TÉCNICO LISBOA

NMR study of Aliquat and C8mim based magnetic and non-magnetic ionic liquids

Rui Miguel de Oliveira Cordeiro

Thesis to obtain the Master of Science Degree in

Engineering Physics

Supervisors: Professor Doutor Pedro José Oliveira Sebastião
Doutora Carla Isabel Lopes Daniel

Examination Committee

Chairperson: Professor Doutor Carlos Manuel dos Santos Rodrigues da Cruz
Supervisor: Professor Doutor Pedro José Oliveira Sebastião
Members of the Committee: Professor Doutor João Luís Maia Figueirinhas
Doutora Marta Cristina Parracho Cançado Corvo

December 2020

Dedicated to my parents...

Acknowledgments

I would like to thank my supervisors, Pedro Sebastião and Carla Daniel, for guiding me throughout this work and for helping me succeed in this undertaking.
I would like to thank Pedro Almeida and Marta Corvo from CENIMAT (FCT/UNL) for allowing me to use their equipment for diffusion measurements and for helping me during that process.
I am also grateful to the professors and colleagues at the Soft Matter Laboratory, and particularly to Carlos Cruz and João Figueirinhas, for their help in conducting X-ray diffractometry and NMR experiments, as well as for expert advice.
A very special thank you to my good friend and colleague Maria Beira, without whom this work would be much poorer. Her support helped me tremendously, and her deep understanding of the kind of systems studied here provided me with much needed insight. I am very grateful to her and look forward to follow her bright future.
I thank my friends, for all the happy memories and encouragement.
I thank my family, for their love and unwavering support for as long as I remember.

Resumo

Efectuámos um estudo de relaxometria e difusometria baseados em RMN de 1H (longitudinal) em misturas de 1%(v/v) de [Aliquat][FeCl4] com [Aliquat][Cl] e DMSO em diferentes concentrações: 50%(v/v) DMSO-d6, 50%(v/v) DMSO-h6 e 99%(v/v) DMSO-h6, respectivamente. Dados experimentais obtidos em estudos anteriores para amostras com 0%, 1% e 10% (v/v) DMSO-d6 foram reajustados a uma única exponencial e são também apresentados. O mesmo estudo foi também efectuado para amostras em que o 1%(v/v) de [Aliquat][FeCl4] foi substituído por [Aliquat][Cl], de forma a isolar a relaxação paramagnética de outros mecanismos de relaxação. Além disso, perfis de difracção de raios-X foram obtidos para todas as amostras. Descobriu-se que o PRE é atenuado significativamente para concentrações elevadas de DMSO, uma vez que o DMSO acima de 50%(v/v) parece solvatar os aniões [FeCl4], diminuindo a sua contribuição para a relaxação paramagnética dos protões de [Aliquat]. Além disso, com o intuito de perceber o efeito da escolha do catião, outro catião foi introduzido, [C8mim], e amostras de [C8mim][Cl] puro e de 99%(v/v) [C8mim][Cl] + 1% (v/v) [C8mim][FeCl4] foram analisadas pelos mesmos métodos usados para as misturas de [Aliquat]. Descobriu-se que o PRE ainda existe nos sistemas de líquidos iónicos magnéticos baseados no catião [C8mim], mas que é menos intenso do que nos sistemas com o catião [Aliquat], e esta diferença aparenta ser maioritariamente devida ao facto da difusão dos aniões [FeCl4] na amostra 99%(v/v) [C8mim][Cl] + 1% (v/v) [C8mim][FeCl4] ser mais rápida quando comparada com a difusão na amostra 99%(v/v) [Aliquat][Cl] + 1% (v/v) [Aliquat][FeCl4].

Palavras-chave: Líquidos Iónicos, Líquidos Iónicos Magnéticos, RMN, Aumento de Relaxação Paramagnética, Relaxometria

Abstract

We performed 1H longitudinal NMR relaxometry and diffusometry study of mixtures of 1%(v/v) of [Aliquat][FeCl4] with [Aliquat][Cl] and DMSO in different concentrations: 50%(v/v) DMSO-d6, 50%(v/v) DMSO-h6 and 99%(v/v) DMSO-h6, respectively. Experimental data obtained in previous studies for samples with 0%, 1% and 10% (v/v) DMSO-d6 were refitted to a single exponential and are also presented. The same study was made for samples in which the 1%(v/v) of [Aliquat][FeCl4] was replaced with [Aliquat][Cl] , in order to isolate the paramagnetic relaxation from other relaxation mechanisms. In addition, X-ray diffraction profiles were collected for all samples. It was found that the PRE significantly attenuates for high DMSO concentrations, as it seems that DMSO above 50%(v/v) solvates the [FeCl4] anions, reducing their contribution to the paramagnetic relaxation of the [Aliquat] protons. Furthermore, in order to understand the effect of cation choice, a different cation was introduced, [C8mim], and pure [C8mim][Cl] samples along with 99%(v/v) [C8mim][Cl] + 1% (v/v) [C8mim][FeCl4] were analysed using the same methods that were used for the [Aliquat] mixtures. It was found that the PRE still exists in the [C8mim] based magnetic ionic liquid systems, but it is less intense than in the [Aliquat] systems, and this difference appears to be mostly due to faster diffusion of the [FeCl4] anions in the 99%(v/v) [C8mim][Cl] + 1% (v/v) [C8mim][FeCl4] sample when compared to 99%(v/v) [Aliquat][Cl] + 1% (v/v) [Aliquat][FeCl4].

Keywords: Ionic Liquids, Magnetic Ionic Liquids, NMR, Paramagnetic Relaxation Enhancement, Relaxometry

Contents

List of Tables

List of Figures

Nomenclature

Experimental Techniques

FFC Fast Field Cycling

PFG Pulse field gradient

General Symbols and Initialisms

$\gamma_{^1H}$ Hydrogen proton gyromagnetic ratio ($2.675 \times 10^8 rad.T^{-1}s^{-1}$)

$\hbar$ Reduced Planck constant ($1.05457 \times 10^{-34} m^2 kg.s^{-1}$)

B Magnetic field (in Tesla)

γ Gyromagnetic ratio

^{35}Cl Chlorine–35

^{37}Cl Chlorine–37

e Charge of the electron ($1.602 \times 10^{-19} C$)

N_A Avogadro's Number

FWHM Full Width at half maximum

NMRD Nuclear magnetic relaxation dispersion

PM Paramagnetic Relaxation

PRE Paramagnetic relaxation enhancement

Rot Rotations and/or reorientations

SNR Signal to noise ratio

ZFS Zero field splitting

Relaxometry Models

BPP Bloembergen, Purcell and Pound

CR Cross-Relaxation

IS Inner Sphere

OPF Order parameter fluctuation

OS Outer Sphere

Parameters

Δ Trace of the zero field splitting tensor

ρ Density

τ_m Exchange time of the inner sphere mechanism

τ_v Correlation time of the zero field splitting fluctuations

τ_{CR} Cross relaxation mechanism's correlation time

τ_{ISRot} Global rotation time for the anion-cation pair

τ_{rot} Rotational correlation time

A_{CR} Cross relaxation mechanism's prefactor

A_{opf} Order parameter fluctuation mechanism prefactor

A_{rot} Rotational mechanism's prefactor

C Paramagnetic particles' molar concentration

d Distance of closest lateral approach for the diffusion

D_{an} Diffusion coefficient for the anion

D_{IL} Diffusion coefficient for the non-magnetic sample

d_{in} Distance between spins for the inner sphere mechanism

D_{MIL} Diffusion coefficient for the magnetic sample

d_{out} Distance between spins for the outer sphere mechanism

F Fraction of the molecule's nuclear spins participating in the inner sphere mechanism

f_{CR} Cross relaxation mechanism's frequency

f_{max} Maximum frequency used for the order parameter fluctuation mechanism

f_{min} Minimum frequency used for the order parameter fluctuation mechanism

G Solvation factor

K Proportion of protons that are Aliquat protons in the 50% DMSO mixtures

M_s Molecular weight

n Spin density

q Number of molecules connected to a paramagnetic center

r Average distance for the diffusional jumps

S Spin of the paramagnetic molecule

Substances

[Aliquat]$^+$[Cl]$^-$ Methyltrioctylammonium Chloride

[Aliquat]$^+$[$FeCl_4$]$^-$ Methyltrioctylammonium Tetrachloroferrate

[C_8mim]$^+$[Cl]$^-$ 1-Octyl-3-Methylimidazolium Chloride

[C_8mim]$^+$[$FeCl_4$]$^-$ 1-Octyl-3-Methylimidazolium Tetrachloroferrate

DMSO Dimethyl sulfoxide

DMSO-d6 Dimethyl sulfoxide with all its hydrogens being deuterium

DMSO-h6 Dimethyl sulfoxide with all its hydrogens being protium

Chapter 1

Introduction

1.1 Thesis Outline

This work is divided into four chapters. The first chapter explains the motivations behind this thesis as well as its objectives, along with an introduction into the subject of ionic liquids. The second chapter explains the theoretical basis for nuclear magnetic relaxation, and introduces the models used for fitting the experimental data. It introduces as well the experimental techniques that were used in this work. The third chapter is where the analysis of the experimental results is both presented and discussed. Finally, the fourth and last chapter presents the main conclusions and suggests future work on this subject.

1.2 Ionic liquids

The term ”Ionic liquid” describes a wide class of liquids which are composed entirely by ions, and have melting point below 100 ºC. Room temperature ionic liquids (RTIL) were the first to be discovered around one hundred years ago, being the first one, ethylammonium nitrate, synthesised in 1914 by Paul Walden [1].

RTIL are generally comprised by organic cations and inorganic anions. Figures 1.1 and 1.2 display some typical cations and anions.

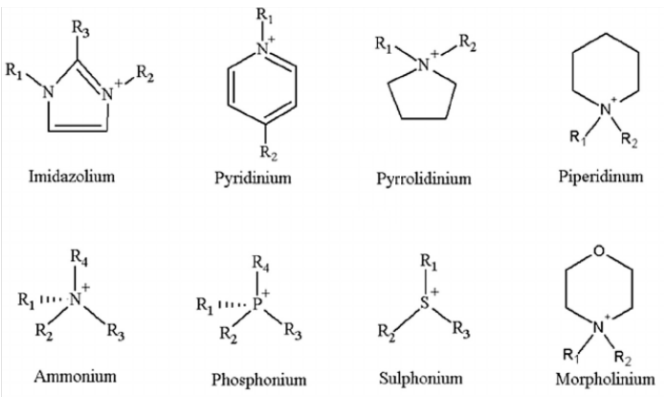

Figure 1.1: Typical IL cations[2].

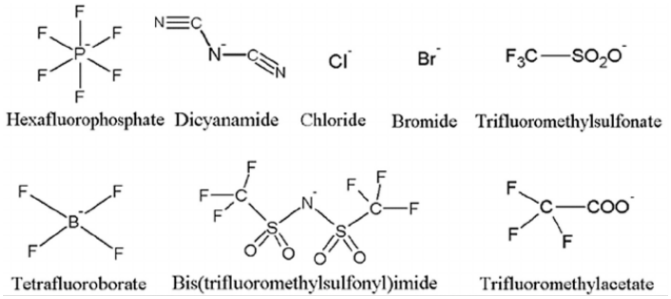

Figure 1.2: Typical IL anions [2].

These substances have a wide set of interesting properties [3, 4], such as:

- A wide liquid range;
- Negligible vapor pressure;
- High thermal stability;
- Are excellent solvents for both polar and nonpolar substances.
- Non-flammability
- Good intrinsic conductivity

These properties make ionic liquids very interesting for future applications and a hot topic of research. Possible applications include chemical separation [5], electrodeposition of aluminum [6], gas storage [7], its use in lithium ion batteries [8], cellulose dissolution [9] and as a catalyst in chemical processes [10, 11].

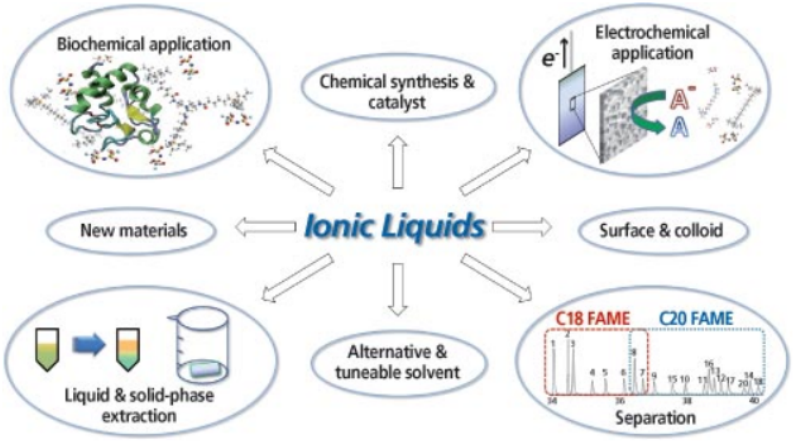

Figure 1.3: Illustration of IL possible applications [12].

However, none looks more promising than the role as solvents, since its very low vapor pressure means they almost do not evaporate. This means less atmospheric contamination and associated health problems, but also an economic advantage as solvent is not wasted. This and the fact that they are usually non-flammable earned them the label of ”green solvents” [13].

Most importantly, the fact that both the cation and the anion can be changed allows the handler to modify the properties of the liquid to its necessities. The number of possible combinations is believed to be in the vicinity of 10^6 for binary ionic liquids, an number which quickly rises if tertiary ionic liquids are considered [14], which basically entails an endless source of combinations to probe for specific applications. This amazing tuneability is at the heart of its promise as future green ”designer solvents”.

Magnetic ionic liquids (MIL) are ionic liquids that incorporate a paramagnetic component in either the cation or the anion. Most common MIL incorporate a transition metal or a lanthanide complex in its anion [15].

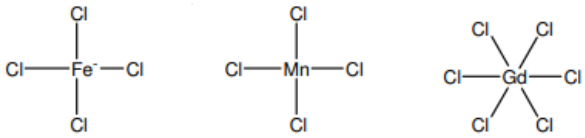

Figure 1.4: Typical MIL anions [15].

Magnetic ionic liquids have all the aforementioned properties of ionic liquids and are also affected by magnetic fields. Some properties, such as viscosity and diffusion coefficient also become magnetic field dependent. In the case of supported magnetic ionic liquid membranes, its permeability has also been found to depend on the magnetic field [16]. Recently, it has been suggested that MIL can also be used as contrast agents [17].

1.3 Motivation

Recent studies [18] discovered significant paramagnetic relaxation enhancement (PRE) on $[\text{Aliquat}]^+$ based magnetic ionic liquids. Subsequent studies [19, 20] analysed the effects of adding small quantities of a co-solvent (DMSO) to the ionic liquid mixture. These studies showed that replacing some of the $[\text{Aliquat}]^+$ for DMSO did not attenuate the PRE as might have been expected. This work tries to build on those previous ones by extending the range of concentrations of the co-solvent in order to understand the underlying molecular dynamics responsible for the PRE in this kind of system. Furthermore, another ionic liquid cation, $[\text{C}_8\text{mim}]^+$, was studied in order to ascertain the effect of cation choice on the PRE.

The different substances studied in this work are displayed in table 1.1, along with its chemical formulas and number of protons. They are also visually presented in figures 1.5, 1.6, 1.7 and 1.8.

	Cations		Co-solvent	Anions	
Name	[Aliquat]$^+$	[C_8mim]$^+$	Dimethyl sulfoxide (DMSO)	Tetrachloroferrate ion	Chloride ion
Chemical formula	$C_{25}H_{54}N^+$	$C_{12}H_{23}N_2^+$	C_2H_6OS	$FeCl_4^-$	Cl^-
Number of protons	54	23	6	0	0

Table 1.1: Substances used in this work.

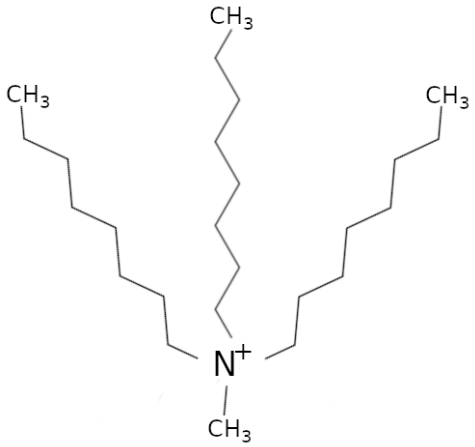

Figure 1.5: [Aliquat]$^+$ cation.

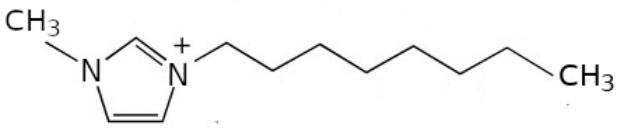

Figure 1.6: [C_8mim]$^+$ cation.

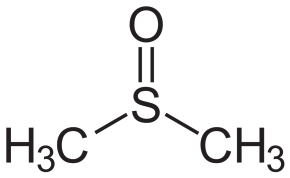

Figure 1.7: Dimethyl sulfoxide.

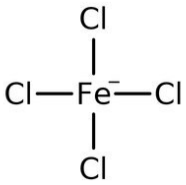

Figure 1.8: Tetrachloroferrate ion.

1.4 Objectives

After the detection of PRE in [Aliquat]$^+$ MIL/IL mixtures in [18], further studies [19, 20] analysed the effect of adding DMSO in small quantities (1% (v/v) and 10%(v/v)) in an attempt to discover the fundamental dynamics that generate the PRE.

In this work, we planned to further complete this study by analysing mixtures of [Aliquat]$^+$ with increasing DMSO concentrations, namely 50%(v/v) and 99% (v/v). Furthermore, since the use of deuterated DMSO for the 99% mixture yields very small signals and is thus impractical, two different samples, one with deuterated and another with protonated DMSO were studied for the 50% (v/v) case in order to

understand the effect of the DMSO protons' relaxation and to connect it to the 99% (v/v) case. Since the paramagnetic relaxation was described by this work by two different models instead of the one model used for both [18–20], the same experimental data for the pure $[Aliquat]^+$ and 1% (v/v) and 10% (v/v) DMSO mixtures shown in [20] was refitted after being gently given by its authors.

All this data for the different samples was then analysed and fitted together to give the full picture of the effect of gradually adding a co-solvent on the PRE for $[Aliquat]^+$ MIL/IL mixtures.

Finally, in order to try to understand how much cation choice impacts the existence of the PRE, another cation, $[C_8mim]^+$, was used to prepare a $[C_8mim]^+$ based magnetic ionic liquid which was then analysed.

Chapter 2

Theoretical overview

2.1 Nuclear magnetic resonance

The experimental techniques used in this work are based on Nuclear Magnetic Resonance. This chapter focuses on introducing the theoretical concepts related to NMR.

2.1.1 Nuclear Spin and the Zeeman Hamiltonian

Elementary particles possess a form of intrinsic angular momentum called spin. Nuclei are a collection of elementary particles, neutrons and protons, each with spin equal to $\frac{1}{2}$. The nuclei behaves as a single particle, with total spin angular momentum I. All nuclei with even number of protons and neutrons have spin equal to 0, while nuclei with odd number of protons and neutrons have integer spin. The remainining nuclei have half-integer spins. Table 2.1 shows some examples of nuclei and their spin.

Nucleus	Spin	Natural Abundance (%)
^{1}H	1/2	99.99
^{2}H	1	0.01
^{12}C	0	98.89
^{13}C	1/2	1.11
^{35}Cl	3/2	75.76
^{37}Cl	3/2	24.24

Table 2.1: Some nucleus and their nuclear spin.

Choosing a direction (usually the direction of an external magnetic field), the projection of spin in that direction is given by the secondary spin quantum number m. There is a magnetic dipole moment $\hat{\mu} = \gamma\hbar\hat{I}$ associated with the spin of the nuclei, where γ is the gyromagnetic ratio, and its projection on the chosen direction is given by $\mu_z = \gamma\hbar m$.

An isolated spin of magnetic moment $\hat{\mu}$ under a magnetic field $\vec{B} = \vec{B}_0$ has a Zeeman Hamiltonian:

$$\hat{\mathcal{H}}_Z = -\hat{\mu}.\vec{B}_0 = -\gamma\hbar\hat{I}.\vec{B}_0. \tag{2.1}$$

Its eigenvalues are the Zeeman levels:

$$E = -m\gamma\hbar B_0. \tag{2.2}$$

This Hamiltonian is only valid for a spin that senses nothing more than an outside magnetic field $\vec{B}_0$. However, this is the case in almost no system. Spins interact with its surroundings, and in practice:

$$\hat{\mathcal{H}} = \hat{\mathcal{H}}_Z + \hat{\mathcal{H}}(t), \tag{2.3}$$

where the second term is a time dependent term that accounts for the other interactions. In practice, this term has both time-dependent and time independent terms. A time independent term that is ubiquitous is the chemical shielding, the magnetic field induced by the movement of surrounding electrons. This induced field is proportional and opposed to the static field:

$$\hat{\mathcal{H}}_{shielding} = \gamma\hbar\hat{I}.\hat{\delta}.\vec{B}_0, \tag{2.4}$$

which results in a Larmor frequency usually downshifted typically by a few ppm (parts per million).

2.1.2 Magnetization

The first phase of any NMR experience is to generate a net magnetization on the substance to be studied, which means that only non zero spin nuclei can be observed using this techniques. For a given magnetic field $\vec{B} = B\hat{e}_z$ a net magnetization will appear in the same direction (the magnetic moments μ_y and μ_x average to 0, therefore there will be no magnetization on those axis), with amplitude given by:

$$\begin{aligned} M = M_z = n\langle\mu_z\rangle &= n\frac{\sum_{\mu_z=-\gamma\hbar I}^{\gamma\hbar I}\mu_z\, exp(-E_\mu/kT)}{\sum_{\mu_z=-\gamma\hbar I}^{\gamma\hbar I} exp(-E_\mu/kT)} = n\gamma\hbar\frac{\sum_{m=-I}^{I} m\, exp\left(\frac{\gamma\hbar mB}{kT}\right)}{\sum_{m=-I}^{I} exp\left(\frac{\gamma\hbar mB}{kT}\right)} \overset{\left(x=\frac{\gamma\hbar BI}{kT}\right)}{=} \\ &= n\gamma\hbar I\frac{d}{dx}\left(ln\Big(\sum_{m=-I}^{I} exp(\frac{x}{I}m)\Big)\right) = n\gamma\hbar I B_I(x), \end{aligned} \tag{2.5}$$

where we used the Zeeman Hamiltonean ($E_\mu = -\mu_z B$) and the last function is called the Brillouin function, $B_I(x) = \frac{2I+1}{2I}coth(x + \frac{x}{2I}) - \frac{1}{2I}coth(\frac{x}{2I})$. For a proton, $x \approx 10^{-3}\frac{B}{T}$, which means that, as $\frac{B}{T}$ is at most of the order of 10^{-2}, $x \leq 10^{-5}$. This means that a high temperature/ low field approximation can be used. Expanding the Brillouin function in a Taylor series around $x = 0$ and keeping only the first term, we get:

$$M \approx \frac{1}{3}n\gamma\hbar(I+1)x = \frac{n\gamma^2\hbar^2 I(I+1)}{3kT}B = \frac{C}{T}B, \tag{2.6}$$

which is called the Curie law, with Curie constant $C = \frac{n\gamma^2\hbar^2 I(I+1)}{3k}$.

2.2 Bloch equations and the resonance condition

The interaction of the total magnetization with the applied magnetic field is described by a set of phenomenological equations called the Bloch equations. Just like an individual magnetic moment experiences a torque caused by a magnetic field, the same is true for the total magnetic moment per unit volume, i.e. the magnetization:

$$\frac{d\vec{M}}{dt} = \gamma\vec{M} \times \vec{B} \tag{2.7}$$

If the magnetization is not aligned with the magnetic field, it will experience a precession motion known as Larmor precession. The frequency is known as the Larmor frequency and is given by:

$$\omega_0 = -\gamma B_0, \tag{2.8}$$

in which the minus sign accounts for the direction of rotation. For instance, a proton has a positive gyromagnetic ratio and will therefore precess clockwise.

Since most NMR experiments use external magnetic fields to change the magnetization of a sample, it is necessary to understand how this is accomplished. The most practical approach is the one used in NMR experiments, which consists in the use of very small fields rotating near the nuclei Larmor frequency to change the magnetization.

To understand how a small field can change the magnetization, it is more natural to look at the problem using a rotating frame.

In a frame rotating with frequency ω along $\hat{e}_z$, the Bloch equation gets modified. In that frame the total derivative of the magnetization with respect to time is given by:

$$\frac{d\vec{M}}{dt} = \frac{\partial\vec{M}}{\partial t} + \vec{\omega} \times \vec{M} \tag{2.9}$$

That modifies the Bloch equation, which mantains the same form as before, only with the magnetic field taking the form of an effective field $\vec{B_{eff}} = \vec{B} + \frac{\vec{\omega}}{\gamma}$, as schematically shown in figure 2.1:

$$\frac{\partial\vec{M}}{\partial t} = \gamma\vec{M} \times (\vec{B} + \frac{\vec{\omega}}{\gamma}) \tag{2.10}$$

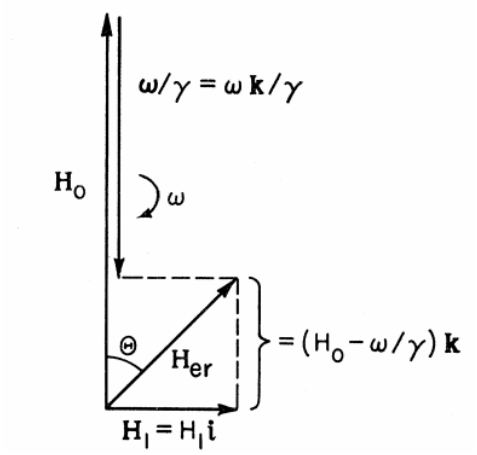

Figure 2.1: Effective magnetic field in the rotating coordinate system (image from [21]).

Because $\vec{B} = -\frac{\vec{\omega_0}}{\gamma}$, we see that if the frequency of the rotating frame is equal to the Larmor frequency of the nuclei, the effective field is zero and the magnetization is a constant in that frame, which implies the aforementioned Larmor precession. When the offset $\Omega = \omega_0 - \omega$ is small, this effective field can be made into a small quantity. If a field rotating at frequency ω in the x-y plane is then created, it can easily overwhelm the z component of the effective field, creating a field on the x-y plane that forces the rotation of the magnetization. This is in essence the phenomena of resonance, in which a small rotating field can produce large effects on the total magnetization, if it is at a frequency close enough to the Larmor frequency in question.

In practice, this rotating field is produced by a coil. This coil has the added benefit of not only producing the RF field but also detecting the signal generated by the sample. The field produced by the coil is in fact linearly polarized that can be decomposed as two circularly polarized fields, one at frequency $\omega = \omega_0$ and the other at frequency $\omega = -\omega_0$, of which only the one at frequency $\omega = \omega_0$ has a relevant effect.

The effective field in the rotating frame is the sum of the static z-field with the radiofrequency field given by the coil:

$$\vec{B}_{eff} = (B_0 - \frac{\omega}{\gamma})\hat{e}_z + B_{rf}\hat{e}_x \tag{2.11}$$

This magnitude of this field is given by:

$$B_{eff} = ((B_0 - \frac{\omega}{\gamma})^2 + B_{rf}^2)^{\frac{1}{2}} = \frac{a}{\gamma} \tag{2.12}$$

in which a is given by:

$$a = ((\omega_0 - \omega)^2 + \omega_{rf}^2)^{\frac{1}{2}} \frac{\gamma}{|\gamma|} \tag{2.13}$$

The angle θ between the effective field B_{eff} and the z-field is given by the following relationships:

$$\tan\theta = \frac{B_{rf}}{B_0 - (\frac{\omega}{\gamma})} = \frac{\omega_{rf}}{\omega_0 - \omega}$$
$$\sin\theta = \frac{\omega_{rf}}{a} \qquad \cos\theta = \frac{\omega_0 - \omega}{a} \tag{2.14}$$

The magnetization will rotate around this effective field. Assuming that it is initially aligned with the z-field, the angle by which it rotates is given by:

$$\cos\alpha = \cos^2\theta + sin^2\theta\cos(at) = 1 - 2\sin^2\theta\sin^2(\frac{1}{2}at) \tag{2.15}$$

It is simple to see that in order to maximize the rotation angle we must have $\sin\theta = 1$, and therefore $\omega = \omega_0$, which is the resonance condition. This also explains why the circularly polarized field with $\omega = -\omega_0$ does not have a relevant effect, since $\sin\theta \ll 1$ and hence why linearly polarized fields are completely acceptable.

When in resonance, the angle of rotation in respect to time is simplified to:

$$\alpha = \arccos(1 - 2\sin^2(\frac{1}{2}\omega_{rf}t)) \Leftrightarrow \alpha = -\gamma B_{rf}t \tag{2.16}$$

The application of such a radiofrequency field in resonance is called a pulse with length t. This pulse is usually designated by the angle α by which the magnetization rotates, if $\alpha = \frac{\pi}{2}$ it is called a $\frac{\pi}{2}$ pulse and the same for any other given angle (ex: a π pulse).

It is important to note that there is an effect of relaxation (described in the next sub-section) competing with the pulse, however, the pulse duration tends to be much shorter than the time needed for relaxation to be relevant and therefore it can be disregarded.

2.3 Relaxation

The equilibrium magnetization relies on the small differences between the populations with field parallel spin and field anti-parallel spin. If a pulse is emitted such that this magnetization is changed, the difference in populations will also vary as a result. The return to the equilibrium of populations is called longitudinal or *spin-lattice relaxation* (T_1).

The emission of a pulse will make the entire spin system rotate, and if the pulse is a $\frac{\pi}{2}$ pulse, the difference of populations will now manifest itself in the $x - y$ plane as phase coherence, having a net magnetization in this direction equal to the previous z-magnetization. There will also be a return to equilibrium of this transverse magnetization, called transverse or *spin-spin relaxation* (T_2). As the processes responsible for T_1 and T_2 aren't the same (although every T_1 inducing process contributes to T_2), these times are different.

These relaxation constants can be added to the Bloch equations as following:

$$\frac{dM_x}{dt} = \gamma M_y B_z - \gamma M_z B_y - \frac{M_x}{T_2} \tag{2.17}$$

$$\frac{dM_y}{dt} = \gamma M_z B_x - \gamma M_x B_z - \frac{M_y}{T_2} \tag{2.18}$$

$$\frac{dM_z}{dt} = \gamma M_x B_y - \gamma M_y B_x - \frac{M_z - M_0}{T_1} \tag{2.19}$$

In this work, we will be concerned exclusively with T_1 and its mechanisms.

It can be shown that the coupling of an isolated spin with a radiation field barely contributes to T_1 relaxation [22]. Instead, coupling with the lattice contributes and that is why T_1 is also called spin-lattice relaxation.

The two kinds of transitions that can contribute will be magnetic dipole or electric quadrupole, since there is no monopole radiation and electric dipole transitions are forbidden by selection rules. Since we will be dealing with ^{1}H exclusively, which has spin $\frac{1}{2}$, its charge distribution is symmetrical and therefore there is no electric quadrupole transition. Therefore, only the magnetic dipole transition is available.

In order for these transitions to occur, the nuclei needs to experience a magnetic field oscillating at specific frequencies. The movement of components of the lattice will generate random magnetic fields at the nuclei. If there is a finite contribution at the frequencies that can induce transitions, then there is a finite probability of transition between spin polarization states, which will eventually put the spin system in thermal equilibrium with the lattice, with the equilibrium Boltzmann populations and the magnetization on the z-axis.

2.4 FID and the spectrum

After the application of a 90º pulse, the magnetization will evolve according to the Bloch equations. In the rotating referential, that yields:

$$M_x(t) = M_0 \cos(\Omega t) \exp(-\frac{t}{T_2}) \tag{2.20}$$

$$M_y(t) = M_0 \sin(\Omega t) \exp(-\frac{t}{T_2}) \tag{2.21}$$

$$M_z(t) = M_0(1 - \exp(-\frac{t}{T_1})) \tag{2.22}$$

The acquisition of this signal results in what is called the Free Induction decay (FID) (shown in figure 2.2), which is of the form of a damped exponential $\sin(\omega_0 t) \exp(-\frac{t}{T_2^*})$, being T_2^* a shorter time than the expected T_2 due to the inevitable presence of magnetic field inhomogenities in the sample.

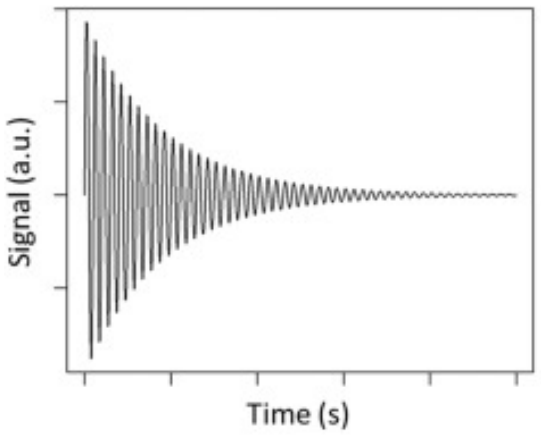

Figure 2.2: Example of a FID.

The detected signal is proportional to the magnetization. The signal function is defined as following:

$$s(t) = S_x(t) + iS_y(t) = S_0 \cos(\Omega t) \exp(-\frac{t}{T_2}) + S_0 \sin(\Omega t) \exp(-\frac{t}{T_2}) = S_0 \exp(i\Omega t) \exp(-\frac{t}{T_2}) \quad (2.23)$$

The Fourier transform (FT) of this signal is called the spectrum, which is the representation of the distribution of different Larmor frequencies of the nuclei in the sample. The FT yields:

$$S(\omega) = \int_{-\infty}^{\infty} s(t) exp(-i\omega t) dt \quad (2.24)$$

Using the signal function, the spectrum becomes:

$$S(\omega) = \int_{-\infty}^{\infty} S_0 \exp(i(\Omega - \omega)t) \exp(-\frac{t}{T_2}) dt \quad (2.25)$$

which is solved to give:

$$S(\omega) = S_0 \frac{\frac{1}{T_2}}{\frac{1}{T_2}^2 + (\Omega - \omega)^2} + iS_0 \frac{(\Omega - \omega)}{\frac{1}{T_2}^2 + (\Omega - \omega)^2} \quad (2.26)$$

2.5 The correlation function and the spectral density

As previously mentioned, fluctuating magnetic fields give origin to relaxation processes. These fluctuations are random, and in order to treat them mathematically we must introduce the correlation function:

$$G(\tau) = \langle B(t) B^*(t + \tau) \rangle_{av} , \quad (2.27)$$

which gives the correlation between two values of the same variable after a finite time τ. In this case, our variable is obviously the magnetic field.A typical form for the correlation function is an exponential decay:

$$G(\tau) = |B(0)^2| \exp\left(-\frac{|\tau|}{\tau_c}\right), \tag{2.28}$$

with the decay time being given by τ_c. This τ_c is entirely dependent of the process by which the random magnetic field fluctuations are created. Furthermore, it obviously depends on the motion of the spins sensing the magnetic field, and therefore on the temperature.

The function that is most often useful, however, is not $G(\tau)$, but its Fourier transform. This function is called the spectral density, and it gives us the amount of power available for relaxation at different frequencies. If the correlation function is an exponential, the spectral density is a Lorentzian curve:

$$J(\omega) = \frac{2\tau_c}{1 + \omega^2 \tau_c^2}. \tag{2.29}$$

2.5.1 Dipole-dipole interaction

As previously stated, magnetic dipole transitions are the main sources for relaxation in spin $\frac{1}{2}$ nuclei, which is the case for the samples studied in this work.

Classically, two dipoles with magnetic moments $\vec{\mu_1}$ and $\vec{\mu_2}$ separated by a vector $\vec{r}$ have the following potential energy:

$$E = \frac{\mu_0}{4\pi r^3}(\vec{\mu_1} \cdot \vec{\mu_2} - 3(\vec{\mu_1} \cdot \vec{r})(\vec{\mu_2} \cdot \vec{r})) \tag{2.30}$$

In the case of two nuclear magnetic dipoles, the previous expression can be treated as a perturbation to the Zeeman Hamiltonian:

$$H_{dip} = \frac{\mu_0 \gamma^2 \hbar^2}{4\pi r^3}(\vec{I_1} \cdot \vec{I_2} - 3(\vec{I_1} \cdot \vec{r})(\vec{I_2} \cdot \vec{r})) \tag{2.31}$$

This Hamiltonian is typically divided into six parts:

$$H_{dip} = \frac{\mu_0 \gamma^2 \hbar^2}{4\pi r^3}(A + B + C + D + E + F), \tag{2.32}$$

which are respectively [22]:

$$A = (1 - 3\cos^2\theta) I_{z1} I_{z2} \tag{2.33}$$

$$B = -\frac{1}{4}(1 - 3\cos^2\theta)(I_1^+ I_2^- + I_1^- I_2^+) \tag{2.34}$$

$$C = -\frac{3}{2}\sin\theta\cos\theta e^{-i\phi}(I_{z1} I_2^+ + I_1^+ I_{z2}) \tag{2.35}$$

$$D = -\frac{3}{2}\sin\theta\cos\theta e^{i\phi}(I_{z1} I_2^- + I_1^- I_{z2}) \tag{2.36}$$

$$E = -\frac{3}{4}\sin^2\theta e^{-2i\phi} I_1^+ I_2^+ \tag{2.37}$$

$$F = -\frac{3}{4}\sin^2\theta e^{2i\phi} I_1^- I_2^- \tag{2.38}$$

Separating the Hamiltonian into its spatial and spin part, the spectral densities are given by the Fourier transforms of the autocorrelation functions of its spatial parts:

$$\overline{F^{(q)}(t)F^{(q')*}(t+\tau)} = \delta_{qq'}G^{(q)}(\tau) \tag{2.39}$$

$$J^{(q)}(\omega) = \int_{-\infty}^{+\infty} G^{(q)}(\tau)e^{-i\omega\tau}d\tau, \tag{2.40}$$

in which the spatial parts are:

$$F^{(0)} = \frac{1-3\cos^2\theta}{r^3} \tag{2.41}$$

$$F^{(1)} = \frac{\sin\theta\cos\theta e^{-i\phi}}{r^3} \tag{2.42}$$

$$F^{(2)} = \frac{\sin^2\theta e^{-2i\phi}}{r^3}. \tag{2.43}$$

Both relaxation rates due to this Hamiltonian can be derived [22]:

$$\frac{1}{T_1} = \frac{3}{2}\left(\frac{\mu_0}{4\pi}\right)^2\gamma^4\hbar^2 I(I+1)(J_1(\omega)+J_2(2\omega)), \tag{2.44}$$

$$\frac{1}{T_2} = \left(\frac{\mu_0}{4\pi}\right)^2\gamma^4\hbar^2 I(I+1)\left(\frac{3}{8}J_0(0)+\frac{15}{4}J_1(\omega)+\frac{3}{8}J_2(2\omega)\right), \tag{2.45}$$

which can be generalized for a system of N spins interacting, as long as as their motions are not correlated:

$$\frac{1}{T_1} = \frac{3}{2}\left(\frac{\mu_0}{4\pi}\right)^2\gamma^4\hbar^2 I(I+1)\sum_{i<j}^{N}(J_1^{ij}(\omega)+J_2^{ij}(2\omega)), \tag{2.46}$$

$$\frac{1}{T_2} = \left(\frac{\mu_0}{4\pi}\right)^2\gamma^4\hbar^2 I(I+1)\sum_{i<j}^{N}\left(\frac{3}{8}J_0^{ij}(0)+\frac{15}{4}J_1^{ij}(\omega)+\frac{3}{8}J_2^{ij}(2\omega)\right), \tag{2.47}$$

These relaxation rates are directly proportional to the value of the spectral densities at three frequencies, zero, the Larmor frequency and its double. These are the specific frequencies of the fluctuating magnetic field that can induce transitions. The spectral density at zero will only affect T_2, however, since flip-flop transitions (in which both spins invert their polarization) do not change the overall z-magnetization but dephase the x-y magnetization, leading to a shortening of T_2.

The spectral density at the Larmor frequency permits transitions in one of the spins, while at the double of the Larmor frequency it permits transitions in which both spins change polarization on the same way. Since both these will change the overall z-magnetization, they both contribute to T_1.

The different relative motions of the magnetic dipole moments will originate different non-zero spectral densities at the frequencies needed for relaxation. Therefore, each of these motions can be catego-

rized as a different relaxation mechanism.

2.6 Spin-lattice relaxation mechanisms

The study performed on this work revolves mainly on the measurement of the spin-lattice relaxation time T_1. As previously discussed, fluctuating magnetic fields at specific frequencies give rise to relaxation. Fluctuating magnetic fields can be generated by different kinds of movements, which constitute separate relaxation mechanisms.

Different kinds of movements have specific correlation times associated to them, and the relaxation rate generated by them will be a function of this correlation time:

$$R_1 = \frac{1}{T_1} = E_c^2 f(\tau_n), \tag{2.48}$$

where E_c is the strenght of the interaction and τ_n the correlation time for the mechanism.

In most cases there will be a combination of more than one of these individual mechanisms. In such a case, it is usually assumed that they are independent, which implies that the total relaxation rate is simply the sum of the individual relaxation rates:

$$\frac{1}{T_1} = \sum_{n=1}^{N} \frac{1}{T_{1n}}, \tag{2.49}$$

where each n represents a relaxation mechanism ($n = 1$ for the rotational relaxation rate, $n = 2$ for the diffusion rate and so on for all relevant mechanisms). In the following sections a review of the mechanisms used in this work is provided:

2.6.1 Rotational diffusion

In the case of spins belonging to the same molecule, the distance between them is almost a constant and only the orientation of the vector between two spins changes in a significant way. This kind of intra-molecular relaxation corresponds to the relative rotational motion between magnetic dipoles and is therefore aptly called rotational diffusion.

In its famous paper [23], Bloembergen, Purcell and Pound (BPP) determined the spectral densities by assuming the rotation of a molecule as the rotation of a rigid sphere in a viscous medium. Using a diffusion equation for the angle between spins, they were able to calculate the following spectral densities:

$$J^{(0)}(\omega) = 6J^{(1)}(\omega) \tag{2.50}$$

$$J^{(1)}(\omega) = \frac{4}{15r^6} \frac{\tau_r}{1 + \omega^2 \tau_r^2} \tag{2.51}$$

$$J^{(2)}(\omega) = 4J^{(1)}(\omega), \tag{2.52}$$

in which r is the average distance between spins.

These densities allowed them to determine the relaxation time T_1. Using $I = \frac{1}{2}$ for both spins:

$$\left(\frac{1}{T_1}\right)_{Rot} = \frac{3}{10}\left(\frac{\mu_0}{4\pi}\right)^2 \frac{\gamma^4\hbar^2}{r^6}\left[\frac{\tau_r}{1+\omega^2\tau_r^2} + \frac{4\tau_r}{1+\omega^2\tau_r^2}\right], \tag{2.53}$$

which is the rotational rate used for this work.

It is also important to note that this model was used as a first approximation, as no other model specific to these systems could be found. In any case, some more elaborate models can be found in the literature [24].

2.6.2 Translational diffusion

In the case of two spins belonging to different molecules, both their respective distances and relative orientation are a function of time. The molecules to which they belong will diffuse with respect to one another, and therefore the relaxation caused by these movements is called translational diffusion.

BPP derived an expression for the translational relaxation time assuming that the molecules follow a diffusion equation. The result, however, gives a relaxation time independent of frequency.

A more satisfactory result was derived by Torrey [25], which assumed instead that the molecules were trapped in a potential well, only allowed to move through a fast random jump between trapped states. He obtained the following spectral densities:

$$\begin{aligned} J^{(k)}(\omega,\tau_d) =& (4k^2-9k+6)\frac{8\pi n\langle r^2\rangle}{45d^5}\frac{1}{\omega^2\tau_d}[(u_+\left(1+\frac{1}{u_-^2+u_+^2}\right)+2)e^{-2u_+}\cos 2u_- \\ &+ u_+\left(1-\frac{1}{u_-^2+u_+^2}\right)+u_-\left(1-\frac{1}{u_-^2+u_+^2}\right)e^{-2u_+}\sin 2u_-] \end{aligned} \tag{2.54}$$

with $u_\pm$ given by:

$$u_\pm = \frac{1}{2}\sqrt{\frac{q(1\pm q)}{\alpha}}, \tag{2.55}$$

and q equal to:

$$q = \frac{\omega\tau_d}{\sqrt{4+(\omega\tau_d)^2}}. \tag{2.56}$$

In the spectral densities, τ_d is the correlation time, $\langle r^2\rangle$ is the mean square jump distance, n is the spin density and d is the minimum distance of approach between the spins.

These densities can be substituted into (2.44) to obtain the relaxation rate for translational diffusion.

The diffusion constant D enters the equation for the relaxation rate through the equality:

$$\langle r^2\rangle = 6\tau_d D. \tag{2.57}$$

Diffusometry and viscometry studies in magnetic ionic liquids have shown that both viscosity and dif-

fusion are magnetic field dependent parameters for magnetic ionic liquids. Since the diffusion coefficient enters the rate equation, there was the need to make it a frequency dependent parameter. Diffusion measurements were only available above $7T$, which means that, together with the coefficient at zero field assumed to be equal to its non-magnetic ionic liquid counterpart (which is magnetic field independent), two points, at $0T$ and $7T$ were available. The lack of justifiable models for the dependence led us to assume the simplest possible model, a linear function of the magnetic field:

$$D(B) = D(0) + \frac{D(7) - D(0)}{7} B, \tag{2.58}$$

with B given in tesla.

2.6.3 Cross-relaxation

Nuclear spins with $I > \frac{1}{2}$ have an additional pathway for relaxation, namely electronic quadrupolar relaxation. This relaxation rate is normally much faster than the magnetic dipole counterpart.

If these spins are present in a given sample, there will be an effect of cross-relaxation to consider. This cross relaxation will be another mechanism to affect the relaxation rates of the spin $\frac{1}{2}$ sample. Since there are chlorine nuclei in the samples to be studied, and both naturally ocurring isotopes ^{35}Cl and ^{37}Cl have spin $I = \frac{3}{2}$, it becomes necessary to include this effect.

Due to the coupling with the external magnetic field, both spin populations are energy reservoirs which can be caracterized by a temperature. The cross relaxation time T_{CR} can be defined as:

$$\frac{d\beta_I}{dt} = -\frac{1}{T_{CR}}(\beta_I - \beta_S), \tag{2.59}$$

with β_I and β_S the inverse spin temperatures for spin $I = \frac{1}{2}$ and spin $S > \frac{1}{2}$, respectively.

Since the spin $S > \frac{1}{2}$ relaxes much faster through quadrupolar relaxation, it will achieve equilibrium with the lattice and therefore any cross relaxation will drive the spin $I = \frac{1}{2}$ population into equilibrium with the lattice.

This interaction occurs when a single I spin exchanges energy with a single S spin. This implies that this interaction is strongest when the Zeeman energy gap of the I spin is equal to one of the energy gaps of the S spin.

The relaxation rate has the following equation [26]:

$$\left(\frac{1}{T_1}\right)_{CR_n} = A_{CR_n} \frac{\tau_{CR_n}}{1 + (\omega - \omega_{CR_n})^2 \tau_{CR_n}^2}, \tag{2.60}$$

with A_{CR_n} being the strength of the interaction and τ_{CR_n} the correlation time associated with the various ω_{CR_n} frequencies.

These frequencies are:

$$\omega_{CR_n} = \omega_Q \pm \gamma_{Cl} B_0 \cos\phi, \tag{2.61}$$

with ω_Q given by:

$$\omega_Q = \frac{3e^2qQ}{4\hbar}, \tag{2.62}$$

where e is the charge of the electron, ϕ is the angle between the z axis of the electric field gradient tensor in the principal axis system of the chlorine nucleus and the external magnetic field and Q is the quadrupole moment.

2.6.4 Order parameter fluctuation

The liquids studied in this work are in the isotropic phase, and therefore show no preferred order as given by a director axis. However, there may be local order in small domains of the sample, caracterized by a local director and a local order parameter tensor.

This local order is not permanent, however, and relaxes with caracteristic time given by:

$$\tau_{OPF} = \frac{\xi^2\nu}{L}, \tag{2.63}$$

with ν being a phenomenological viscosity coefficient, ξ the lenght of the ordered domain and L an elastic constant.

The spectral density due to the order parameter fluctuations can be calculated [24]:

$$J_1(\omega) = \frac{k_BT\sqrt{\nu}}{4\sqrt{2}\pi L^{3/2}}\Big(\frac{\tau_0}{1+\sqrt{1+\omega^2\tau_{OPF}^2}}\Big)^{1/2}. \tag{2.64}$$

For small Larmor frequencies ($\omega\tau_{OPF} << 1$), this simplifies to a frequency independent rate:

$$\frac{1}{T_1}_{OPF} \propto J_1(\omega) = \frac{k_BT\xi}{4\sqrt{2}\pi L^2}, \tag{2.65}$$

while for large Larmor frequencies ($\omega\tau_{OPF} >> 1$), it simplifies to a $\omega^{-1/2}$ dependence in the frequency:

$$\frac{1}{T_1}_{OPF} \propto J_1(\omega) = \frac{k_BT\sqrt{\nu}}{4\sqrt{2}\pi L^{3/2}}\omega^{-1/2}. \tag{2.66}$$

The actual formula used to fit the experimental data in this work is:

$$\frac{1}{T_1}_{OPF} = \frac{A_{opf}}{\sqrt{f}}\int_0^{f_{max}/f}\frac{\sqrt{x}}{1+(x+f_{min}/f)^2}dx, \tag{2.67}$$

in which f_{min} and f_{max} are respectively the minimum and maximum cutoff frequencies for the OPF relaxation and $A_{opf} \propto \frac{\nu^{1/2}}{L^{3/2}}$. The maximum cutoff is directly related to the minimum distance involved in this fluctuation, which is the length of a single molecule, while the minimum cutoff relates to the maximum distance involved in the OPF, which is the size of the ordered domain.

2.6.5 Paramagnetic Relaxation

The presence of paramagnetic molecules in a sample is a very strong source for relaxation. Unpaired electrons' spin interacts with the nuclei spin and the modulation of this interaction will give rise

to fast relaxation, being most often the dominant relaxation mechanism even for small quantities of the paramagnetic material.

The total relaxation rate will be the sum of two rates, the diamagnetic rate due to the contributions in the absence of the paramagnetic species $\left(\frac{1}{T_1}\right)_d$ and the paramagnetic rate due to the presence of the paramagnetic species $\left(\frac{1}{T_1}\right)_p$:

$$\frac{1}{T_1} = \left(\frac{1}{T_1}\right)_d + \left(\frac{1}{T_1}\right)_p \tag{2.68}$$

The paramagnetic rate is also a sum of different contributions. In this work, we will consider two different components, inner-sphere (IS) and outer-sphere (OS) relaxation:

$$\left(\frac{1}{T_1}\right)_p = \left(\frac{1}{T_1}\right)_{OS} + \left(\frac{1}{T_1}\right)_{IS} \tag{2.69}$$

2.6.5.1 Inner Sphere

The inner sphere contribution is due to the temporary coordination between protons and the paramagnetic particle. The relaxation due to this coordination is governed by two times, the relaxation time if the coordination is permanent and the mean lifetime of this coordination (the inverse of the exchange rate). Therefore, $\left(\frac{1}{T_1}\right)_{IS}$ is given by:

$$\left(\frac{1}{T_1}\right)_{IS} = \frac{P_m}{T_{1m} + \tau_m}, \tag{2.70}$$

where P_m is the mole fraction of bound solvent protons and τ_m is the mean lifetime of the coordination.

In the case of diluted solutions, which is valid for all samples studied in this work, P_m is given by:

$$P_m = qF\frac{m_s[m]'}{1000\rho}, \tag{2.71}$$

in which q is the number of solvent molecules connected to a paramagnetic particle, F is the fraction of protons of the molecule bound to the paramagnetic center, m_s is the molar mass of the solvent, ρ is the density of the solution in kg/L and $[m]'$ is the molar concentration of paramagnetic particles in $mmol/L$.

The relaxation rate in the absence of exchange has two components, one due to the dipole-dipole interaction between the unpaired electron and the proton spin $\left(\frac{1}{T_{1m}^{dd}}\right)$ and one due to the contact interaction between them $\left(\frac{1}{T_{1m}^{sc}}\right)$:

$$\frac{1}{T_{1m}} = \frac{1}{T_{1m}^{dd}} + \frac{1}{T_{1m}^{sc}} \tag{2.72}$$

They are given by the following expressions [27]:

$$\frac{1}{T_{1m}^{dd}} = \frac{2}{15}\left(\frac{\mu_0}{4\pi}\right)^2 \frac{\gamma_S^2\gamma_I^2\hbar^2}{r_{IS}^6} S(S+1)\left[\frac{3\tau_{c1}}{1+\omega_I^2\tau_{c1}^2} + \frac{7\tau_{c2}}{1+\omega_S^2\tau_{c2}^2}\right], \tag{2.73}$$

$$\frac{1}{T_{1m}^{sc}} = \frac{2}{3}\left(\frac{A}{\hbar}\right)^2 S(S+1)\left[\frac{\tau_{e1}}{1+\omega_S^2\tau_{e1}^2}\right], \tag{2.74}$$

where γ_S is the gyromagnetic ratio of the electron and γ_I is the gyromagnetic ratio of the proton, r_{IS} is the distance between spins I and S and $A/\hbar$ is the Fermi-contact coupling constant between both spins.

The correlation times in both expressions are themselves a sum of different contributions:

$$\begin{aligned} \tau_{c1}^{-1} &= \tau_R^{-1} + T_{1e}^{-1} + \tau_m^{-1}, \\ \tau_{e1}^{-1} &= T_{1e}^{-1} + \tau_m^{-1}, \end{aligned} \tag{2.75}$$

in which τ_R is the rotational correlation time of the pair formed by the paramagnetic complex and the coordinated protons and T_{1e} is the electron longitudinal relaxation time. For $S > 1/2$, T_{1e} is given by the modulation of the zero field splitting interaction (ZFS). The ZFS is the splitting of the electronic energy levels at zero magnetic field caused by the anisotropy of the electric field and spin-orbit coupling [28]. Although monoexponential analytical results are only valid for $S = 1$, for $S > 1$ the following result is valid in the case of extreme narrowing ($\omega_S \tau_v << 1$):

$$T_{1e}^{-1} = \left(T_{1e}^{-1}\right)^{ZFS} = \frac{1}{25}\Delta^2[4S(S+1) - 3]\left[\frac{\tau_v}{1+\omega_S^2\tau_v^2} + \frac{4\tau_v}{1+4\omega_S^2\tau_v^2}\right], \tag{2.76}$$

in which Δ is the average value of the ZFS interaction in units of s^{-1} and τ_v is the correlation time of the ZFS fluctuations. A similar result is obtained for T_{2e} under the same assumption of extreme narrowing:

$$T_{2e}^{-1} = \left(T_{1e}^{-1}\right)^{ZFS} = \frac{1}{50}\Delta^2[4S(S+1) - 3]\left[\frac{5\tau_v}{1+\omega_S^2\tau_v^2} + \frac{2\tau_v}{1+4\omega_S^2\tau_v^2} + 3\tau_v\right], \tag{2.77}$$

2.6.5.2 Outer Sphere

The outer sphere contribution is the contribution generated by the diffusion of protons in the vicinity of paramagnetic centers.

This contribution is given by [29]:

$$\frac{1}{T_1}_{OS} = \frac{32\pi}{405}\left(\frac{\mu_0}{4\pi}\right)^2 \gamma_S^2\gamma_I^2\hbar^2\frac{n_m N_a}{aD}S(S+1)\left[j_2(\omega_I - \omega_S) + 3j_1(\omega_I) + 6j_2(\omega_I + \omega_S)\right], \tag{2.78}$$

with ω_I and ω_S the proton and electron Larmor frequencies, n_m the spin density of the paramagnetic molecules and N_a the Avogadro number, a is the effective distance between the electron and proton spins and D is the effective diffusion coefficient given by the sum of the diffusion coefficients of both species ($D = D_I + D_S$).

The spectral densities j_k are given by:

$$j_k(\omega) = \frac{9}{4}Re\left\{\frac{4 + z_k}{9 + 9z_k + 4z_k^2 + z_k^3}\right\}, \tag{2.79}$$

with

$$z_k = \sqrt{i\omega\tau_D + \tau_D/T_{ke}}. \tag{2.80}$$

The diffusion correlation time τ_D satisfies $\tau_D = a^2/D$ and T_{ke} is the electronic relaxation time given by (2.76) and (2.77) following the same assumption of extreme narrowing. These expressions for the spectral densities are not unique though, and alternative expressions can be found in [30].

2.7 Experimental Methods

The samples used in this work were prepared at the Faculdade de Ciências e Tecnologia - UNL and at the Faculdade de Farmácia - UL using a procedure described in references [31, 32].

The experimental techniques used in this work were NMR relaxometry, NMR diffusometry and X-ray diffractometry. NMR relaxometry forms the experimental core of this work, since all the models used to predict the microscopic dynamics of the system are made to fit the relaxometry curves obtained from this method. The great amount of parameters used in the models required the use of other experimental techniques in order to fix parameters. NMR diffusometry was helpful to determine diffusion coefficients, while X-ray diffractometry provided estimates on molecular sizes and intermolecular characteristic distances.

These techniques will be discussed in detail on the following sections.

2.7.1 NMR relaxometry

In order to cover as much of the frequency spectrum as possible, three different magnets were used, a home developed desktop low field spectrometer [33] that can measure T_1 for proton Larmor frequencies ranging from 10 KHz to 9 MHz, a medium field iron core electromagnet *Bruker BE-30* capable of probing fields from 9 MHz to 90.5 MHz and a *Bruker Widebore* superconducting magnet that operates at 7T (300 MHz) controlled by an *Avance II* NMR console. These magnets are on display in figures 2.3, 2.4 and 2.5.

Due to the fact that the signal to noise ratio (SNR) varies with approximately $B^{3/2}$, low fields have increasing noise. In order to avoid that, the low field spectrometer uses a different kind of technique called fast field cycling (FFC) and can be referred to as an FFC spectrometer.

Figure 2.3: FFC spectrometer used for low field measurements.

Figure 2.4: Electromagnet used for medium field measurements.

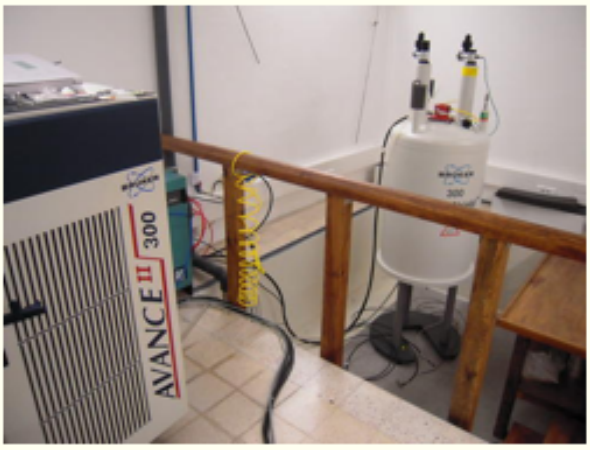

Figure 2.5: Superconducting magnet used for $B = 7T$.

The technique used for medium and high magnetic fields was an inversion recovery technique. It consists on applying an initial π pulse, therefore inverting the direction of the magnetization, letting it evolve for a time τ and then applying a $\pi/2$ pulse that rotates the magnetization to the $x - y$ plane, where it can be measured. Figure 2.6 shows a scheme of such an experiment.

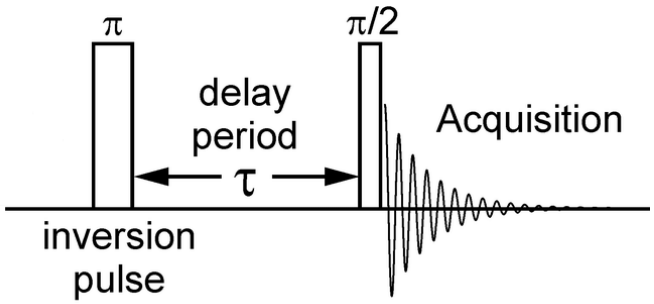

Figure 2.6: Inversion recovery experiment scheme.

It is done for several values of τ, at which point one has experimental data to adjust. A typical curve is shown in figure 2.7. If it is mono-exponential, a relaxation rate (T_1) can be obtained for that field:

$$I = I_0 \left(1 - 2exp\left(-\frac{\tau}{T_1}\right)\right) + (I_{inf} - I_0). \tag{2.81}$$

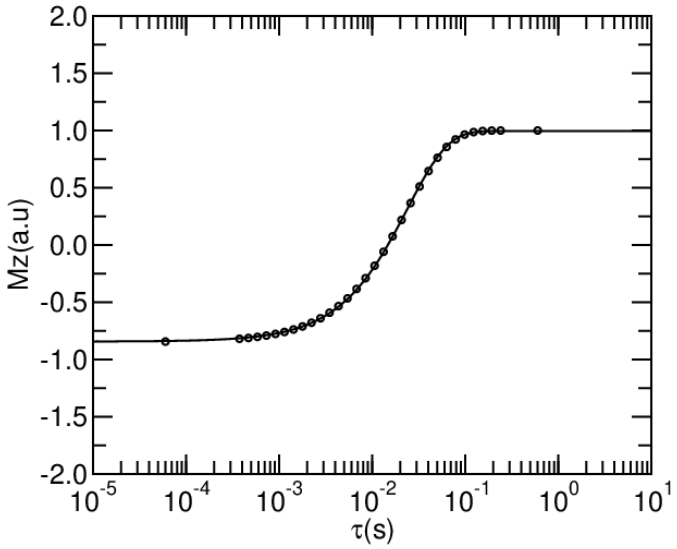

Figure 2.7: Example of an inversion recovery experimental curve.

For the case of the FFC technique, there is no inversion pulse applied. Instead, a relatively high magnetic field (called the polarization field, B_p) is applied, allowing the sample to reach an equilibrium magnetization in that field. The field is then switched to a lower field (the evolution field, B_e), where the magnetization will evolve for a time τ, only to be switched to another higher field (the detection field, B_d) from where the magnetization, still in the z-axis, immediately receives a $\pi/2$ pulse in order to be measured. A scheme of the FFC experiment is displayed in figure 2.8. The fact that the measurement is made at an higher field circumvents the SNR problem, which was the objective. This technique then goes through multiple values of τ which will give the experimental data needed to obtain the relaxation rate for the low magnetic field considered. The switching of the fields has a time on the order of miliseconds (typically between 2.5 and 3 miliseconds), which makes this technique unviable for relaxation times in that vicinity (or smaller). The relaxation rate will be given by the fitting of the function:

$$I = I_0 exp\left(-\frac{\tau}{T_1}\right) + C, \tag{2.82}$$

where T_1 is the relaxation time for $B = B_e$.

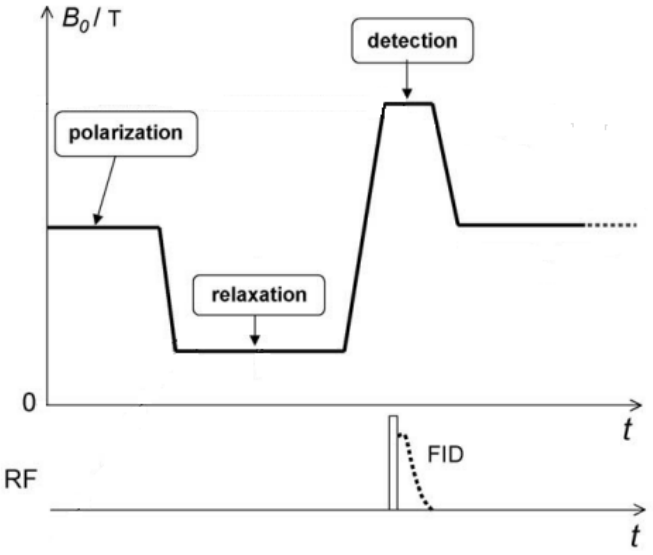

Figure 2.8: FFC experiment scheme [34].

For both FFC and inversion recovery techniques, there is a need to let the magnetization reach an equilibrium value before repeating the measurement for another τ. The waiting time used for all our experiments was at least $5T_1$ ($5T_1(B_p)$ for the FFC technique).

2.7.2 NMR diffusometry

Diffusion measurements were conducted at the CENIMAT at FCT/UNL using a 7T (300MHz) superconducting magnet with a *Bruker Diff 30* diffusion probe and an *Avance III* NMR console. The technique used to make these measurements is known as pulsed field gradient NMR (PFG). PFG is a more complex form of a Hahn spin-echo pulse sequence [35], this is a $\pi/2$ pulse, followed by some waiting time τ and a π pulse that will, after waiting another time τ, refocus the signal, generating an echo. PFG adds to this Hahn sequence two gradients, one before and another after the π pulse, caracterized by gradient duration δ, gradient intensity g and time between gradients Δ. A scheme of the PFG experiment is shown in figure 2.83.

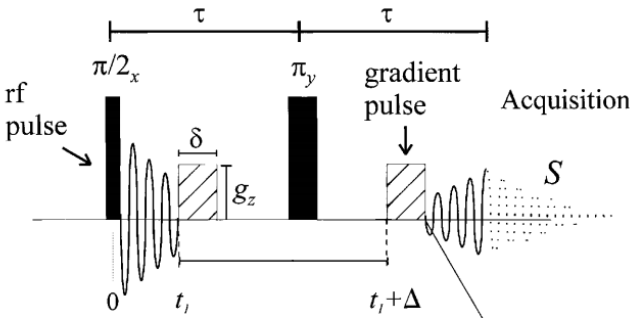

Figure 2.9: PFG visualization (from [36]).

In this specific case, a modified PFG (Pulsed gradient stimulated echo) was used. This technique contains an additional radiofrequency pulse which allows the diffusion time to be limited by T_1 instead of

T_2. The diffusion will attenuate the echo, and the signal is given by [36]:

$$I = I_0 exp\left\{-\gamma_{proton}^2 g^2 D\delta^3 \left(\frac{\Delta}{\delta} - \frac{1}{3}\right)\right\}. \tag{2.83}$$

Choosing the values of δ and Δ carefully, and iterating for different values of g, an experimental curve can be obtained to recover D. An example of such a curve is shown in figure 2.10.

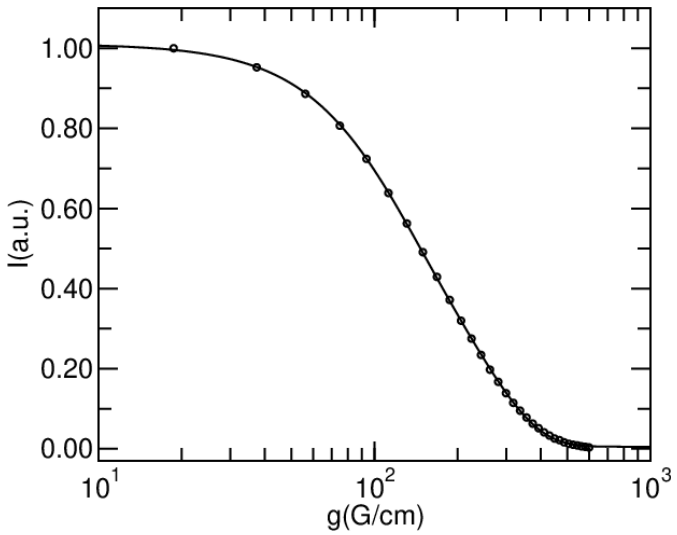

Figure 2.10: Example of a PFG experimental curve.

2.7.3 X-ray diffractometry

X-ray diffractometry measurements were made using the X-ray diffractometer shown in figure 2.11. In these experiments, a sample is placed between an X-ray source and a semi-circular *INEL* gas curved detector. The detector will then provide the angular distribution of the incident radiation intensity. In order to average out possible anisotropies, the sample is rotated at constant angular velocity during the acquisitions.

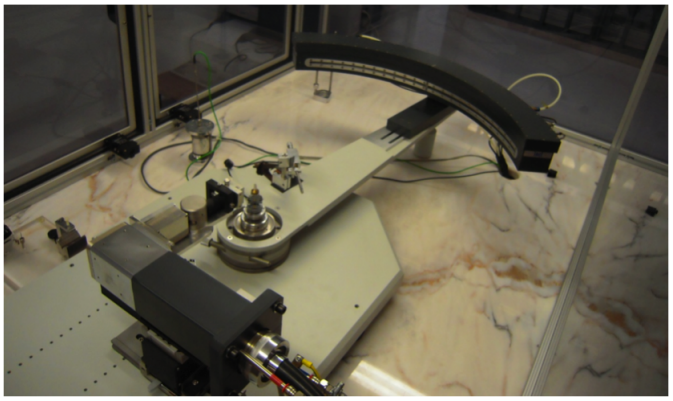

Figure 2.11: X-ray diffractometer used in this work.

This angular distribution of radiation intensity contains information about the microscopic structure of the sample. The Bragg formula for diffraction peaks gives:

$$n\lambda = 2dsin\theta, \tag{2.84}$$

where λ is the wavelenght of the radiation and d is the relevant distance. In the case of crystals, d is the distance between crystallographic planes. In the case of liquid samples such as the ones studied in this work, d is related to the molecular distances. Normally, the experimental data are analysed transforming θ to the reciprocal scale using:

$$q = \frac{4\pi sin(\theta)}{\lambda}. \tag{2.85}$$

While the location of the peaks gives us the repeating distances on the sample, the form of the peaks will also contain information, namely the mean size of the ordered domains in the sample. This is given by the Scherrer equation:

$$L = \frac{\lambda K}{\Delta_{\frac{1}{2}}(2\theta)cos\theta} = \frac{2\pi K}{\Delta_{\frac{1}{2}}(q)}, \tag{2.86}$$

where K is a constant close to unity and $\Delta_{\frac{1}{2}}$ is the full width at half maximum of the adjusting function (FWHM). In this case, a sum of Lorentzian functions was adjusted to the different peaks, and FWHM is the one corresponding to the Lorentzian function of the specific peak.

Chapter 3

Results

3.1 Preface to the analysis

3.1.1 Monoexponential assumption

A NMRD (nuclear magnetic relaxation dispersion) was obtained for each of the samples studied. It is the fit of the models introduced in Chapter 2 to this NMRD that conveys the information we seek about the values of the relevant parameters of the system, which in its turn will allow us to take conclusions about the molecular dynamics in play. Each point of this NMRD is given by a singular inversion recovery or FFC experiment, which provides magnetization data can then be fitted to one or multiple exponential functions, yielding therefore one or more values of T_1 for each Larmor frequency.

In the studies [18–20] which we intend to expand upon, two values of T_1 were obtained for each Larmor frequency, namely a smaller T_{11} associated with the slower movements of the CH_2 protons and a bigger T_{12} associated with the faster movements of the CH_3 protons at the end of the aliphatic chains of the [Aliquat]$^+$ molecule.

These studies detected a bi-exponential decay as well for the 50%(v/v) DMSO samples, both protonated and deuterated, and a monoexponential decay for the 99% (v/v) DMSO-h6. The monoexponential decay for the 99%(v/v) DMSO-h6 was attributed to the fact that most of the magnetization decay of the last sample is associated with the protons of the DMSO, which are expected to display the same average relaxation time for a given frequency. The same was true for the diffusion measurements, which also exhibited bi-exponential behaviour for the 50%(v/v) case and monoexponential for the 99%(v/v) case.

Everything seems therefore consistent with a bi-exponential analysis such as the one used in the aforementioned studies. However, the approach used in this work was to use a monoexponential analysis.

There are two main reasons for this choice. The first one is that the faster times obtained for the relaxation in the FFC frequency range for both 50%(v/v) DMSO samples were smaller than the field switching time of the FFC. This makes a true assessment of these times impossible, since most of the relaxation will occur at a field different than the detection field as it is supposed to happen. The second is that the proportions of each exponential, which were constant at the aforementioned works and that

give meaning to these rates by associating them with specific spin populations were simply not constant. They varied wildly for different frequencies and for each sample. It was possible to fit them at the values used in the aforementioned works, but it provided ineffective fits. Other fixed populations that reflected a different spin population reality were also tried, but they displayed the same problem.

In the end, for these reasons already stated, it was decided that a monoexponential fit was the best approach for this work. This included refitting the data for pure [Aliquat]$^+$ as well as 1%(v/v) and 10%(v/v) DMSO-d6 analysed in [19, 20] using a single exponential for each NMRD point.

These NMRD were all obtained using the same approach and could therefore be compared and fitted together using the *fitteia* software at *fitteia.org*.

The [C_8mim]$^+$ samples were already monoexponential by nature, and therefore can be readily analysed as such. Furthermore, the fact that both analysis are monoexponential allows us to directly compare the NMRD profiles and fitting parameters from both [C_8mim]$^+$ and [Aliquat]$^+$ based samples.

3.1.2 Fixed parameters

The enormous quantity of parameters involved in each NMRD fit made it imperative to obtain some knowledge from independent methods in order to fix some of them. In order to do so, additional sources of information were used, namely X-ray diffractometry and diffusion measurements. Diffusion measurements were made, allowing us to retrieve diffusion coefficients for each sample. These measurements, which were made at a field of 7 T, gave diffusion coefficients who were then fixed for the non-magnetic ionic liquids and that varied accordingly to (2.58) for the magnetic ionic liquids. X-ray diffractometry measurements allowed for knowledge of typical microscopic distances in each mixture. Here, we considered that the average jumping distance in the diffusion model can be estimated from the peak representing the smaller distances in each diffraction profile. Furthermore, the outer-sphere distance parameter was assumed to be one fourth of the longest distances obtained from the X-ray diffraction profiles, roughly corresponding to the distance between the polar region and the center of mass of each cation.

Another parameter that was estimated was the spin density for each sample, a parameter that can be calculated knowing the density (ρ), molecular weight (M_s) and the numbers of protons per molecule. Both ρ and M_s were also fixed, M_s being calculated while ρ was measured gravimetrically using a pycnometer for the samples with 1% (v/v), 10% (v/v) and without DMSO and calculated for the remaining. In the case of a mixture, it also needs to be multiplied by its volume fraction (V_f). In the case of protonated DMSO, one also has to add that contribution. For example, for a mixture of [Aliquat][Cl] with 10% DMSO-d6 (v/v) it is:

$$n_{10DMSO} = 54\frac{0.9\rho N_A}{M_w}, \tag{3.1}$$

since [Aliquat]$^+$ has 54 protons and the volume fraction is 90% (N_A is Avogadro's number).

The parameter A_{rot} that describes the strength of the proton relaxation due to molecular rotations was also calculated by choosing a preferential axis of rotation using a representation of the molecules within the software *Avogadro* [37]. From there, an average effective distance between spins can be

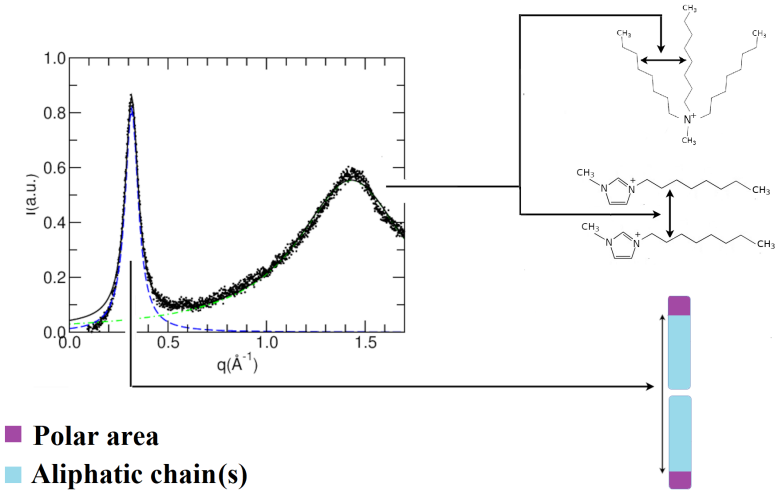

Figure 3.1: Scheme showing the interpretation of the relationship between the X-ray peaks and the distances at the molecular level. The peak on the small angles corresponds to the distance between polar areas of two molecules directly opposing one another (the rectangles represent either an [Aliquat]$^+$ or [C_8mim]$^+$ cation), while the peak on large angles corresponds to the distance between the chains of the cations.

obtained and A_{rot} calculated [38]. The concentration of paramagnetic centers (C) was also fixed. It was measured by inductively coupled plasma for the sample without DMSO, and was measured by flame atomic absorption spectrometry for the samples with 1% (v/v) and 10% (v/v) DMSO, while it was calculated for the remaining samples. It was also assumed that q, the number of molecules participating in the inner sphere mechanism per paramagnetic center was constant and equal to 1. The fraction of proton spins per molecule interacting by inner sphere (F) was constant for a given species, namely $\frac{9}{54}$ for the [Aliquat]$^+$ ion and $\frac{8}{23}$ for the [C_8mim]$^+$ ion, corresponding to the hydrogen protons in the immediate vicinity of the paramagnetic species (namely, those close to the polar regions). Lastly, the paramagnetic spin S of the [$FeCl_4$]$^-$ ion is constant and equal to 2.5.

3.1.3 Contact coupling and τ_m hypothesis

The inner sphere mechanism is caracterized by two kinds of relaxation inducing couplings, the dipolar coupling and the contact coupling between two spins (see equations 2.73 to 2.76). The contact coupling demands that both spins, in this case one of the unpaired electronic spins of [$FeCl_4$]$^-$ ion and a proton from the respective cation are in close proximity. Since the fits were sucessfully performed in the absence of the contact interaction, we saw no need to add yet another parameter to the set of parameters. The fact that it can be approximately zero also seems plausible due to the fact that the outside Cl atoms should shield any nearby protons from direct contact with the Fe atom.

There were two parameters which, while belonging to two different mechanisms, were considered to be correlated. These are τ_m and D_{an}, the exchange time of the inner sphere interaction and the diffusion of the anion. It was considered that diffusion of the anion occurs by discrete events with an average time between them equal to τ_m. That is, the anion diffuses together with the cation for a time τ_m, then it breaks out from the electrostatic interaction and diffuses with constant D_{an} until it settles on

another cation's vicinity. This diffusion by random jumps has an average jump distance relation that is similar to the Torrey model, i.e.:

$$\langle r^2 \rangle = n_d \tau_m D_{an}, \tag{3.2}$$

where n_d is a constant that depends on the dimensionality of the diffusion, being $n_d = 6$ for three dimensional diffusion, $n_d = 4$ for two dimensional diffusion and $n_d = 2$ for one dimensional diffusion. This implies that τ_m can be described completely in terms of D_{an} by:

$$\tau_m = \frac{\langle r^2 \rangle}{n_d D_{an}}, \tag{3.3}$$

as long as n_d and $\langle r^2 \rangle$ is given.

For the [Aliquat]$^+$ samples, it was reasoned that the average distance travelled would be the average distance between two contiguous polar regions of the [Aliquat]$^+$ ion, which is roughly equal to two times the distance between [Aliquat]$^+$ aliphatic chains. This distance is the distance given by the X-ray diffraction measurements for the peak in the larger angles, which is referred here as d_{ch}. Since the polar regions of the [Aliquat]$^+$ ions define a layer or region with a small thickness, the diffusivity was considered to be two-dimensional, and therefore $n_d = 4$. Then, for all [Aliquat]$^+$ based samples, the relationship used was:

$$\tau_m = \frac{2d_{ch}2d_{ch}}{4D_{an}} = \frac{d_{ch}^2}{D_{an}}. \tag{3.4}$$

This relationship generated τ_m values similar to the ones obtained in a fit without this restriction, and therefore seems to be valid for the [Aliquat]$^+$ based samples.

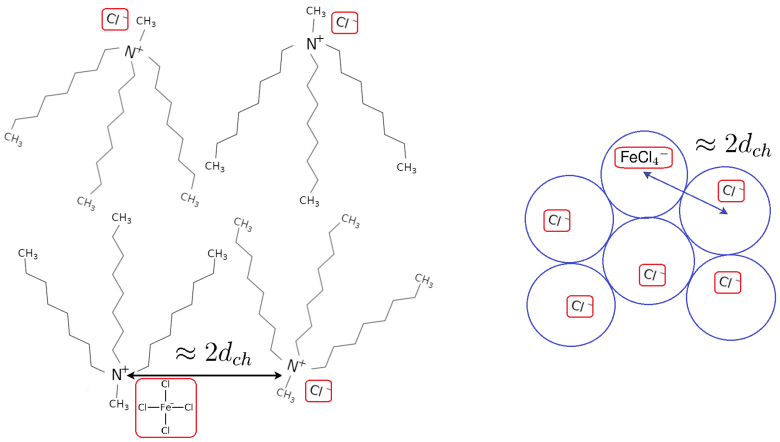

Figure 3.2: Illustration of the distance between polar areas of the [Aliquat]$^+$ ions, which is equal to approximately $2d_{ch}$. The right part of the image is a cross section of the [Aliquat]$^+$ ions viewed in the direction of the aliphatic chains (in blue).

For the [C_8mim]$^+$ sample case, the same approach was used. However, since the [C_8mim]$^+$ ion only

has one aliphatic chain, the average distance between two contiguous polar regions of $[C_8mim]^+$ ions is now equal to the distance between $[C_8mim]^+$ aliphatic chains (while it was twice that in the $[Aliquat]^+$ case). The reasoning for the diffusivity is the same as the $[Aliquat]^+$ case, being the case that its polar regions also form a surface, and therefore the following formula should apply:

$$\tau_m = \frac{d_{ch} d_{ch}}{4D_{an}} = \frac{d_{ch}^2}{4D_{an}}. \tag{3.5}$$

However, this formula did not actually accurately represent the experimental data. It was found that a formula like (3.4), that does not have a factor of 4 in the denominator, was more accurate in describing the experimental data.

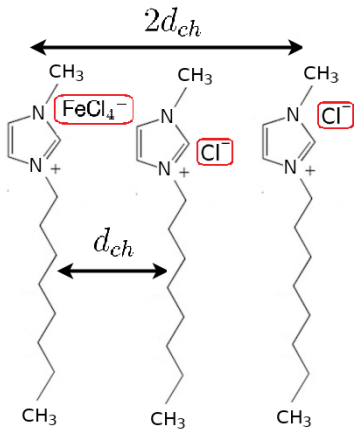

Figure 3.3: Illustration of the distance between polar areas of the $[C_8mim]^+$ ions, which is equal to approximately d_{ch}. However, $[FeCl_4]^-$ ions seem to diffuse on average $2d_{ch}$.

This seems to imply that the diffusion process is not to the closest neighbour, but that it instead diffuses on average twice as much, to the second neighbour. There is, however, the alternative possibility that the diffusion process is not two-dimensional. This would still give average diffusion distances bigger than the distance between polar regions, around $\sqrt{2}d_{ch}$ for one-dimensional diffusion and $\sqrt{6}d_{ch}$ for three dimensional diffusion.

3.2 $[Aliquat]^+$ based ionic liquids

The basis of the $[Aliquat]^+$ based ionic liquid mixtures used in this work is the $[Aliquat]^+$ ion. This cation is represented in Figure 1.5. It is constituted by three distinct chains uniting in an nitrogen atom also connected to a methyl group. The excess charge of this cation is located around the nitrogen. Its chemical formula is $C_{25}H_{54}N^+$, whence it can be seen that it has 54 protons.

The two anions used in these samples were $[Cl]^-$ and $[FeCl_4]^-$. For the paramagnetic mixtures, a fixed 1%(v/v) of $[Aliquat][FeCl_4]$ was used (the rest being $[Aliquat][Cl]$ and DMSO).

The solvent used in these samples, DMSO, is represented in Figure 1.7. Its chemical formula is C_2H_6OS. When mention is made to deuterated DMSO, it is meant that all six protons are substituted by

deuterium (also called DMSO-d6 for brevity). Protonated DMSO only has common hydrogen (protium), and can be referred to as DMSO-h6 for brevity.

3.2.1 Experimental results

In this section the experimental results will be presented. For the sake of consistency, the results will be presented starting from the samples with lower DMSO concentrations and finishing on the sample with the most (to conserve space, only the name of the relevant MIL is shown in the title of its corresponding section). The X-ray diffraction spectra are shown first, highlighting the relevant distances for each mixture. Afterwards, the full NMRD results are shown pairwise, one for the sample with 1% [Aliquat][$FeCl_4$] and one for its counterpart without it. It makes sense to do so since the parameters regarding non-paramagnetic relaxation were assumed to be constant for both samples, and were obtained from the sample without [Aliquat][$FeCl_4$] . For the paramagnetic mixture, the sum of these non-paramagnetic contributions is displayed as a single curve named "Bulk", in order to not distract from the most important contribution, the paramagnetic relaxation.

q	1
F	$\frac{9}{54}$
S	2.5

Table 3.1: Parameters that were the same for all [Aliquat]$^+$ samples.

The NMRD fits were not performed individually. Instead, a global fit was performed for two groups of experimental data, the group of samples without [Aliquat][$FeCl_4$] and the group of samples with [Aliquat][$FeCl_4$] . The pdf reports for both these global adjustments are displayed in Appendix A. This approach has the benefit of allowing us to assign the same value to parameters thought to be common to multiple samples, thereby reducing the complexity of the analysis in a system of many parameters. The most notable difference was evident for the group of magnetic samples, in which after individual fits displayed similar Δ values for all individual deuterated DMSO samples, a single Δ was used.

3.2.1.1 99% (v/v) [Aliquat][Cl] + 1% (v/v) [Aliquat][$FeCl_4$]

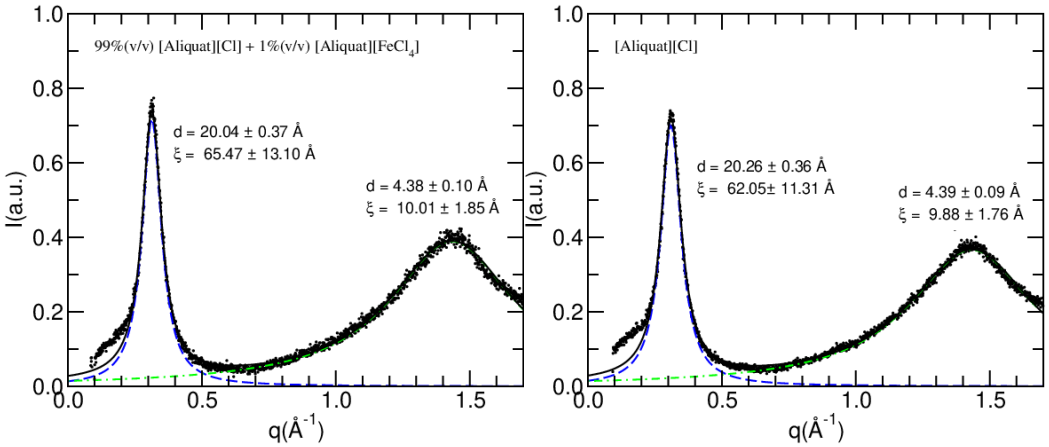

Figure 3.4: X-ray diffractometry spectra obtained for pure [Aliquat]$^+$ mixtures at 25ºC (without any DMSO present). The left image is the spectrum obtained for the relevant MIL, which contains an additional 1% (v/v) [Aliquat][$FeCl_4$] .

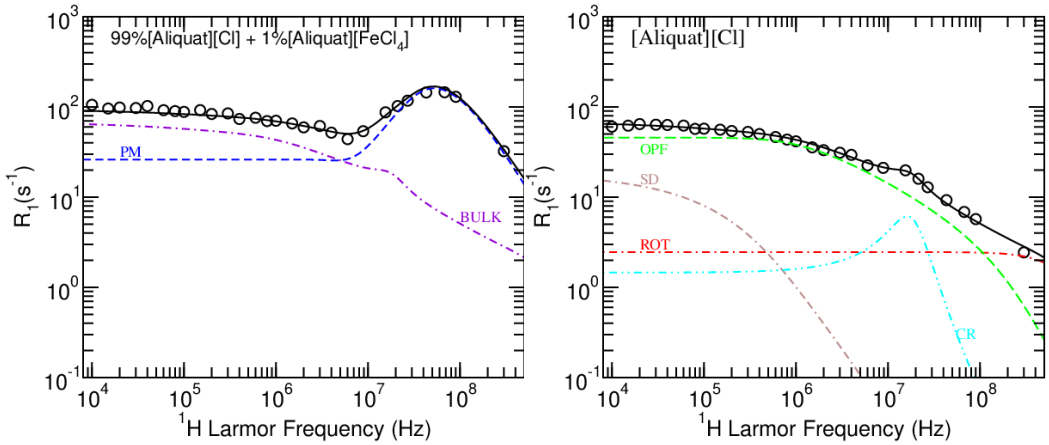

Figure 3.5: Relaxation rate dependence on the proton Larmor frequency obtained for pure [Aliquat]$^+$ mixtures at 25ºC (without any DMSO present). The left image is the relevant MIL, which contains an additional 1% (v/v) [Aliquat][$FeCl_4$] .

Parameters	[Aliquat][Cl]	99% (v/v) [Aliquat][Cl] + 1% (v/v) [Aliquat][$FeCl_4$]
τ_{rot}(10^{-11} s)	10 ± 1	
D_{IL} (10^{-12} m^2s^{-1})	2 ± 2	-
D_{MIL} (10^{-12} m^2s^{-1})	-	5 ± 5
r(10^{-10} m)	$4\ ^{+30}_{-4}$	
d(10^{-10} m)	19 ± 2	
A_{opf}(10^4 $s^{-\frac{3}{2}}$)	6.4 ± 0.2	
f_{min}(10^5 s^{-1})	6.9 ± 0.5	
f_{max}(10^8 s^{-1})	2.6 ± 0.5	
A_{CR}(10^7 s^{-2})	6 ± 1	
τ_{CR}(10^{-7} s)	1.1 ± 0.4	
f_{CR}(10^7 s^{-1})	1.6 ± 0.3	
Δ(10^{10} s^{-1})	-	1.07 ± 0.01
D_{an} (10^{-10} m^2s^{-1})	-	0.8 ± 0.2
d_{out}(10^{-10} m)	-	6.4 ± 0.2
τ_v(10^{-11} s)	-	2.9 ± 0.2
τ_{ISRot}(10^{-9} s)	-	5 ± 2
d_{in}(10^{-10} m)	-	4.53 ± 0.06

Table 3.2: Parameters obtained for [Aliquat][Cl] and [Aliquat][$FeCl_4$] mixtures without DMSO at 25ºC. Additional parameters common to both systems not obtained by the fitting of the NMRD: $n = 7.1 \times 10^{22}$ cm^{-3} (*); $\rho = 1.03$ kg dm^{-3}; $M_s = 0.4$ kg mol^{-1} (*); $C = 12$ mmol dm^{-3}; $A_{rot} = 5 \times 10^9$ s^{-2} (*). Calculated values are followed by (*).

3.2.1.2 98% (v/v) [Aliquat][Cl] + 1% (v/v) [Aliquat][$FeCl_4$] + 1%(v/v) DMSO-d6

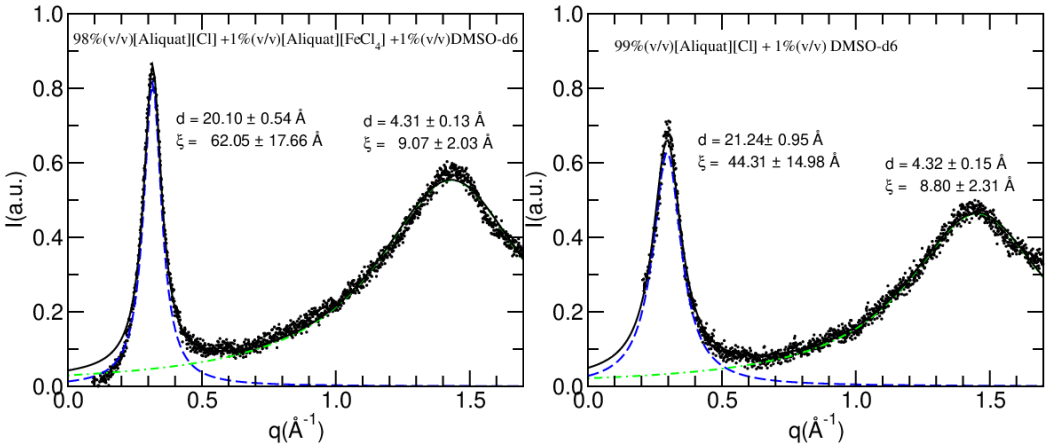

Figure 3.6: X-ray diffractometry spectra obtained for 1% (v/v) deuterated DMSO and $[Aliquat]^+$ mixtures at 25ºC. The left image is the spectrum obtained for the relevant MIL, which contains an additional 1% (v/v) [Aliquat][$FeCl_4$] .

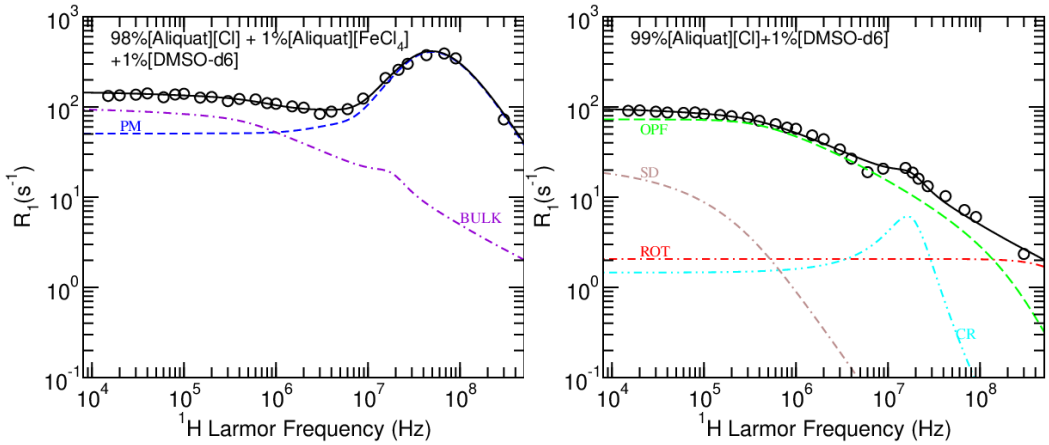

Figure 3.7: Relaxation rate dependence on the proton Larmor frequency obtained for 1% (v/v) deuterated DMSO and $[Aliquat]^+$ mixtures at 25ºC. The left image is the relevant MIL, which contains an additional 1% (v/v) [Aliquat][$FeCl_4$] .

Parameters	99% (v/v) [Aliquat][Cl] +1% (v/v) DMSO-d6	98% (v/v) [Aliquat][Cl] + 1% (v/v) [Aliquat][$FeCl_4$] +1% (v/v) DMSO-d6
τ_{rot}(10^{-11} s)	8 ± 1	
D_{IL} (10^{-12} m^2s^{-1})	1.1 ± 0.2	-
D_{MIL} (10^{-12} m^2s^{-1})	-	1.5 ± 0.4
r(10^{-10} m)	$4\ ^{+30}_{-4}$	
d(10^{-10} m)	19 ± 6	
A_{opf}(10^4 $s^{-\frac{3}{2}}$)	6.6 ± 0.2	
f_{min}(10^5 s^{-1})	3.1 ± 0.3	
f_{max}(10^8 s^{-1})	3.0 ± 0.6	
A_{CR}(10^7 s^{-2})	6 ± 1	
τ_{CR}(10^{-7} s)	1.1 ± 0.4	
f_{CR}(10^7 s^{-1})	1.6 ± 0.3	
Δ(10^{10} s^{-1})	-	1.07 ± 0.01
D_{an} (10^{-10} m^2s^{-1})	-	0.74 ± 0.08
d_{out}(10^{-10} m)	-	5.1 ± 0.2
τ_v(10^{-11} s)	-	3.9 ± 0.3
τ_{ISRot}(10^{-9} s)	-	5 ± 2
d_{in}(10^{-10} m)	-	4.00 ± 0.04

Table 3.3: Parameters obtained for [Aliquat][Cl] and [Aliquat][$FeCl_4$] mixtures with 1% (v/v) DMSO-d6 at 25ºC. Additional parameters common to both systems not obtained by the fitting of the NMRD: $n = 7 \times 10^{22}$ cm^{-3} (*); $\rho = 0.89$ kg dm^{-3}; $M_s = 0.38$ kg mol^{-1} (*); $C = 14.4$ mmol dm^{-3}; $A_{rot} = 5 \times 10^9$ s^{-2} (*). Calculated values are followed by (*).

3.2.1.3 89%(v/v) [Aliquat][Cl] +1%(v/v) [Aliquat][$FeCl_4$] +10%(v/v) DMSO-d6

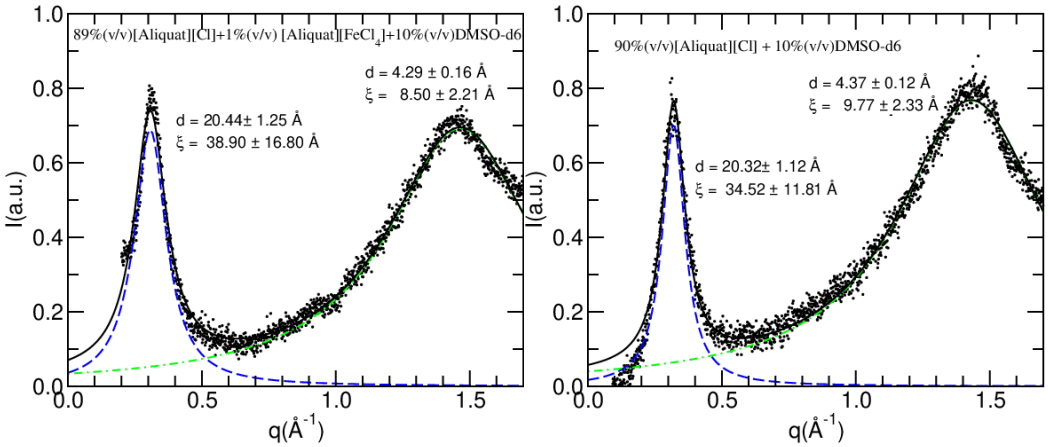

Figure 3.8: X-ray diffractometry spectra obtained for 10% (v/v) deuterated DMSO and $[Aliquat]^+$ mixtures at 25ºC. The left image is the spectrum obtained for the relevant MIL, which contains an additional 1% (v/v) [Aliquat][$FeCl_4$] .

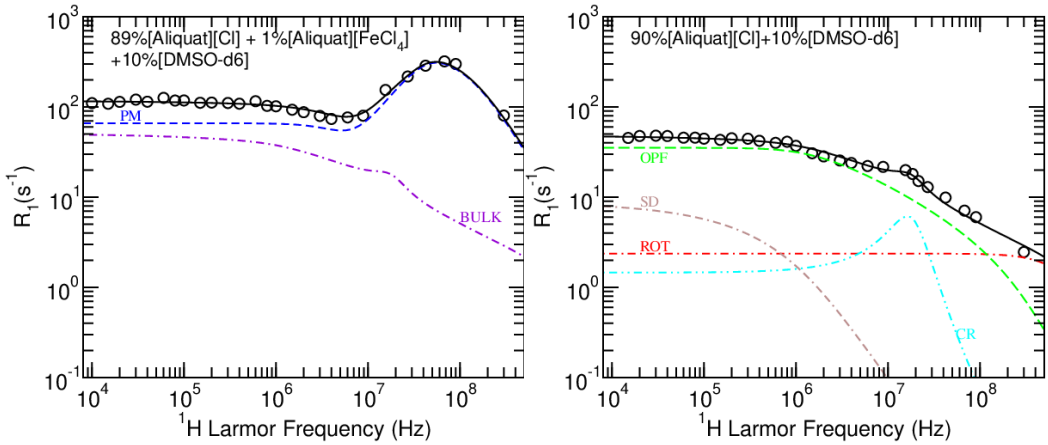

Figure 3.9: Relaxation rate dependence on the proton Larmor frequency obtained for 10% (v/v) deuterated DMSO and $[Aliquat]^+$ mixtures at 25ºC. The left image is the relevant MIL, which contains an additional 1% (v/v) [Aliquat][$FeCl_4$] .

Parameters	90% (v/v) [Aliquat][Cl] +10% (v/v) DMSO-d6	89% (v/v) [Aliquat][Cl] + 1% (v/v) [Aliquat][$FeCl_4$] +10% (v/v) DMSO-d6
τ_{rot}(10^{-11} s)	9 ± 1	
D_{IL} (10^{-12} m^2s^{-1})	3.28 ± 0.07	-
D_{MIL} (10^{-12} m^2s^{-1})	-	3.70 ± 0.06
r(10^{-10} m)	$4^{\pm 5}_{-4}$	
d(10^{-10} m)	16 ± 2	
A_{opf}(10^4 $s^{-\frac{3}{2}}$)	5.9 ± 0.2	
f_{min}(10^5 s^{-1})	9.7 ± 0.7	
f_{max}(10^8 s^{-1})	3.4 ± 0.7	
A_{CR}(10^7 s^{-2})	5.6 ± 0.9	
τ_{CR}(10^{-7} s)	1.1 ± 0.3	
f_{CR}(10^7 s^{-1})	1.6 ± 0.2	
Δ(10^{10} s^{-1})	-	1.07 ± 0.01
D_{an} (10^{-10} m^2s^{-1})	-	0.52 ± 0.08
d_{out}(10^{-10} m)	-	5.18 ± 0.08
τ_v(10^{-11} s)	-	2.5 ± 0.2
τ_{ISRot}(10^{-9} s)	-	1.7 ± 0.5
d_{in}(10^{-10} m)	-	4.00 ± 0.04

Table 3.4: Parameters obtained for [Aliquat][Cl] and [Aliquat][$FeCl_4$] mixtures with 10% (v/v) DMSO-d6 at 25ºC. Additional parameters common to both systems not obtained by the fitting of the NMRD: $n = 6.4 \times 10^{22}$ cm^{-3} (*); $\rho = 0.92$ kg dm^{-3}; $M_s = 0.27$ kg mol^{-1} (*); $C = 14.7$ mmol dm^{-3}; $A_{rot} = 5 \times 10^9$ s^{-2} (*). Calculated values are followed by (*).

3.2.1.4 49% (v/v) [Aliquat][Cl] +1%(v/v) [Aliquat][$FeCl_4$] +50%(v/v) DMSO-d6

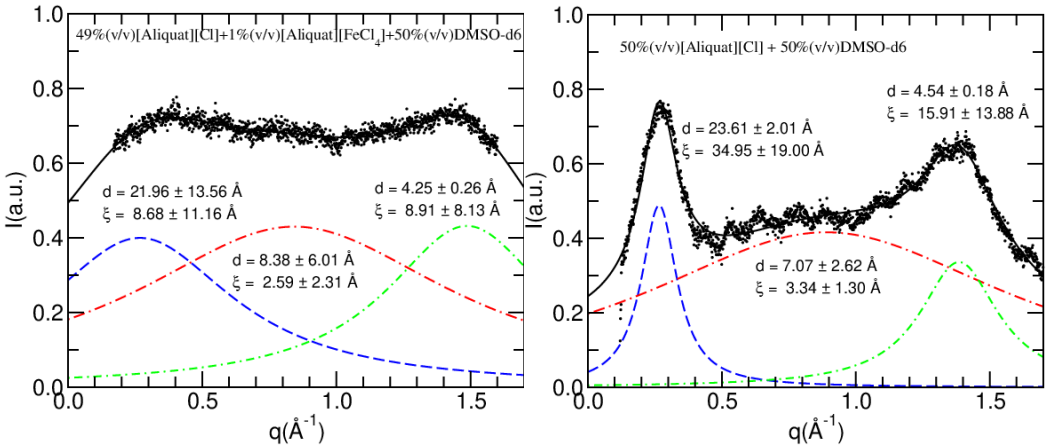

Figure 3.10: X-ray diffractometry spectra obtained for 50% (v/v) deuterated DMSO and $[Aliquat]^+$ mixtures at 25ºC. The left image is the spectrum obtained for the relevant MIL, which contains an additional 1% (v/v) [Aliquat][$FeCl_4$] .

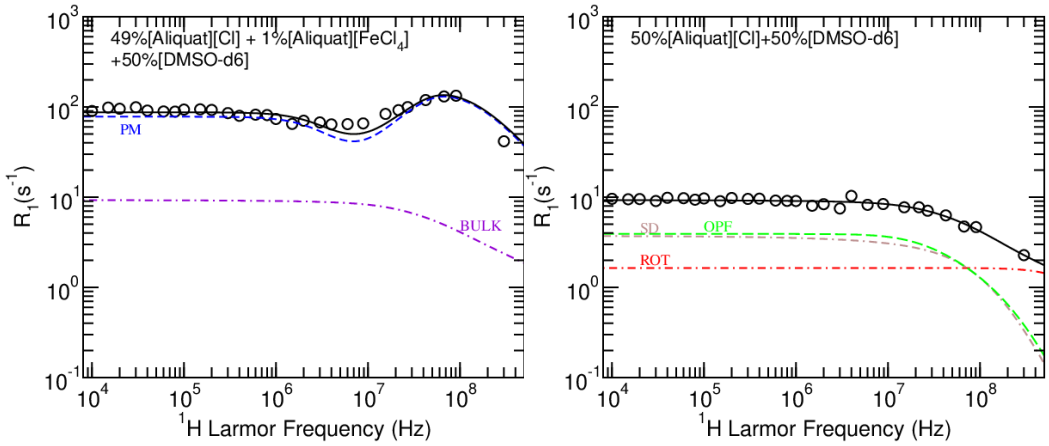

Figure 3.11: Relaxation rate dependence on the proton Larmor frequency obtained for 50% (v/v) deuterated DMSO and $[Aliquat]^+$ mixtures at 25ºC. The left image is the relevant MIL, which contains an additional 1% (v/v) [Aliquat][$FeCl_4$] .

Parameters	50% (v/v) [Aliquat][Cl] +50% (v/v) DMSO-d6	49% (v/v) [Aliquat][Cl] + 1% (v/v) [Aliquat][$FeCl_4$] +50% (v/v) DMSO-d6
τ_{rot}(10^{-11} s)	6.6 ± 0.6	
D_{IL} (10^{-12} m^2s^{-1})	$30\ ^{+40}_{-30}$	-
D_{MIL} (10^{-12} m^2s^{-1})	-	70 ± 20
r(10^{-10} m)	4.3 ± 0.3	
d(10^{-10} m)	3.44 ± 0.09	
A_{opf}(10^4 $s^{-\frac{3}{2}}$)	3.1 ± 0.2	
f_{min}(10^5 s^{-1})	140 ± 20	
f_{max}(10^8 s^{-1})	3.5 ± 0.9	
Δ(10^{10} s^{-1})	-	1.07 ± 0.01
D_{an} (10^{-10} m^2s^{-1})	-	0.98 ± 0.09
d_{out}(10^{-10} m)	-	4.64 ± 0.05
τ_v(10^{-11} s)	-	1.41 ± 0.04
τ_{ISRot}(10^{-9} s)	-	$1\ ^{+4}_{-1}$
d_{in}(10^{-10} m)	-	4.00 ± 0.06

Table 3.5: Parameters obtained for [Aliquat][Cl] and [Aliquat][$FeCl_4$] mixtures with 50% (v/v) DMSO-d6 at 25ºC. Additional parameters common to both systems not obtained by the fitting of the NMRD: $n = 3.54 \times 10^{22}$ cm^{-3} (*); $\rho = 1.04$ kg dm^{-3}(*); $M_s = 0.13$ kg mol^{-1} (*); $C = 12$ mmol dm^{-3}(*); $A_{rot} = 5 \times 10^9$ s^{-2} (*). Calculated values are followed by (*).

3.2.1.5 49%(v/v) [Aliquat][Cl] +1%(v/v) [Aliquat][$FeCl_4$] +50%(v/v) DMSO-h6

The x-ray obtained for the 50 % (v/v) deuterated DMSO pair of samples was also used for this pair of samples. This is an approximation which was considered plausible due to the fact that the typical distances of consideration should not be greatly affected by a small change of molecular weight of the DMSO molecule.

The connection between the paramagnetic curves of both deuterated and protonated DMSO samples was made through the use of two constants, K for the inner sphere and G for the outer sphere mechanism.

It was considered that only the [Aliquat]$^+$ protons relax through the inner sphere mechanism, since the rotational correlation only exists between the [Aliquat]$^+$ and [$FeCl_4$]$^-$ ions. Therefore, DMSO protons, which relaxation we can now also observe, only take part in the outer sphere mechanism. In order to connect the inner sphere relaxation of both deuterated and protonated DMSO samples, a multiplicative factor K, the fraction of [Aliquat]$^+$ protons in the sample, was calculated, and the inner sphere curve was the one obtained for the deuterated case multiplied by this factor K. Therefore, since all inner sphere parameters are the same, only the K factor will be presented on this table, while the rest of these parameters was presented on the 50% (v/v) DMSO-d6 table and can therefore be omitted from this one.

$$R_{1IS}^{50\%DMSO-h6} = R_{1IS}^{50\%DMSO-d6} \times K \tag{3.6}$$

Regarding the outer sphere mechanism, analysis of the fits for 99 %(v/v) DMSO-h6 made it apparent that its Δ had to be significantly different from the rest of the samples containing deuterated DMSO. This fact can be explained if the [$FeCl_4$]$^-$ are solvated by DMSO at high concentrations of this solvent. Since at 99 %(v/v) DMSO-h6 we almost only observe DMSO protons, we are bound to see most of the outer sphere relaxation of this protons while [$FeCl_4$]$^-$ is in this solvated state, while for lower, deuterated DMSO concentrations we only observe the [Aliquat]$^+$ protons' outer sphere relaxation, which only happens in a significant manner for instances where the [$FeCl_4$]$^-$ ion is close to the [Aliquat]$^+$ protons. This train of thought shows that in the 50 %(v/v) protonated DMSO samples, in which there is a high DMSO concentration and we observe both [Aliquat]$^+$ and DMSO protons' relaxation, we should see both outer sphere contributions, both for the solvated and the non-solvated [$FeCl_4$]$^-$ ions. Therefore, this reasoning led us to estimate the outer sphere contribution of this samples as a sum of the outer sphere relaxation of the 50 %(v/v) DMSO-d6 and the 99 %(v/v) DMSO-h6 samples, weighted by a factor G which roughly expresses this solvation and is therefore called the solvation factor. Therefore, since the outer sphere parameters are presented in the 50% (v/v) deuterated DMSO and 99 % (v/v) DMSO-h6 samples tables, only the G factor will be presented on this table (aside from the outer sphere distances, which were allowed to vary).

$$R_{1OS}^{50\%DMSO-h6} = R_{1OS}^{99\%DMSO-h6} \times G + R_{1OS}^{50\%DMSO-d6} \times (1-G) \tag{3.7}$$

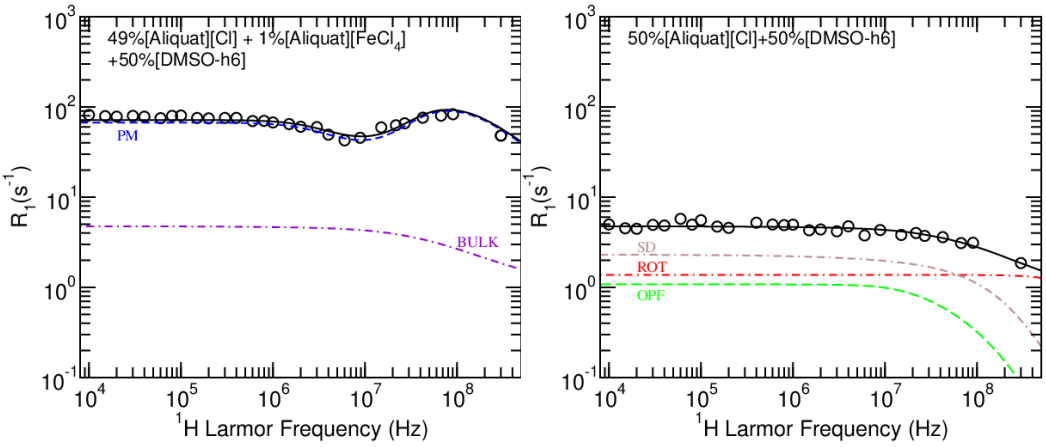

Figure 3.12: Relaxation rate dependence on the proton Larmor frequency obtained for 50% (v/v) protonated DMSO and $[Aliquat]^+$ mixtures at 25ºC. The left image is the relevant MIL, which contains an additional 1% (v/v) $[Aliquat][FeCl_4]$.

Parameters	50% (v/v) [Aliquat][Cl] +50% (v/v) DMSO-h6	49% (v/v) [Aliquat][Cl] + 1% (v/v) [Aliquat][$FeCl_4$] +50% (v/v) DMSO-h6
G	-	0.34 ± 0.05
τ_{rot}(10^{-11} s)	4.9 ± 0.3	
D_{IL} (10^{-12} m^2s^{-1})	$70\ ^{+90}_{-70}$	-
D_{MIL} (10^{-12} m^2s^{-1})	-	124 ± 113
r(10^{-10} m)	4.3 ± 0.3	
d(10^{-10} m)	4.05 ± 0.09	
A_{opf}(10^4 $s^{-\frac{3}{2}}$)	0.84 ± 0.08	
f_{min}(10^5 s^{-1})	129 ± 20	
f_{max}(10^8 s^{-1})	3 ± 2	
d_{Outer1}(10^{-10} m)	-	5.00 ± 0.09
d_{Outer2}(10^{-10} m)	-	2.88 ± 0.06

Table 3.6: Parameters obtained for [Aliquat][Cl] and [Aliquat][$FeCl_4$] mixtures with 50% (v/v) DMSO-h6 at 25ºC. OS parameters except d_{Outer1} and d_{Outer2} are common to both 50 %(v/v) DMSO-d6 and the 99 %(v/v) DMSO-h6 samples and are present on tables 3.5 and 3.7. IS parameters are the same as for 50 %(v/v) DMSO-d6 and are also present on table 3.5. Additional parameters common to both systems not obtained by the fitting of the NMRD: $n = 6.1 \times 10^{22}$ cm^{-3} (*); $A_{rot} = 5.6 \times 10^9$ s^{-2} (*); $K = 0.65$ (*). Calculated values are followed by (*).

3.2.1.6 1%(v/v) [Aliquat][$FeCl_4$] + 99%(v/v) DMSO-h6

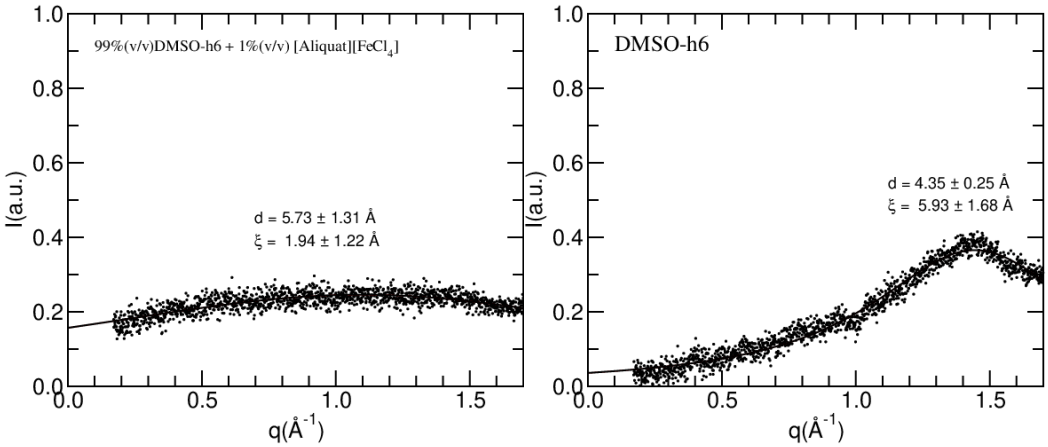

Figure 3.13: X-ray diffractometry spectra obtained for 99% (v/v) protonated DMSO and 1% (v/v) [Aliquat][$FeCl_4$] (left image) and pure DMSO (right image) at 25ºC.

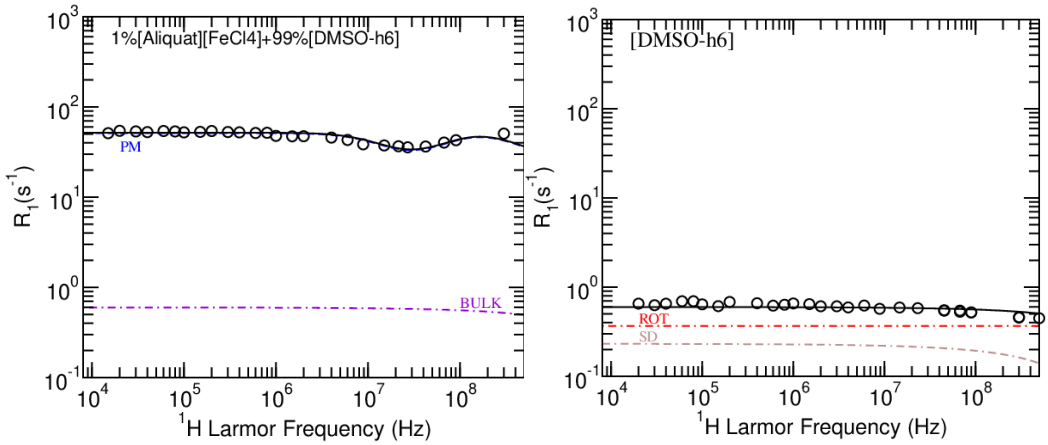

Figure 3.14: Relaxation rate dependence on the proton Larmor frequency obtained for 99% (v/v) protonated DMSO and 1% (v/v) [Aliquat][$FeCl_4$] (left image) and pure DMSO (right image) at 25ºC.

Parameters	DMSO-h6	1% (v/v) [Aliquat][$FeCl_4$] + 99% (v/v) DMSO-h6
τ_{rot}(10^{-11} s)	1.24 $\pm$ 0.03	
D_{IL} (10^{-12} m^{2}s^{-1})	600 $^{+700}_{-600}$	-
D_{MIL} (10^{-12} m^{2}s^{-1})	-	600 $\pm$ 500
r(10^{-10} m)	4 $\pm$ 0.5	
d(10^{-10} m)	4.1 $\pm$ 0.2	
Δ(10^{10} s^{-1})	-	2.68$\pm$ 0.06
D_{an} (10^{-10} m^{2}s^{-1})	-	2.9 $\pm$ 0.3
d_{out}(10^{-10} m)	-	2.88 $\pm$ 0.03
τ_v(10^{-11} s)	-	0.67 $\pm$ 0.03
τ_{ISRot}(10^{-9} s)	-	1 $^{+15}_{-1}$
d_{in}(10^{-10} m)	-	4.0 $\pm$ 0.2

Table 3.7: Parameters obtained for 1%(v/v) [Aliquat][$FeCl_4$] with 99% (v/v) DMSO-h6 and for pure DMSO at 25ºC. Additional parameters common to both systems not obtained by the fitting of the NMRD: $n = 5.12\times10^{22}$ cm^{-3} (*); $\rho = 1.1$ kg dm^{-3}(*); $M_s = 0.08$ kg mol^{-1} (*); $C = 12$ mmol dm^{-3}(*); $A_{rot} = 6.28\times10^{9}$ s^{-2} (*). Calculated values are followed by (*).

3.3 $[C_8mim]^+$ based ionic liquids

$[C_8mim]^+$ based ionic liquids are formed by $[C_8mim]^+$ cations in conjunction with a chosen anion. The anions used for the samples studied are the same as in the [Aliquat]$^+$ studies, namely Cl^- and $[FeCl_4]^-$. The $[C_8mim]^+$ cation is represented in Figure 1.6. This cation is constituted by an aromatic ring (imidazolium) connected to an aliphatic chain with eight carbons on one side and a CH_3 on the opposite side. Its excess positive charge is located at one of the nitrogens of the imidazolium ring. $[C_8mim]^+$ chemical formula is $C_{12}H_{23}N_2^+$, from where it can be seen that it has 23 protons.

3.3.1 Experimental results

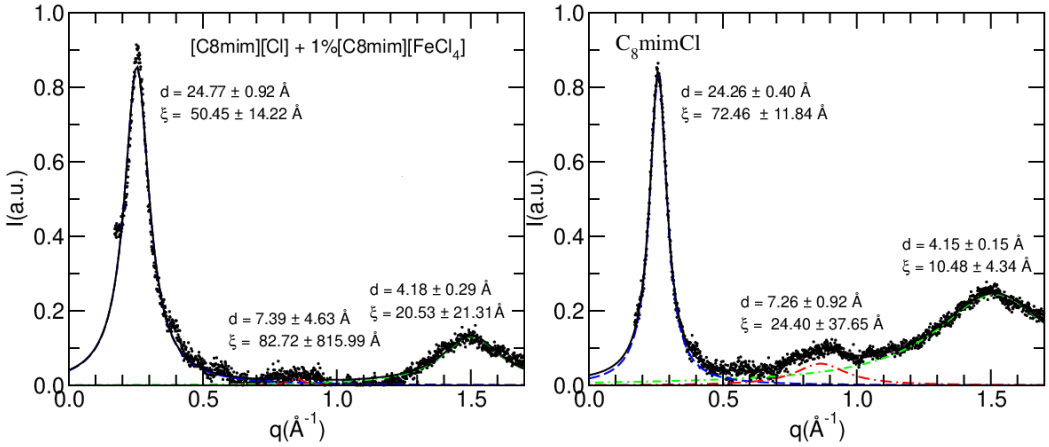

Figure 3.15: X-ray diffractometry spectra obtained for 99% (v/v) $[C_8mim][Cl]$ and 1% (v/v) $[C_8mim][FeCl_4]$ (left image) and pure $[C_8mim][Cl]$ (right image) at 25ºC.

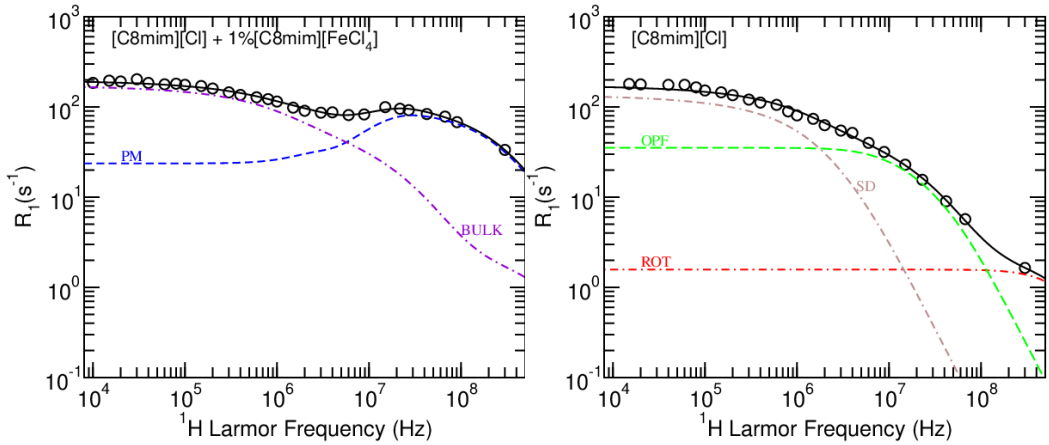

Figure 3.16: Relaxation rate dependence on the proton Larmor frequency obtained for pure $[C_8mim][Cl]$ and $[C_8mim][Cl]$ with 1% (v/v) $[C_8mim][FeCl_4]$ at 25ºC.

Parameters	[C_8mim][Cl]	99% (v/v) [C_8mim][Cl] + 1% (v/v) [C_8mim][$FeCl_4$]
τ_{rot}(10^{-11} s)	11 ± 2	
D_{IL} (10^{-12} m^{2}s^{-1})	$0.7\ ^{+0.8}_{-0.7}$	-
D_{MIL} (10^{-12} m^{2}s^{-1})	-	$10\ ^{+20}_{-10}$
r(10^{-10} m)	4.3 ± 0.3	
d(10^{-10} m)	4.94 ± 0.07	
A_{opf}(10^4 s$^{-\frac{3}{2}}$)	21.5 ± 0.8	
f_{min}(10^5 s^{-1})	56 ± 4	
f_{max}(10^8 s^{-1})	0.55 ± 0.04	
Δ(10^{10} s^{-1})	-	0.62 ± 0.05
D_{an} (10^{-10} m^{2}s^{-1})	-	3.4 ± 0.3
d_{out}(10^{-10} m)	-	7.8 ± 0.3
τ_v(10^{-11} s)	-	7 ± 2
τ_{ISRot}(10^{-9} s)	-	$10\ ^{+50}_{-10}$
d_{in}(10^{-10} m)	-	6.2 ± 0.2

Table 3.8: Parameters obtained for pure [C_8mim][Cl] and [C_8mim][Cl] with 1% (v/v) [C_8mim][$FeCl_4$] at 25ºC. Additional parameters common to both systems not obtained by the fitting of the NMRD: $n = 5.27 \times 10^{22}$ cm^{-3} (*); $\rho = 1.01$ kg dm^{-3}(*); $M_s = 0.23$ kg mol^{-1} (*); $C = 26$ mmol dm^{-3}(*); $A_{rot} = 3 \times 10^9$ s^{-2} (*); $F = \frac{8}{23}$ (*). Calculated values are followed by (*).

Chapter 4

Discussion and Conclusions

4.1 Discussion of the results

In this section the results we obtained will be discussed. For the [Aliquat]$^+$ based samples, the comparison will be made in terms of increasing DMSO percentage. By discussing the behaviour of each parameter with the addition of different quantities of DMSO, we hope to explain the effects caused by its gradual addition. For the [C_8mim]$^+$ samples, we hope to understand what happens to each parameter when the cation is replaced, and therefore a comparison will be made between the [Aliquat]$^+$ samples without DMSO and the [C_8mim]$^+$ samples.

4.1.1 [Aliquat][Cl] samples without $[FeCl_4]^-$

The T_1 relaxation of the magnetic samples is dominated by the paramagnetic mechanisms. In order to understand the other mechanisms at play, which give valuable insight into the dynamical features of the system, non-magnetic samples were analysed.

In figure 4.7 is shown the NMRD for each non-paramagnetic [Aliquat]$^+$ based sample.

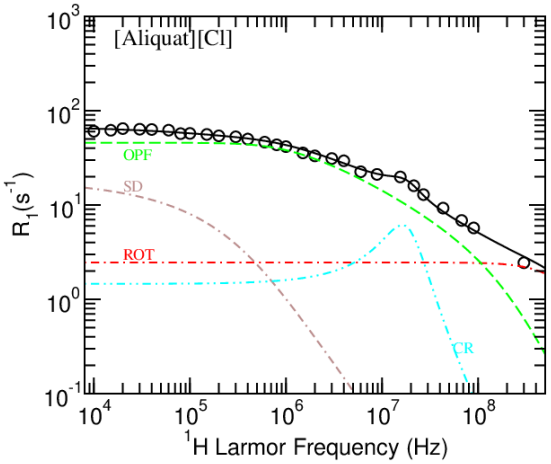

Figure 4.1: 0% DMSO

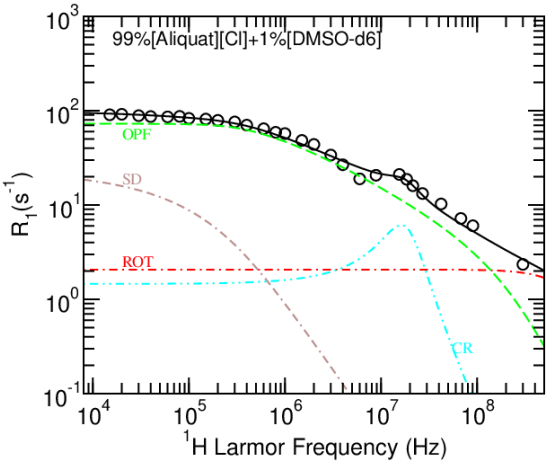

Figure 4.2: 1% DMSO-d6 (v/v)

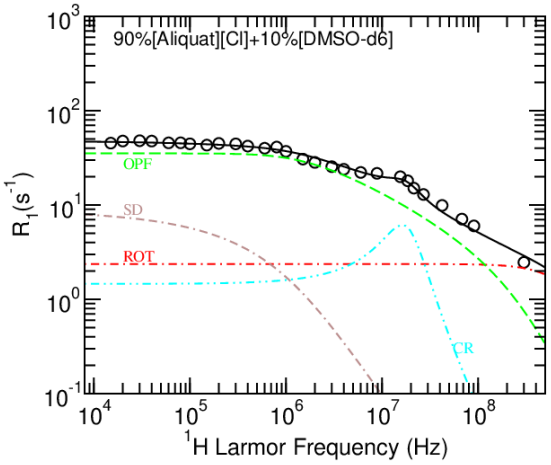

Figure 4.3: 10% DMSO-d6 (v/v)

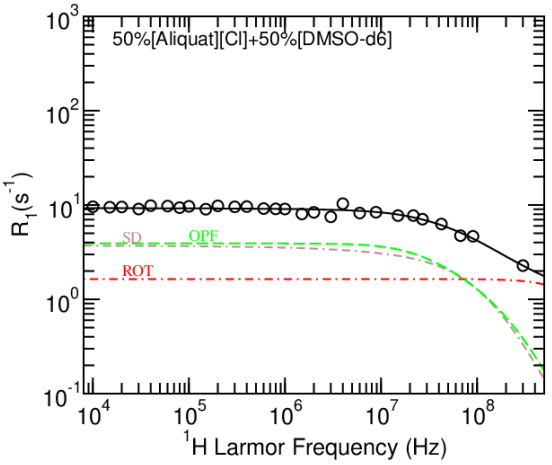

Figure 4.4: 50% DMSO-d6 (v/v)

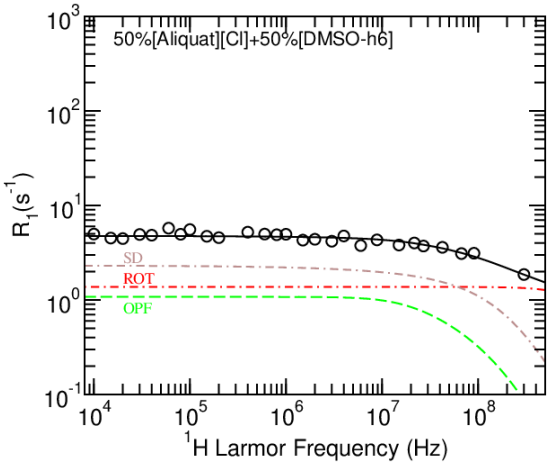

Figure 4.5: 50% DMSO-h6 (v/v)

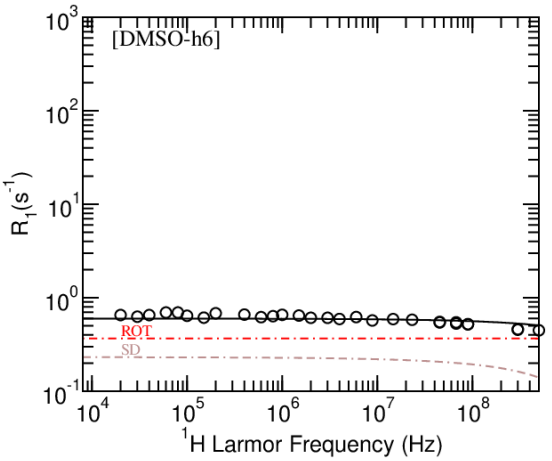

Figure 4.6: 99% DMSO-h6 (v/v)

Figure 4.7: All $[Aliquat]^+$ based non-paramagnetic samples' NMRD (ordered by DMSO percentage).

There were several relaxation mechanisms used in the description of these samples. One describes the rotations, another the diffusional motions, an order parameter fluctuation mechanism for collective motions, and cross relaxation.

- **Rotations**

Of the mechanisms common to all samples, the rotational mechanism has the smallest relaxation contribution, as seen in 4.7. [Aliquat]$^+$ molecules are relatively anisotropic and should therefore, have more than one axis of rotation. However, since it is a relatively weak mechanism, and in order to avoid having multiple rotation relaxation contributions, which would be difficult to distinguish, only one average rotational mechanism was considered. This allows us to have an average rotational correlation time that describes the average rotation of the molecules in the system. The following table compiles the rotational correlation times for the different samples:

DMSO % (v/v)	$\tau_{rot}(10^{-11}$ s)
0 % (d6)	10 ± 1
1 % (d6)	8 ± 1
10 % (d6)	9 ± 1
50 % (d6)	6.6 ± 0.6
50 % (h6)	4.9 ± 0.3
100 % (h6)	1.24 ± 0.03

Table 4.1: Rotational correlation times by sample (ordered by DMSO percentage).

The samples with 0,1 and 10% (v/v) DMSO-d6 seem to have similar correlation times, implying similar average rotation speeds for the [Aliquat]$^+$ molecules in these samples. For bigger concentrations of DMSO, there is a noticeable decrease in rotational correlation times. Since smaller correlation times imply faster rotation, the smaller correlation time for 50% (v/v) DMSO-d6 compared to the samples with less DMSO is evidence for a faster average rotation of [Aliquat]$^+$ molecules with increasing DMSO concentration. There is also a decrease in correlation times from the deuterated to the protonated 50% (v/v) DMSO samples. This is an average of the rotational mechanisms for both [Aliquat]$^+$ and DMSO protons. DMSO itself has a smaller correlation time, as can be seen from the pure DMSO sample, which leads the average correlation time down from the deuterated to the protonated 50% (v/v) DMSO sample. The smaller correlation time for DMSO in relation to [Aliquat]$^+$ is most likely due to its small size, which allows for faster rotation relative to the [Aliquat]$^+$ molecules.

- **Diffusion**

For the diffusion mechanism, there are several relevant parameters. The average jumping distance r was constrained by X-ray diffraction measurements, while the diffusion coefficient was measured through diffusion measurements and the spin density n was calculated. The only parameter re-

maining is the distance of lateral closest approach, d. The following table contains the values obtained for the [Aliquat]$^+$ samples:

DMSO % (v/v)	$d(10^{-10}$ m)
0 % (d6)	19 ± 2
1 % (d6)	19 ± 6
10 % (d6)	16 ± 2
50 % (d6)	3.44 ± 0.09
50 % (h6)	4.05 ± 0.09
100 % (h6)	4.1 ± 0.2

Table 4.2: Distance of lateral closest approach by sample (ordered by DMSO percentage).

There is an enormous difference between the results from 0,1 and 10 % (v/v) DMSO-d6 samples and the other. This seems to be consistent with fundamentally different kinds of diffusion. For the 0,1 and 10% (v/v) DMSO-d6 the distances obtained are consistent with the distances between the center of mass of two contiguous [Aliquat]$^+$ molecules. This suggests that the diffusion is made by the molecule as a whole, and that there is no liberty of motion between the aliphatic chains. For the 50% (v/v) DMSO-d6 case, the distance obtained is consistent with the distance between aliphatic chains, suggesting the the diffusion we indirectly observe is the individual diffusion of each chain. This seems to imply that while small quantities of DMSO do not fundamentally alter the diffusion of [Aliquat]$^+$ molecules, bigger quantities of DMSO free up the individual chains, allowing them to diffuse independently of the main [Aliquat]$^+$ molecule. For the 50% (v/v) DMSO-h6 diffusion we observe a weighted average of the DMSO and the [Aliquat]$^+$ diffusions which seems to be close to the diffusion of pure DMSO.

- **OPF**

The Order Parameter Fluctuation mechanism depends on three parameters, A_{opf}, f_{min} and f_{max}, which are named the OPF prefactor and minimum and maximum cutoff frequency, respectively. Table 4.3 compiles its values for the studied samples:

DMSO % (v/v)	A_{opf}(10^4 $s^{-\frac{3}{2}}$)	f_{max}(10^8 s^{-1})	f_{min}(10^5 s^{-1})
0 % (d6)	6.4 $\pm$ 0.2	2.6 $\pm$ 0.5	6.9 $\pm$ 0.5
1 % (d6)	6.6 $\pm$ 0.2	3.0 $\pm$ 0.6	3.1 $\pm$ 0.3
10 % (d6)	5.9 $\pm$ 0.2	3.4 $\pm$ 0.7	9.7 $\pm$ 0.7
50 % (d6)	3.1 $\pm$ 0.2	3.5 $\pm$ 0.9	140 $\pm$ 20
50 % (h6)	0.84 $\pm$ 0.08	3 $\pm$ 2	129 $\pm$ 20

Table 4.3: OPF mechanism parameters by sample (ordered by DMSO percentage).

Firstly, it is important to note that since the OPF mechanism depends on the establishment of locally ordered domains, it is only relevant when there is an anisometric molecule such as $[Aliquat]^+$ that can generate these domains. As DMSO is a relatively small molecule with small anisometry, this mechanism was not found in the pure DMSO sample.

We start by looking at the A_{opf} values. This parameter exhibits an overall trend of decline with increasing DMSO concentration. Since $A_{opf} \propto \frac{\nu^{1/2}}{L^{3/2}}$, this change can either be from the phenomenological viscosity coefficient ν or from the elastic constant L. While there is no information as to how the elastic constant might change with DMSO concentration, it is known [19] that even small quantities of DMSO decrease the viscosity coefficent of the sample. Since ν will most likely decrease if the sample viscosity decreases, this explains why A_{opf} decreases with DMSO concentration. For the 50% (v/v) DMSO-h6 case, since the OPF mechanism only applies to the $[Aliquat]^+$ protons and both $[Aliquat]^+$ and DMSO protons are now observed, the whole mechanism is now only a fraction of what it was for the deuterated sample and therefore its prefactor (A_{opf}) must decrease.

The second relevant parameter is the maximum cutoff frequency, which appears to be relatively constant for all samples. Since f_{max} is a function of the smallest distance involved in the collective motions, which is the roughly the length of $[Aliquat]^+$ molecule, this was its expected behaviour, as this length should not change much with DMSO concentration.

The last parameter relevant to the OPF mechanism is the minimum cutoff frequency, which is related to the maximum distance involved in the OPF mechanism, increasing as the maximum distance decreases. Both 50% (v/v) DMSO samples give f_{min} values within error of the other, as expected, since there is no fundamental difference in the OPF mechanism's distances for both samples. For the deuterated DMSO samples, there is a notorious increase in f_{min}, with the exception of 1% (v/v). This increase of f_min implies a decrease in the maximum distance for the OPF mechanism with the addition of DMSO, which seems to indicate that the presence of DMSO, for moderate (10% (v/v)) to high (50% (v/v)) concentrations, gradually destroys the long range co-

ordination of [Aliquat]$^+$ molecules. The exception of the 1% (v/v) DMSO case seems to indicate that DMSO, in lower concentrations, actually helps this long range coordination and increases the size of the correlated [Aliquat]$^+$ domains.

- **Order parameter fluctuation and Diffusion - Relative importance**

  The two strongest mechanisms for relaxation in non-magnetic samples are the order parameter fluctuation (also referred to as OPF) and the diffusion. While analysing the experimental data, it was found that it was possible to make each one of these mechanisms dominant over the other. While initially it was reasoned that the diffusion curve should be the dominant one, new data for pure [Aliquat][Cl] samples at different temperatures ([39], displayed in Appendix B) shows that a coherent analysis can only be performed if the OPF mechanism is the dominant one, since it was the only way to ensure that the f_{min} of the OPF mechanism did not decrease with temperature for the [Aliquat][Cl] samples, which would imply that the correlated domains would actually increase in size with temperature, a fact that seems implausible. In light of that new data, the present analysis shown in this work has the OPF mechanism as the dominant one.

- **Cross relaxation**

  Another relatively weak mechanism was cross relaxation. There was evidence for this mechanism in the form of an high frequency peak in the 0, 1 and 10% (v/v) DMSO samples, but not for any other sample. The peaks were all very similar, and consistent with a fit using the same parameters for each sample. The parameters are shown in the following table:

A_{CR}(10^7 s^{-2})	6 ± 1
τ_{CR}(10^{-7} s)	1.1 ± 0.4
f_{CR}(10^7 s^{-1})	1.6 ± 0.3

Table 4.4: Cross relaxation parameters for 0,1 and 10% (v/v) DMSO samples.

4.1.2 [Aliquat][Cl] samples with $[FeCl_4]^-$

For the samples containing $[FeCl_4]^-$, the main pathway for relaxation was paramagnetic relaxation caused by the interaction between $[FeCl_4]^-$ unpaired electrons' spins and individual protons. This interaction can however happen in two different ways, one when the molecule containing the protons diffuses by the $[FeCl_4]^-$ ion, and another where the molecule and the $[FeCl_4]^-$ ion are motionally correlated, rotating together and at a relatively small distance from one another. The first is modelled by the OS model, while the latter is modelled by the IS model. The sum between these two models is the full paramagnetic relaxation.

The fact that both models sum to the total paramagnetic relaxation means that they are competing models, and that changing the parameters of one implies changing the parameters of the other.

There were situations where different balances between both models were numerically possible. The fits obtained are, however, the result of a long thought on each individual parameter and its physical consequences.

There is however, one substantial improvement that could be made. The parameter D_{an}, the diffusion of the anion, dominates the total diffusion of the OS mechanism and therefore the relaxation rate is very sensitive to its variation. While it was allowed to vary in each individual fit, it is possible to measure it for each sample. This would allow a better estimation for the rest of the parameters, and is therefore an important improvent to be made for this work.

Figure 4.14 shows the NMRD for each paramagnetic [Aliquat]$^+$ based sample. While displaying the results in chapter 3 both the IS and OS curves were summed into a general paramagnetic contribution. Figure 4.14 shows both curves separately in order to display their relative importance. In the case of 50%(v/v) DMSO, there are two OS contributions as already discussed in section 3.2.1.5.

- **Parameters shared between IS and OS mechanisms**

  There are three main parameters common to both mechanisms (excluding the spin $S = 2.5$), Δ and τ_v and D_{an}. Although D_{an} originally only enters the OS mechanism, the τ_m hypothesis discussed in the previous chapter also makes it a parameter for the IS mechanism. The following table contains the values obtained for the three parameters:

DMSO % (v/v)	$\Delta(10^{10}$ s$^{-1})$	$\tau_v(10^{-11}$ s)	D_{an} (10^{-10} m^{2}s^{-1})
0 % (d6)	1.07 ± 0.01	2.9 ± 0.2	0.8 ± 0.2
1 % (d6)		3.9 ± 0.3	0.74 ± 0.08
10 % (d6)		2.5 ± 0.2	0.52 ± 0.08
50 % (d6)		1.41 ± 0.04	0.98 ± 0.09
99 % (h6)	2.68 ± 0.06	0.67 ± 0.03	2.9 ± 0.3

Table 4.5: Parameters shared by the OS and IS mechanisms by sample (ordered by DMSO percentage).

The value of Δ is a measure of the total energy of the ZFS interaction and is directly connected to the immediate vicinity of the $[FeCl_4]^-$ ion. It was reasonable to assume that since the $[FeCl_4]^-$ ions reside mainly in the polar areas of the [Aliquat]$^+$ molecules, the value of Δ should be reasonably independent of the quantity of DMSO and the numerical fitting of the data was made for a single value of Δ for every sample with deuterated DMSO. The fact that the sample with 99 % (v/v) DMSO-h6 had to be adjusted with a much higher value for Δ led us to make the assumption that this represents a fundamentally different chemical environment for the $[FeCl_4]^-$ ions in this sample, namely that it is mostly solvated by the DMSO molecules instead of residing in the polar areas of the [Aliquat]$^+$ molecules.

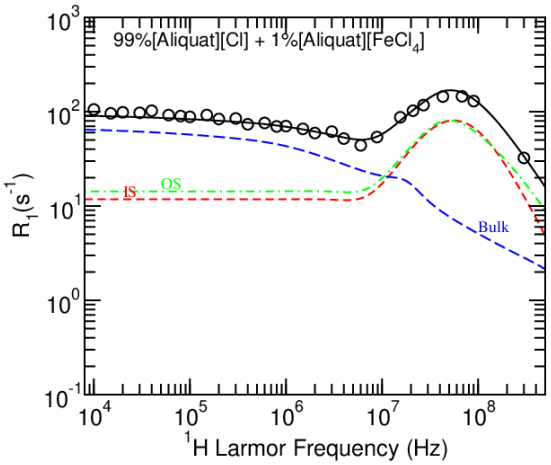

Figure 4.8: 0% DMSO

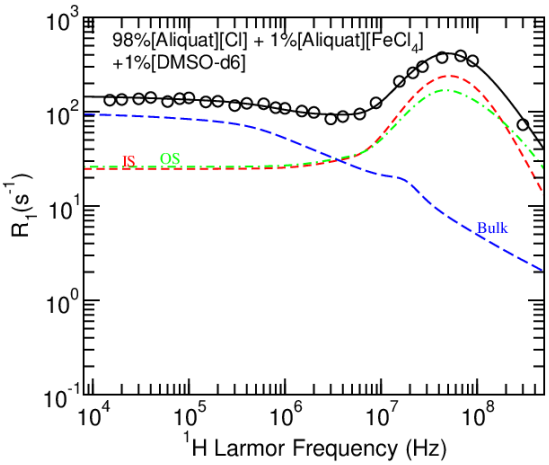

Figure 4.9: 1% DMSO-d6 (v/v)

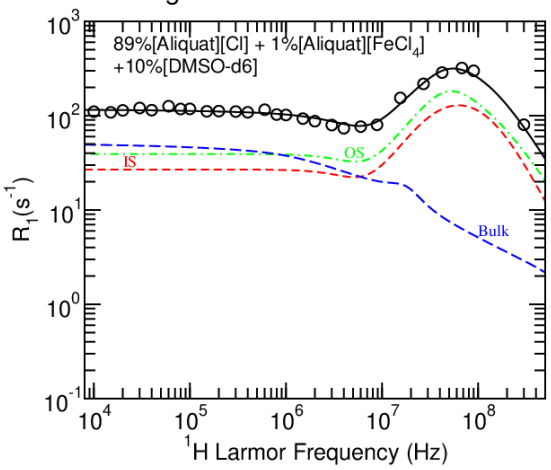

Figure 4.10: 10% DMSO-d6 (v/v)

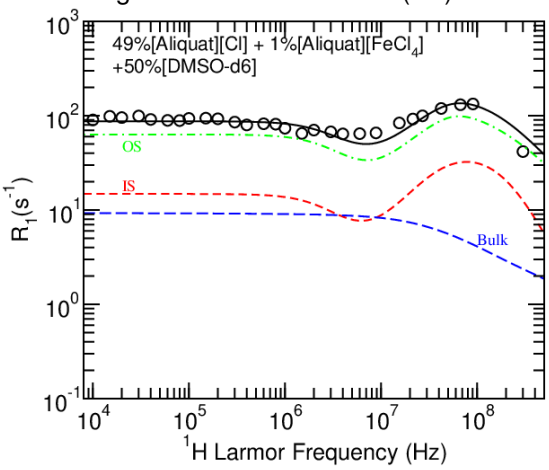

Figure 4.11: 50% DMSO-d6 (v/v)

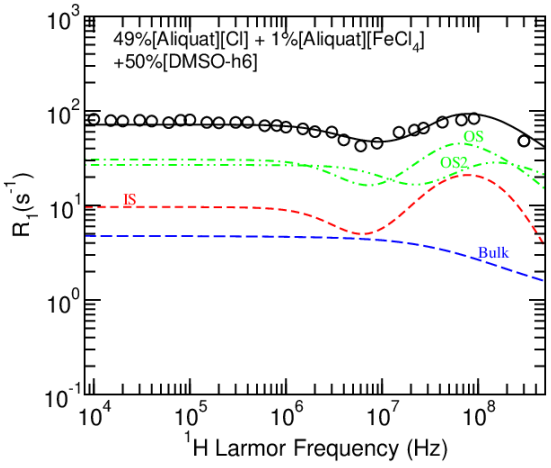

Figure 4.12: 50% DMSO-h6 (v/v)

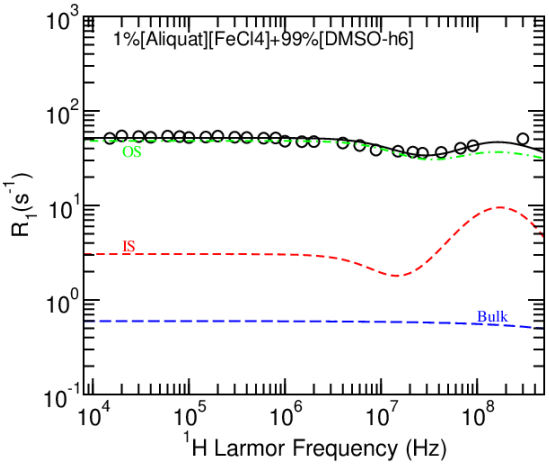

Figure 4.13: 99% DMSO-h6 (v/v)

Figure 4.14: All $[Aliquat]^+$ based paramagnetic samples' NMRD (IS in red, both OS in green, Bulk in blue, ordered by DMSO percentage).

The fact that the balance between IS and OS seems to be roughly 1:1 in the samples with 0%, 1 % and 10% (v/v) DMSO-d6 while the OS gains relative relevance for the 50% and 99% (v/v) DMSO-h6 samples seems to corroborate that there is solvation by DMSO for the 50% and 99% (v/v) DMSO samples. For the 50% (v/v) DMSO-d6 case, since only the [Aliquat]$^+$ protons are visible, the Δ was assumed to be mostly derived from the close [$FeCl_4$]$^-$ ions in the polar areas of the [Aliquat]$^+$ molecules, which was already reasoned to be similar to the value for the samples with less DMSO. For the 50% (v/v) DMSO-h6 case however, since both [Aliquat]$^+$ and DMSO protons are now visible, one should observe [$FeCl_4$]$^-$ ions both solvated and in the polar areas of the [Aliquat]$^+$ molecules. This led to a numerical fit consisting in a weighted sum between two different OS, one with each Δ. The IS was assumed to have Δ corresponding to the non-solvated [$FeCl_4$]$^-$ ions. The weighted sum's factor was called the solvation factor $G = 0.34 \pm 0.05$, which seems to indicate that in the 50% (v/v) DMSO samples 34% of all proton relaxation by OS is due to solvated [$FeCl_4$]$^-$ ions. Knowing this solvation factor, it is possible to estimate the fraction of [$FeCl_4$]$^-$ ions that are solvated by DMSO molecules for the 50%(v/v) DMSO-h6 sample (which should be the same for the 50%(v/v) DMSO-d6 sample). It was found that this fraction is somewhere in the interval $[0.29; 0.47]$, meaning that the percentage of [$FeCl_4$]$^-$ ions solvated by DMSO molecules is at least 29% and at most 47%.

The correlation time for the ZFS fluctuations, τ_v, seems to decrease with increasing DMSO concentration, apart from a notorious increase for the 1% (v/v) DMSO sample. τ_v is mainly determined by the number of collisions per unit time between the [$FeCl_4$]$^-$ ions and the environment, which seems to indicate that for the deuterated samples, where the [$FeCl_4$]$^-$ ion is located near the polar areas of the [Aliquat]$^+$ molecules, increasing DMSO concentration will increase the collisions with the [$FeCl_4$]$^-$ ion. The 1% (v/v) DMSO-d6 case is once again the exception in this trend, as it was before for the OPF minimum cutoff frequency, which implies that DMSO in small concentrations actually stabilizes the local dynamics near the polar area of the [Aliquat]$^+$ molecule, diminishing the number of collisions per unit time. For the 99% (v/v) DMSO-h6 case, one observes the behaviour of [$FeCl_4$]$^-$ ions near DMSO molecules, which seem to collide with the [$FeCl_4$]$^-$ ion more frequently than the cases where the ion was near the [Aliquat]$^+$ molecule. Finally, it is necessary to mention that the 50% (v/v) DMSO-h6 was a mixture between the two cases, having the 50% (v/v) DMSO-d6 τ_v for the IS and one of the OS curves, and the 99% (v/v) DMSO-h6 τ_v for the other OS curve.

The diffusion coefficient for the [$FeCl_4$]$^-$ ion, D_{an}, seems to not vary much for the deuterated samples, fluctuating between 0.5 and 1(10^{-10} m^2s^{-1}). For the 99% (v/v) DMSO-h6 sample however, it increases by a factor of three, closer to the diffusion of the DMSO molecules $\approx 6\times10^{-10}$ m^2s^{-1}, which makes sense if the [$FeCl_4$]$^-$ ions are mostly solvated in the 99% (v/v) DMSO-h6 sample. The 50 % (v/v) DMSO-h6 sample was again a mixture, having the 50% (v/v) DMSO-d6 D_{an} for the IS and one of the OS curves, and the 99% DMSO-h6 D_{an} for the other OS curve.

- **Inner sphere**

  After the discussion of the parameters shared by both paramagnetic mechanisms and considering the τ_m hypothesis, there are only two parameters of interest obtainable by the numerical fits, τ_{ISrot} and d_{in}. As the inner sphere contribution for 50% (v/v) DMSO-h6 is a scaled version (by the fraction K) of the 50 % (v/v) DMSO-d6, its parameters are the same and therefore omitted.

  The values of τ_{ISrot} and d_{in} obtained were the following:

DMSO % (v/v)	τ_{ISRot}(10^{-9} s)	d_{in}(10^{-10} m)
0 % (d6)	5 ± 2	4.53 ± 0.06
1 % (d6)	5 ± 2	4.00 ± 0.04
10 % (d6)	1.7 ± 0.5	4.00 ± 0.04
50 % (d6)	$1\ ^{+4}_{-1}$	4.00 ± 0.06
99 % (h6)	$1\ ^{+15}_{-1}$	4.0 ± 0.2

Table 4.6: Rotational correlation time and distance between spins for the IS mechanism (ordered by DMSO percentage).

The rotational correlation time for the inner sphere mechanism, τ_{ISrot}, is a measure of the rotational speed of the complex formed by the [Aliquat]$^+$ molecule and the [$FeCl_4$]$^-$ ion. It decreases with DMSO concentration, which means that the rotation of the complex becomes faster with DMSO concentration. This means that while the addition of 1% (v/v) DMSO does not fundamentally alter the rotational dynamic of the [Aliquat][$FeCl_4$] complex, larger concentrations do, starting from at least 10% (v/v) DMSO. They do so in a way such that the rotation becomes faster, which seems to imply that the presence of enough DMSO liberates the rotation of the complex.

The distance between spins for the IS mechanism, d_{in}, is an average of the distance between the [$FeCl_4$]$^-$ ion and the [Aliquat]$^+$ protons participating in the IS relaxation. The distance is relatively constant, excluding the sample without DMSO, which seems to be higher. This seems to imply that the presence of DMSO, even in small quantities, approximates the [$FeCl_4$]$^-$ ion from the polar areas of the [Aliquat]$^+$ molecule, while increasing the DMSO quantity to higher concentrations seems to have no further effect.

- **Outer sphere**

  The only relevant parameter belonging to the OS mechanism that has not yet been discussed is the distance between spins for the OS interaction, d_{out}. Its values are presented in the following table:

DMSO % (v/v)	$d_{out}(10^{-10}$ m)
0 % (d6)	6.4 $\pm$ 0.2
1 % (d6)	5.1 $\pm$ 0.2
10 % (d6)	5.18 $\pm$ 0.08
50 % (d6)	4.64 $\pm$ 0.05
99 % (h6)	2.88 $\pm$ 0.03

Table 4.7: Distance between spins for the OS mechanism (ordered by DMSO percentage).

There is a constant decrease in the distance between spins for the OS interaction. The values up to 50 % (v/v) DMSO describe the OS mechanism in the vicinity of the $[Aliquat]^+$ protons, and this decrease seems to suggest that the presence of DMSO approximates the $[FeCl_4]^-$ ion from the $[Aliquat]^+$ molecule. As for the 99% (v/v) DMSO case, the distance is to the DMSO molecules' protons, and is therefore a measure of the effective distance between the $[FeCl_4]^-$ ion and DMSO protons when diffusing around DMSO molecules.

4.1.3 $[C_8mim][Cl]$ sample without $[FeCl_4]^-$

We begin by analysing the effect of changing the cation to $[C_8mim]^+$ on the non-paramagnetic relaxation components. Figure 4.17 shows the comparison between $[C_8mim][Cl]$ and [Aliquat][Cl] NMRD.

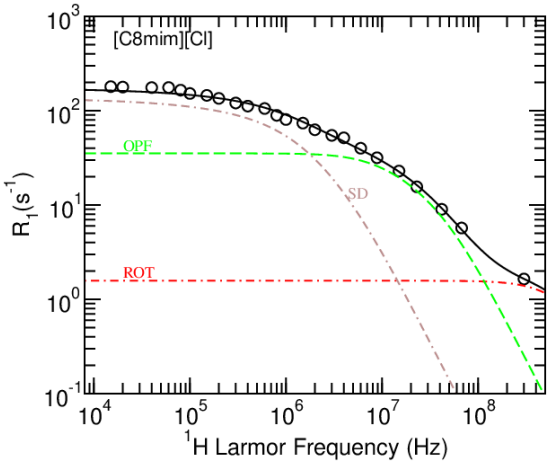

Figure 4.15: $[C_8mim][Cl]$

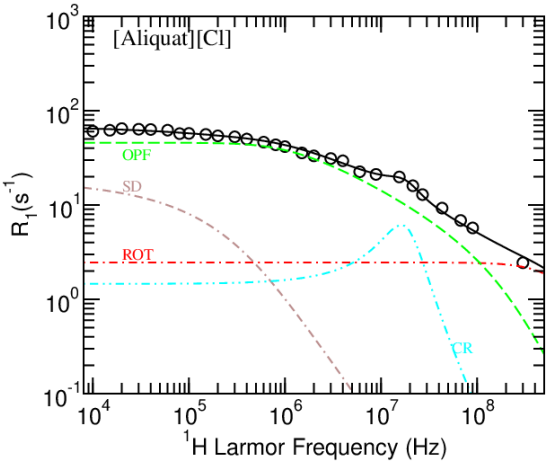

Figure 4.16: [Aliquat][Cl]

Figure 4.17: $[C_8mim][Cl]$ and [Aliquat][Cl] NMRD.

The following table shows a comparison between pure [Aliquat][Cl] and pure $[C_8mim][Cl]$ parameters:

Parameters	[C_8mim][Cl]	[Aliquat][Cl]
n (10^{22} cm^{-3})	5.27*	7.1*
A_{rot}(10^9 s^{-2})	3*	5*
τ_{rot}(10^{-11} s)	11 ± 2	10 ± 1
D_{IL} (10^{-12} m^{2}s^{-1})	$0.7\ ^{+0.8}_{-0.7}$	2 ± 2
r(10^{-10} m)	4.3 ± 0.3	$4\ ^{+30}_{-4}$
d(10^{-10} m)	4.94 ± 0.07	19 ± 2
A_{opf}(10^4 s$^{-\frac{3}{2}}$)	21.5 ± 0.8	6.4 ± 0.2
f_{min}(10^5 s^{-1})	56 ± 4	6.9 ± 0.5
f_{max}(10^8 s^{-1})	0.55 ± 0.04	2.6 ± 0.5

Table 4.8: Comparison between [C_8mim][Cl] and [Aliquat][Cl] parameters at 25ºC. (*) Calculated values

Firstly, there is no visible cross relaxation contribution on the [C_8mim]$^+$ sample, and therefore this mechanism was not used in the fitting.

For the rotational contribution, while the A_{rot} is bigger for the [Aliquat][Cl] sample, there is virtually no difference between rotational correlation times, which seems to suggest that the rotational speeds of both cations are the same. For the diffusion contribution, there are some fundamental differences. The diffusion coefficient for [C_8mim][Cl] is smaller than for [Aliquat][Cl] . Both average jump distances (r) are similar, while the distance of lateral closest approach (d) is very different. The similar average jump distances are explained by the fact that the x-ray peak for smaller distances, which encodes the lateral distances between molecules, has almost equal values. The big difference between the distance of lateral closest approach for both samples is explained by the fact that, for [Aliquat]$^+$, the diffusion is made by the molecule as a whole, and the distance is of the order of the distances between the center of mass of two contiguous [Aliquat]$^+$ molecules, while for [C_8mim]$^+$, a smaller molecule with only one aliphatic chain, this distance is simply of the order of the distance between molecules, which is also of the same order as r.

For the OPF contribution, there is a big difference between samples. While the intensity of the overall mechanism seems to increase for the [C_8mim][Cl] sample, the minimum cutoff frequency increases by a factor of roughly ten, implying a much shorter distance for the domains of correlated [C_8mim]$^+$ molecules in comparison to the [Aliquat]$^+$ molecules. The maximum cutoff frequency decreases for the [C_8mim][Cl] sample, which is surprising, since the [C_8mim]$^+$ molecule has a smaller size.

4.1.4 [C_8mim][Cl] sample with $[FeCl_4]^-$

With the non-paramagnetic contributions already discussed, it is time to focus on the differences between paramagnetic relaxation when the cation is changed from $[Aliquat]^+$ to $[C_8mim]^+$. Figure 4.20 shows both the NMRD of both 99%(v/v)[Aliquat][Cl] + 1%(v/v)[Aliquat][$FeCl_4$] and 99%(v/v)[C_8mim][Cl] + 1%(v/v)[C_8mim][$FeCl_4$] samples. Figure 4.21 shows the contributions from the OS and IS mechanisms for the 99%(v/v)[C_8mim][Cl] + 1%(v/v)[C_8mim][$FeCl_4$] sample separately in order to understand its relative importance.

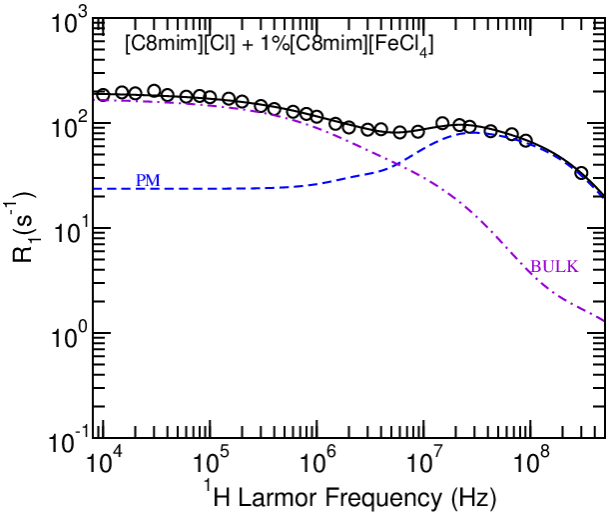

Figure 4.18: [C_8mim][Cl]+1%(v/v)[C_8mim][$FeCl_4$]

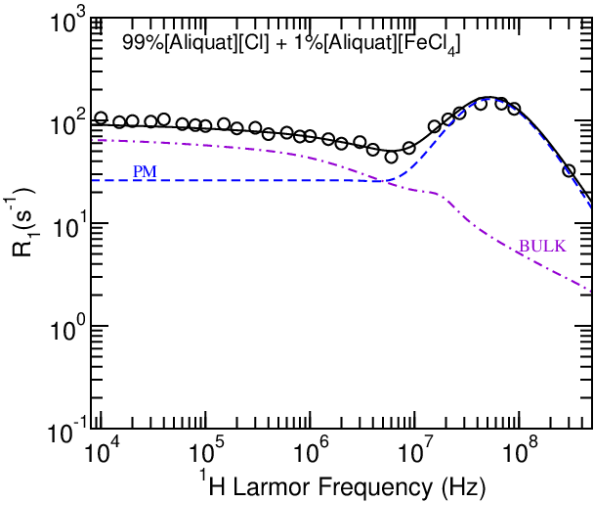

Figure 4.19: [Aliquat][Cl]+1%(v/v)[Aliquat][$FeCl_4$]

Figure 4.20: 99%(v/v)[C_8mim][Cl]+1%(v/v)[C_8mim][$FeCl_4$] and 99%(v/v)[Aliquat][Cl]+1%(v/v)[Aliquat][$FeCl_4$] NMRD.

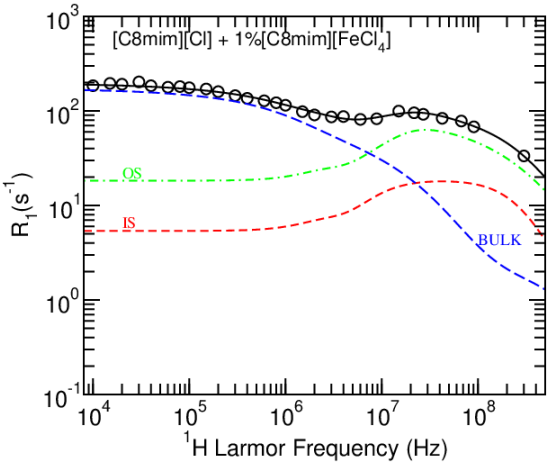

Figure 4.21: 99%(v/v)[C_8mim][Cl] + 1%(v/v)[C_8mim][$FeCl_4$] with OS and IS curves separated (IS curve red, OS curve green, Bulk curve blue).

Comparing the NMRD in figure 4.20, we can see that the high frequency relaxation rate due to paramagnetic relaxation is smaller for 99%(v/v)[C_8mim][Cl] + 1%(v/v)[C_8mim][$FeCl_4$] than for 99%(v/v)[Aliquat][Cl] + 1%(v/v)[Aliquat][$FeCl_4$] . The PRE displayed by 99%(v/v)[C_8mim][Cl] + 1%(v/v)[C_8mim][$FeCl_4$] is therefore smaller than the one for 99%(v/v)[Aliquat][Cl] + 1%(v/v)[Aliquat][$FeCl_4$] .

While in the 99%(v/v)[Aliquat][Cl] + 1%(v/v)[Aliquat][$FeCl_4$] sample both the IS and OS curves are similar in value (figure 4.8), in figure 4.21 we can see that in the 99%(v/v)[C_8mim][Cl] + 1%(v/v)[C_8mim][$FeCl_4$] sample the OS mechanism is stronger than the IS mechanism.

The following table summarizes the relevant parameters:

Parameters	99%(v/v)[C_8mim][Cl] +1%(v/v)[C_8mim][$FeCl_4$]	99%(v/v)[Aliquat][Cl] +1%(v/v)[Aliquat][$FeCl_4$]
$\Delta(10^{10}$ s$^{-1})$	0.62$\pm$ 0.05	1.07 $\pm$ 0.01
$\tau_v(10^{-11}$ s)	7 $\pm$ 2	2.9 $\pm$ 0.2
D_{MIL} (10^{-12} m^{2}s^{-1})	10 $^{+20}_{-10}$	5 $\pm$ 5
D_{an} (10^{-10} m^{2}s^{-1})	3.4 $\pm$ 0.3	0.8 $\pm$ 0.2
$\tau_{ISRot}(10^{-9}$ s)	10 $^{+50}_{-10}$	5 $\pm$ 2
$d_{in}(10^{-10}$ m)	6.2 $\pm$ 0.2	4.53 $\pm$ 0.06
$d_{out}(10^{-10}$ m)	7.8 $\pm$ 0.3	6.4 $\pm$ 0.2
C (mmol dm^{-3})	26*	12

Table 4.9: Comparison between 99%(v/v)[C_8mim][Cl] + 1%(v/v)[C_8mim][$FeCl_4$] and 99%(v/v)[Aliquat][Cl] + 1%(v/v)[Aliquat][$FeCl_4$] parameters for paramagnetic relaxation at 25ºC. (*) Calculated values

The values of Δ are different for the different samples, which is most likely simply a consequence of the different chemical surroundings for the $[FeCl_4]^-$ ions.

The value of τ_v is bigger for the 99%(v/v)[C_8mim][Cl] + 1%(v/v)[C_8mim][$FeCl_4$] sample than its value for the 99%(v/v)[Aliquat][Cl] + 1%(v/v)[Aliquat][$FeCl_4$] sample. Since τ_v is modulated by collisions of the $[FeCl_4]^-$ ion with its surroundings, this appears to imply that there is a smaller frequency of collisions for the $[FeCl_4]^-$ ions when the cation is $[C_8mim]^+$ than when the cation is $[Aliquat]^+$.

Both diffusions, that of the cation (D_{MIL}) and of the anion (D_{an}) are bigger for the 99%(v/v)[C_8mim][Cl] + 1%(v/v)[C_8mim][$FeCl_4$] sample than for the 99%(v/v)[Aliquat][Cl] + 1%(v/v)[Aliquat][$FeCl_4$] sample. While the change of value for D_{MIL} does not alter the shape of the NMRD in a substantial way, the fourfold increase in the diffusion of the anion has a profound effect on it, severely decreasing the relaxation rate in the high frequency region, and therefore the PRE, for the sample with [C_8mim][$FeCl_4$] when compared to the sample with [Aliquat][$FeCl_4$] .

As for the rotational correlation time for the inner sphere mechanism, τ_{ISrot}, there is a twofold increase in its value for the sample with [C_8mim][$FeCl_4$] when compared to the sample with [Aliquat][$FeCl_4$] . This seems to indicate that the [C_8mim][$FeCl_4$] complex rotates slower than the [Aliquat][$FeCl_4$] complex does. There is however a great deal of uncertainty associated with this value, and conclusions

derived from it are generally unreliable.

Both distances, the one associated with the IS mechanism (d_{in}) and the one associated with the OS mechanism (d_{out}) are bigger for the 99%(v/v)[C_8mim][Cl] + 1%(v/v)[C_8mim][$FeCl_4$] sample than for the 99%(v/v)[Aliquat][Cl] + 1%(v/v)[Aliquat][$FeCl_4$] sample. This is the second main factor (along with the bigger value for D_{an}) contributing for the reduction of the PRE in the sample with [C_8mim][$FeCl_4$] when compared to the sample with [Aliquat][$FeCl_4$] . The bigger distance for d_{in}, in particular, causes the IS mechanism to lose importance in the total paramagnetic relaxation.

Finally, it is important to mention that the concentration of paramagnetic particles is bigger for the 99%(v/v)[C_8mim][Cl] + 1%(v/v)[C_8mim][$FeCl_4$] sample than for the 99%(v/v)[Aliquat][Cl] + 1%(v/v)[Aliquat][$FeCl_4$] sample. This makes the paramagnetic part of the NMRD of the sample with [C_8mim][$FeCl_4$] greater by a factor of $\frac{26}{12} \approx 2.17$ than it should be if we were to compare it in equal conditions to the 99%(v/v)[Aliquat][Cl] + 1%(v/v)[Aliquat][$FeCl_4$] NMRD curve. This makes the reduction of the PRE, already visible when comparing the NMRD curves, even more apparent.

4.2 Conclusions

One of the two main purposes of this work was to discover the effect on the PRE displayed by $[Aliquat]^+$ based magnetic ionic liquids by the addition of a co-solvent, in this case DMSO. This goal has been fulfilled, and it has been observed that, while for relatively small quantities of DMSO (1 and 10% (v/v)) there was no notable attenuation of this PRE, for 50%(v/v) and 99% (v/v) there was a substantial reduction. This reduction appears to be caused by the fact that the addition of large quantities of DMSO effectively separates some of the $[FeCl_4]^-$ ions from the $[Aliquat]^+$ cations, causing a reduction of the IS mechanism by disassembling some of the [Aliquat][$FeCl_4$] complexes.

The other main objective was to discover what happened to the PRE if the cation is changed. This comparison was made with another, simpler cation, $[C_8mim]^+$, and it showed that changing the cation dramatically alters the PRE. In this specific case, 99%(v/v)[C_8mim][Cl] + 1%(v/v)[C_8mim][$FeCl_4$] exhibits a lower relaxation rate due to paramagnetic relaxation mechanisms than 99%(v/v)[Aliquat][Cl] + 1%(v/v)[Aliquat][$FeCl_4$] . This difference seems to be mainly caused by a faster diffusion of the $[FeCl_4]^-$ ions in the sample with [C_8mim][$FeCl_4$] , suggesting that bigger PRE can be generated in systems where this diffusion is slowed.

Another important conclusion to retrieve from this work is the major importance of collective motions in the relaxation rate of both $[C_8mim]^+$ and $[Aliquat]^+$ based ionic liquid systems. These collective motions seem to be attenuated by the presence of larger quantities of DMSO, but exist at least up to 50%(v/v).

4.3 Future Work

The results obtained in this work would benefit from an accurate determination of the diffusion coefficient for the $[FeCl_4]^-$ ions. It would also be useful to better understand the regions between 10% and 50%(v/v)

DMSO and 50% and 99%(v/v) DMSO, by studying intermediate systems with DMSO concentrations between those studied in this work. Also, it would be important to study different cations with dimensions and structure between $[C_8mim]^+$ and [Aliquat]$^+$ cations, to see if the PRE is something between those obtained in this work or radically different. Furthermore, studying systems with other anions, such as $GdCl_6{}^{3-}$, would help to understand the effect of the metal anion used. Finally, it would be interesting to compare the results obtained in this work with molecular dynamics simulations [40].

Bibliography

[1] P. Walden. Molecular weights and electrical conductivity of several fused salts. *Bulletin de l'Académie impériale des sciences de St. Pétersbourg*, 1914.

[2] J. Wang, J. Luo, S. Feng, H. Li, W. Yinhua, and X. Zhang. Recent development of ionic liquid membranes. *Green Energy & Environment*, 2016.

[3] K. Seddon. Ionic liquids for clean technology. *Journal of Chemical Technology & Biotechnology*, 68:351–356, 1997.

[4] K. Marsh, J. Boxall, and R.Lichtenthaler. Room temperature ionic liquids and their mixtures—a review. *Fluid Phase Equilibria*, 219(1):93–98, 2004.

[5] A.Berthod, M. Ruiz-Ángel, and S.Carda-Broch. Ionic liquids in separation techniques. *Journal of Chromatography A*, 1184(1):6–18, 2008.

[6] T. Jiang, M. Brym, G. Dubé, A. Lasia, and G. Brisard. Electrodeposition of aluminium from ionic liquids: Part i—electrodeposition and surface morphology of aluminium from aluminium chloride (alcl3)–1-ethyl-3-methylimidazolium chloride ([emim]cl) ionic liquids. *Surface and Coatings Technology*, 201(1):1–9, 2006.

[7] D. Tempel, P. Henderson, J. Brzozowski, R. Pearlstein, and H. Cheng. High gas storage capacities for ionic liquids through chemical complexation. *Journal of the American Chemical Society*, 130(2): 400–401, 2008.

[8] M. Ishikawa, T. Sugimoto, M. Kikuta, E. Ishiko, and M. Kono. Pure ionic liquid electrolytes compatible with a graphitized carbon negative electrode in rechargeable lithium-ion batteries. *Journal of Power Sources*, 162(1):658 – 662, 2006.

[9] R. Remsing, R. Swatloski, R. Rogers, and G.Moyna. Mechanism of cellulose dissolution in the ionic liquid 1-n-butyl-3-methylimidazolium chloride: a 13c and 35/37cl nmr relaxation study on model systems. *Chemical Communications*, (12):1271–1273, 2006.

[10] J.Sun, W. Cheng, W. Fan, Y. Wang, Z. Meng, and S. Zhang. Reusable and efficient polymer-supported task-specific ionic liquid catalyst for cycloaddition of epoxide with co2. *Catalysis Today*, 148(3):361 – 367, 2009.

[11] S. Ding, M. Radosz, and Y. Shen. Ionic liquid catalyst for biphasic atom transfer radical polymerization of methyl methacrylate. *Macromolecules*, 38(14):5921–5928, 2005.

[12] C. Kulsing, Y. Nolvachai, H. Hügel, and P. Marriott. Developments in gas chromatography using ionic liquid stationary phases. *LC GC Europe*, pages 434–440, 2015.

[13] S. Mallakpour and M. Dinari. *Green Solvents II*. Springer, 2012.

[14] R.Rogers and K. Seddon. Ionic liquids–solvents of the future? *Science*, 302(5646):792–793, 2003.

[15] E.Santos, J. Albo, and A. Irabien. Magnetic ionic liquids: synthesis, properties and applications. *RSC Advances*, 4:40008–40018, 2014.

[16] E. Santos, J. Albo, C. Daniel, C. Portugal, J. Crespo, and A. Irabien. Permeability modulation of supported magnetic ionic liquid membranes (smilms) by an external magnetic field. *Journal of Membrane Science*, 430:56–61, 2013.

[17] C. Daniel, F. Chávez, C. Portugal, J. Crespo, and P. Sebastião. ^{1}h nmr relaxation study of a magnetic ionic liquid as a potential contrast agent. *The Journal of Physical Chemistry B*, 119(35):11740–11747, 2015.

[18] C. I. Daniel, F. V. Chávez, G. Feio, C. A. Portugal, J. G. Crespo, and P. J. Sebastião. ^{1}H NMR relaxometry, viscometry and PFG NMR studies of magnetic and nonmagnetic ionic liquids. *The Journal of Physical Chemistry B*, 117(39):11877–11884, 2013.

[19] M. Beira. Nmr study of the molecular dynamics in magnetic and non-magnetic ionic liquids. Master's thesis, Instituto Superior Técnico - Universidade de Lisboa, 2016.

[20] M. Beira, C. I. Daniel, P. L. Almeida, M. C. Corvo, A. A. Rosatella, C. A. M. Afonso, and P. J. Sebastião. 1h nmr relaxometry and diffusometry study of magnetic and nonmagnetic ionic liquid-based solutions: Cosolvent and temperature effects. *The Journal of Physical Chemistry B*, 121(51): 11472–11484, 2017.

[21] I. I. Rabi, N. F. Ramsey, and J. Schwinger. Use of rotating coordinates in magnetic resonance problems. *Rev. Mod. Phys.*, 26:167–171, Apr 1954. doi: 10.1103/RevModPhys.26.167.

[22] A. Abragam. *The principles of nuclear magnetism*. Claredon Press, Oxford, 1961.

[23] N. Bloembergen, E. M. Purcell, and R. V. Pound. Relaxation effect in nuclear magnetic resonance absorption. *Physical Review*, 73(7):679–712, Apr. 1948.

[24] R. Dong. *Nuclear Magnetic Resonance of Liquid Crystals*. Springer, 1997.

[25] H. C. Torrey. Nuclear spin relaxation by translational diffusion. *Physical Review*, 92(4):962–969, Nov. 1953.

[26] R. Kimmich, F. Winter, W. Nusser, and K.-H. Spohn. Interactions and fluctuations deduced from proton field – cycling relaxation spectroscopy of polypeptides, DNA, muscles, and algae. *Journal of Magnetic Resonance*, 68:263–282, 1986.

[27] N. Bloembergen and L. O. Morgan. Proton relaxation times in paramagnetic solutions. effects of electron spin relaxation. *Journal of Chemical Physics*, 34(3):842–850, 1961.

[28] A. Carrington and G. Luckhurst. Electron spin resonance line widths of transition metal ions in solution. relaxation through zero-field splitting. *Molecular Physics*, 8(2):125–132, 1964.

[29] A. Merbach, L. Helm, and E. Tóth. *The Chemistry of Contrast Agents in Medical Magnetic Resonance Imaging*. Wiley, 2013.

[30] I. Bertini, C. Luchinat, G. Parigi, and E. Ravera. *NMR of paramagnetic molecules*. Elsevier, 2016.

[31] R. E. del Sesto, T. M. McCleskey, A. K. Burrell, G. A. Baker, J. D. Thompson, B. L. Scott, J. S. Wilkes, and P. Williams. Structure and magnetic behavior of transition metal based ionic liquids. *Chemical communications*, 28(4):447–449, 2008.

[32] J. Albo, E. Santos, L. Neves, S. Simeonov, C. Afonso, J. Crespo, and A. Irabien. Separation performance of CO_2 through supported magnetic ionic liquid membranes (SMILMs). *Separation and Purification Technology*, 97:26–33, 2012.

[33] D. Sousa, G. Marques, J. Cascais, and P. Sebastião. Desktop fast-field cycling nuclear magnetic resonance relaxometer. *Solid State Nuclear Magnetic Resonance*, 38(1):36–43, 2010.

[34] R. Kimmich and E. Anoardo. Field-cycling nmr relaxometry. *Progress in Nuclear Magnetic Resonance Spectroscopy*, 44(4):257–320, 2004.

[35] E. Hahn. Spin echoes. *Physical Review*, 80(4):580–594, Nov. 1950.

[36] W. S. Price. Pulsed-field gradient nuclear magnetic resonance as a tool for studying translational diffusion: Part 1. basic theory. volume 9, pages 299–336. 1997.

[37] Avogadro: an open-source molecular builder and visualization tool. version 1.2.0. `http://avogadro.cc/`.

[38] P. J. O. Sebastião. *Estudo da dinâmica molecular em cristais líquidos com polimorfismos peculiares*. PhD thesis, Instituto Superior Técnico - Universidade de Lisboa, Jan. 1993.

[39] Aliquatcl nmrd for different temperatures - part of an article to be published - gently ceded by maria beira.

[40] P. Morgado, K. Shimizu, J. M. S. S. Esperança, P. M. Reis, L. P. N. Rebelo, J. N. Canongia Lopes, and E. J. M. Filipe. Using 129xe nmr to probe the structure of ionic liquids. *The Journal of Physical Chemistry Letters*, 4(16):2758–2762, 2013.

Appendix A

Global fits

This Appendix includes two pdf reports, one for the global fit of all [Aliquat]$^+$ and DMSO mixtures without [Aliquat][$FeCl_4$] , and another for the global fit of all [Aliquat]$^+$ and DMSO mixtures with 1%(v/v) [Aliquat][$FeCl_4$] . What is shown here is a plot of the global fits, and that is why the ”fixed” qualifier appears after each parameter. In reality, each individual fit has several independent free parameters, typically between 6 and 9. The name of the parameters used on this work are different than those appearing on the pdf reports, and table A.1 corresponds the terminology of the pdf reports with that used in the rest of this work.

tau	$\Leftrightarrow$	τ_{rot}	f0c	$\Leftrightarrow$	f_{CR}
a	$\Leftrightarrow$	d	k	$\Leftrightarrow$	K
rtorr	$\Leftrightarrow$	r	tr	$\Leftrightarrow$	τ_{ISRot}
Aopf	$\Leftrightarrow$	A_{opf}	tv	$\Leftrightarrow$	τ_v
f0	$\Leftrightarrow$	f_{min}	r	$\Leftrightarrow$	d_{in}
fcM	$\Leftrightarrow$	f_{max}	DOSani	$\Leftrightarrow$	D_{an}
ac	$\Leftrightarrow$	A_{CR}	l	$\Leftrightarrow$	d_{out}
tauc	$\Leftrightarrow$	τ_{CR}	frac	$\Leftrightarrow$	F

Table A.1: Correspondence between the name of the parameters in the pdf reports and in the rest of this work (pdf report - left; rest of the work - right). The number on the left of the parameters in the pdf report is the DMSO concentration (50d - DMSO-d6; 50p - DMSO-h6).

fitteia Report

(internet based fitter service)

The Art of Model Fitting to Experimental Results[1]

Subject	Globalfits, Global_fit_non_magnetic_Aliquat_samples
Date	Thursday 24th September, 2020, 18:41
Affiliation	ruimanuk@hotmail.com 2.80.224.80
Abstract	Fit report produced with the fit results of function: y= (T_4==1) ? BPP(f, T_1, tau1): (T_4==2) ? BPP(f, T_1, tau10):(T_4==3) ? BPP(f, T_1, tau50p):(T_4==4) ? BPP(f, T_1, tau50d):(T_4==5) ? BPP(f, T_1, tau99):BPP(f, T_1, tau0) + (T_4==1) ? Torrey1(f, a1, rtorr1, T_2, rtorr1*rtorr1*1e-20/(6*T_3)):(T_4==2) ? Torrey1(f, a10, rtorr10, T_2, rtorr10*rtorr10*1e-20/(6*T_3)):(T_4==3) ? Torrey1(f, a50p, rtorr50p, T_2, rtorr50p*rtorr50p*1e-20/(6*T_3)) :(T_4==4) ? Torrey1(f, a50d, rtorr50d, T_2, rtorr50d*rtorr50d*1e-20/(6*T_3)):(T_4==5) ? Torrey1(f, a99, rtorr99, T_2, rtorr99*rtorr99*1e-20/(6*T_3)):(T_4==6) ? Torrey1(f, a0, rtorr0, T_2, rtorr0*rtorr0*1e-20/(6*T_3)): 1e-9 + (T_4==1) ? OPF(f, Aopf1, f01, 0.0, fcM1, 30):(T_4==2) ? OPF(f, Aopf10, f010, 0.0, fcM10, 30):(T_4==3) ? OPF(f, Aopf50p, f050p, 0.0, fcM50p, 30):(T_4==4) ? OPF(f, Aopf50d, f050d, 0.0, fcM50d, 30):(T_4==6) ? OPF(f, Aopf0, f0of0, 0.0, fcM0, 30) :1e-9 + (T_4==1) ? CROSSRELAX(f, ac1, tauc1, f0c1):(T_4==2) ? CROSSRELAX(f, ac10, tauc10, f0c10):(T_4==6) ?CROSSRELAX(f, ac0, tauc0, f0c0): 1e-9 to the 168 experimental points, considering 0 free parameters.

$tau0 = 9.84 \times 10^{-11}$ (fixed)	$Aopf50d = 30808$ (fixed)
$tau1 = 8.27 \times 10^{-11}$ (fixed)	$Aopf50p = 8378.8$ (fixed)
$tau10 = 9.47 \times 10^{-11}$ (fixed)	$f0of0 = 6.871 \times 10^{+05}$ (fixed)
$tau50d = 6.57 \times 10^{-11}$ (fixed)	$f01 = 3.1073 \times 10^{+05}$ (fixed)
$tau50p = 4.91 \times 10^{-11}$ (fixed)	$f010 = 9.734 \times 10^{+05}$ (fixed)
$tau99 = 1.24 \times 10^{-11}$ (fixed)	$f050d = 1.38 \times 10^{+07}$ (fixed)
$a0 = 18.75$ (fixed)	$f050p = 1.29 \times 10^{+07}$ (fixed)
$a1 = 19.139$ (fixed)	$fcM0 = 2.63 \times 10^{+08}$ (fixed)
$a10 = 16.185$ (fixed)	$fcM1 = 3.01 \times 10^{+08}$ (fixed)
$a50d = 3.4378$ (fixed)	$fcM10 = 3.42 \times 10^{+08}$ (fixed)
$a50p = 4.0492$ (fixed)	$fcM50d = 3.46 \times 10^{+08}$ (fixed)
$a99 = 4.0492$ (fixed)	$fcM50p = 2.86 \times 10^{+08}$ (fixed)
$rtorr0 = 4.388$ (fixed)	$ac0 = 5.55 \times 10^{+07}$ (fixed)
$rtorr1 = 4.32$ (fixed)	$ac1 = 5.55 \times 10^{+07}$ (fixed)
$rtorr10 = 4.37$ (fixed)	$ac10 = 5.55 \times 10^{+07}$ (fixed)
$rtorr50d = 4.26$ (fixed)	$tauc0 = 1.11 \times 10^{-07}$ (fixed)
$rtorr50p = 4.26$ (fixed)	$tauc1 = 1.11 \times 10^{-07}$ (fixed)
$rtorr99 = 4.35$ (fixed)	$tauc10 = 1.11 \times 10^{-07}$ (fixed)
$Aopf0 = 64116$ (fixed)	$f0c0 = 1.62 \times 10^{+07}$ (fixed)
$Aopf1 = 65585$ (fixed)	$f0c1 = 1.62 \times 10^{+07}$ (fixed)
$Aopf10 = 59045$ (fixed)	$f0c10 = 1.62 \times 10^{+07}$ (fixed)

$\chi^2[6] = 22.8826$	$\chi^2[5] = 15.6453$
$\chi^2[4] = 11.3268$	$\chi^2[3] = 13.952$
$\chi^2[2] = 23.234$	$\chi^2[1] = 7.73858$
$\chi^2_t = 94.7794$	

[1] "The Art of Model Fitting to Experimental Results", P.J. Sebastião, *Eur. J. Phys.* **35** (2014) 015017

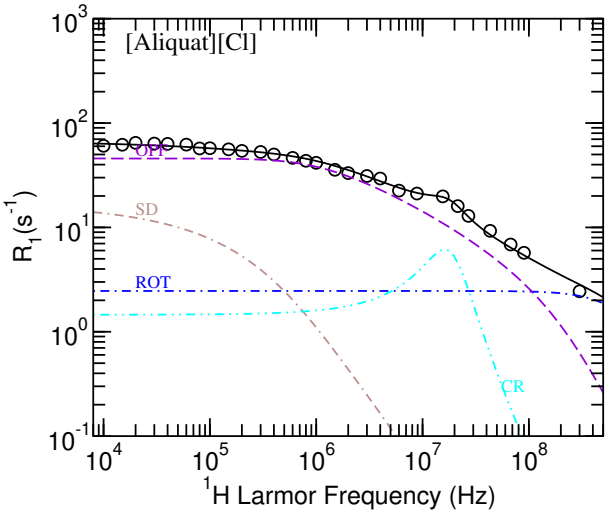

globalnonmagnetic-1.pdf

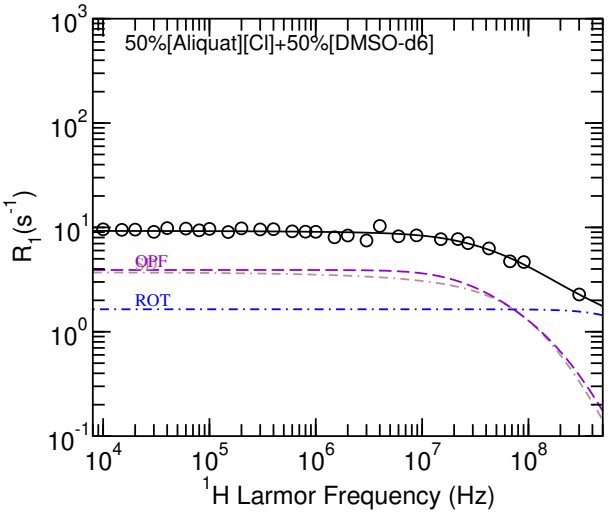

globalnonmagnetic-4.pdf

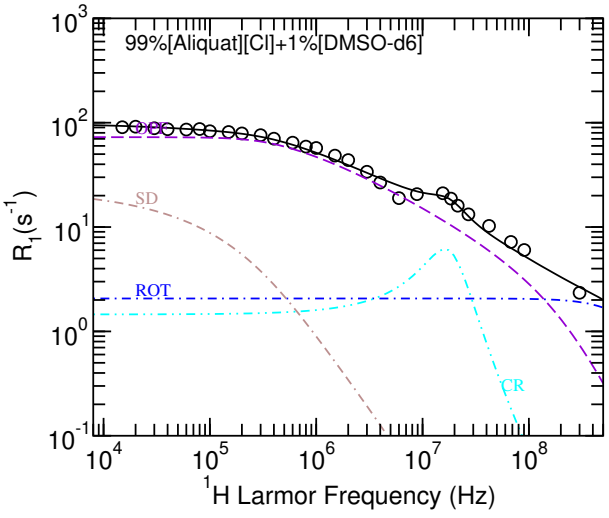

globalnonmagnetic-2.pdf

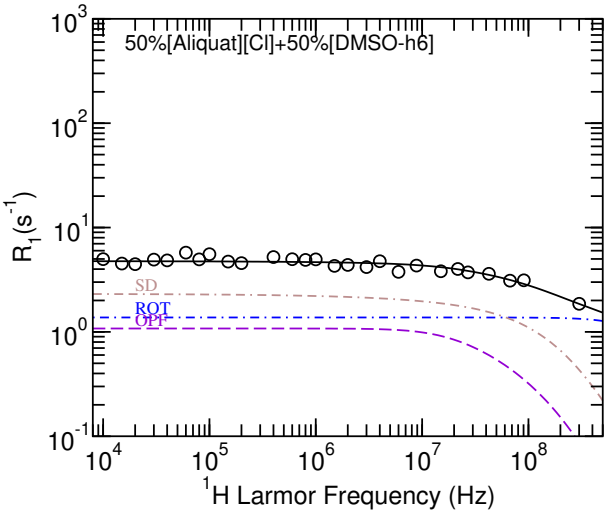

globalnonmagnetic-5.pdf

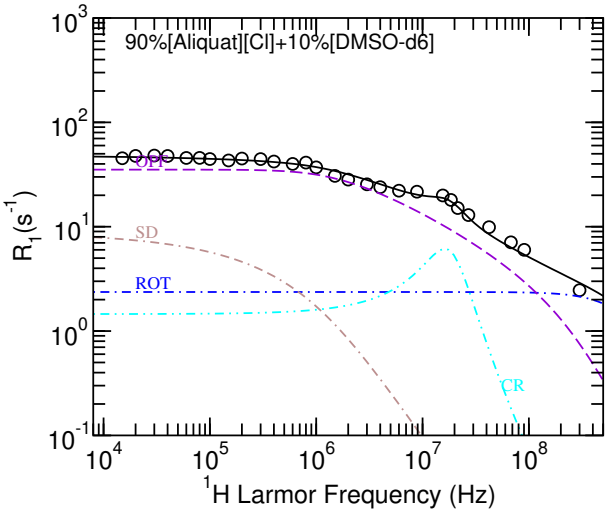

globalnonmagnetic-3.pdf

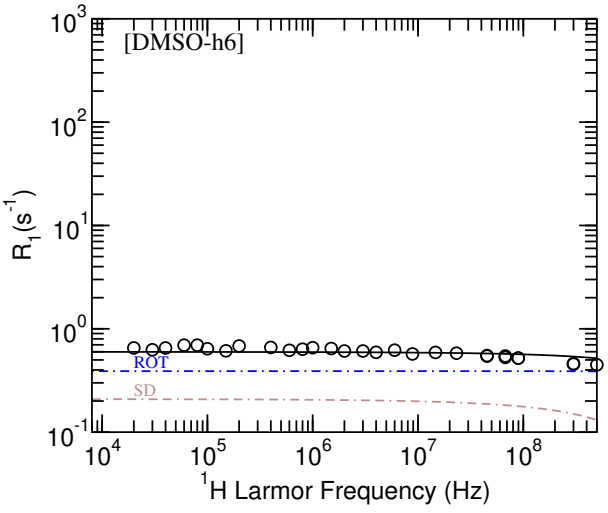

globalnonmagnetic-6.pdf

fitteia Report

(internet based fitter service)

The Art of Model Fitting to Experimental Results[1]

Subject	Globalfits, Global_fit_magnetic_Aliquat_samples
Date	Thursday 24th September, 2020, 18:58
Affiliation	ruimanuk@hotmail.com 2.80.224.80
Abstract	Fit report produced with the fit results of function: y= (T_22==1) ? k*Inner(f, 12.0, 1.0, 0.12682, 1.037, frac, 2.50000e + 00, (4.2600e + 00*4.2600e + 00*1e-20)/DOSani50, tr50d, tv50, r50d, Delta250, 0.0): (T_22==2) ? Inner(f, T_19, T_1, T_20, T_21, frac, T_2, (T_10*T_10*1e-20)/DOSani50, tr50d, tv50, r50d, Delta250, 0.0): (T_22==3) ? Inner(f, T_19, T_1, T_20, T_21, frac, T_2, (T_10*T_10*1e-20)/DOSani10d, tr10d, tv10d, r10d, Delta2, 0.0): (T_22==4) ? Inner(f, T_19, T_1, T_20, T_21, frac, T_2, (T_10*T_10*1e-20)/DOSani1d, tr1d, tv1d, r1d, Delta2, 0.0) : (T_22==5)? Inner(f, T_19, T_1, T_20, T_21, frac, T_2, (T_10*T_10*1e-20)/DOSani99, tr99, tv99, r99, Delta299, 0.0) : Inner(f, T_19, T_1, T_20, T_21, frac, T_2, (T_10*T_10*1e-20)/DOSani0, tr0, tv0, r0, Delta2, 0.0) + (T_22==1) ? G*R1OSabhf(f, T_4, T_2, l50p*1e-10, (T_5 + f*(T_6-T_5)/3e8) + DOSani50, tv50, Delta250) : (T_22==2) ? R1OSabhf(f, T_4, T_2, l50d*1e-10, (T_5 + f*(T_6-T_5)/3e8) + DOSani50, tv50, Delta250) : (T_22==3) ? R1OSabhf(f, T_4, T_2, l10d*1e-10, (T_5 + f*(T_6-T_5)/3e8) + DOSani10d, tv10d, Delta2) :(T_22==4) ? R1OSabhf(f, T_4, T_2, l1d*1e-10, (T_5 + f*(T_6-T_5)/3e8) + DOSani1d, tv1d, Delta2): (T_22==5) ?R1OSabhf(f, T_4, T_2, l99*1e-10, (T_5 + f*(T_6-T_5)/3e8) + DOSani99, tv99, Delta299): R1OSabhf(f, T_4, T_2, l0*1e-10, (T_5 + f*(T_6-T_5)/3e8) + DOSani0, tv0, Delta2) + BPP(f, T_7, T_8) + Torrey1(f, T_9, T_10, T_11, T_10*T_10*1e-20/(6*(T_5 + f*(T_6-T_5)/3e8))) + OPF(f, T_12, T_13, 0.0, T_14, T_15) + CROSSRELAX(f, T_16, T_17, T_18) + (T_22==1) ? (1-G)*R1OSabhf(f, T_4, T_2, l50p2*1e-10, (T_5 + f*(T_6-T_5)/3e8) + DOSani99, tv99, Delta299): (T_22==2) ? 1e-10: (T_22==3) ? 1e-10: (T_22==4) ? 1e-10: (T_22==5) ? 1e-10: 1e-10 to the 165 experimental points, considering 0 free parameters.

$k = 0.649$ (fixed)	$r10d = 4 \times 10^{-10}$ (fixed)
$G = 0.61742$ (fixed)	$r1d = 4 \times 10^{-10}$ (fixed)
$Delta299 = 7.17 \times 10^{+20}$ (fixed)	$r0 = 4.53 \times 10^{-10}$ (fixed)
$Delta250 = 1.15 \times 10^{+20}$ (fixed)	$DOSani99 = 2.89 \times 10^{-10}$ (fixed)
$Delta2 = 1.15 \times 10^{+20}$ (fixed)	$DOSani50 = 9.8 \times 10^{-11}$ (fixed)
$tr99 = 1.45 \times 10^{-09}$ (fixed)	$DOSani10d = 5.27 \times 10^{-11}$ (fixed)
$tr50d = 1.45 \times 10^{-09}$ (fixed)	$DOSani1d = 7.35 \times 10^{-11}$ (fixed)
$tr10d = 1.72 \times 10^{-09}$ (fixed)	$DOSani0 = 8.2 \times 10^{-11}$ (fixed)
$tr1d = 4.68 \times 10^{-09}$ (fixed)	$l99 = 2.8826$ (fixed)
$tr0 = 4.79 \times 10^{-09}$ (fixed)	$l50d = 4.6361$ (fixed)
$tv99 = 6.69 \times 10^{-12}$ (fixed)	$l50p = 4.9989$ (fixed)
$tv50 = 1.41 \times 10^{-11}$ (fixed)	$l50p2 = 2.8826$ (fixed)
$tv10d = 2.45 \times 10^{-11}$ (fixed)	$l10d = 5.191$ (fixed)
$tv1d = 3.9 \times 10^{-11}$ (fixed)	$l1d = 5.0725$ (fixed)
$tv0 = 2.93 \times 10^{-11}$ (fixed)	$l0 = 6.4238$ (fixed)
$r99 = 4 \times 10^{-10}$ (fixed)	$frac = 0.16667$ (fixed)
$r50d = 4 \times 10^{-10}$ (fixed)	

$\chi^2[6] = 9.15848$ $\chi^2[2] = 9.80443$

$\chi^2[1] = 18.0777$ $\chi^2[3] = 10.2707$

[1] "The Art of Model Fitting to Experimental Results", P.J. Sebastião, *Eur. J. Phys.* **35** (2014) 015017

$\chi^2[4] = 55.5519$ $\chi^2[5] = 27.1918$
$\chi^2_t = 130.055$

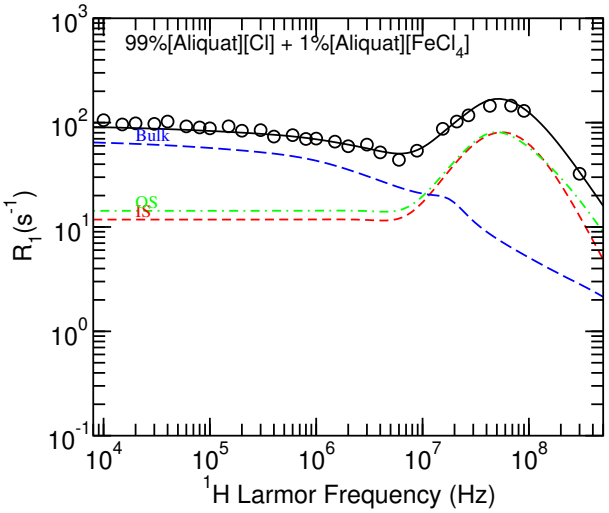

globalmagnetic-1.pdf

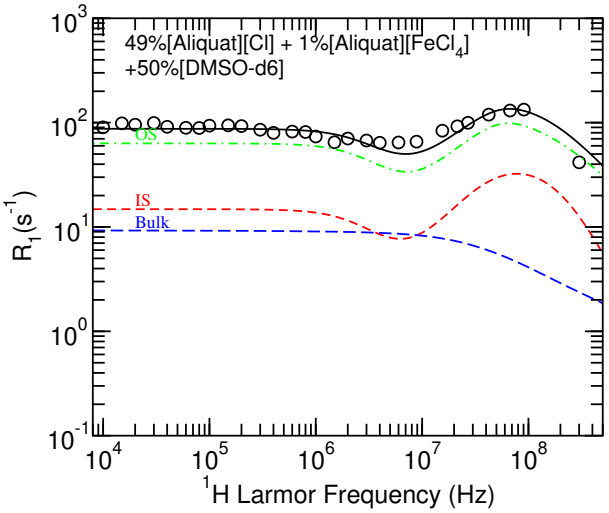

globalmagnetic-4.pdf

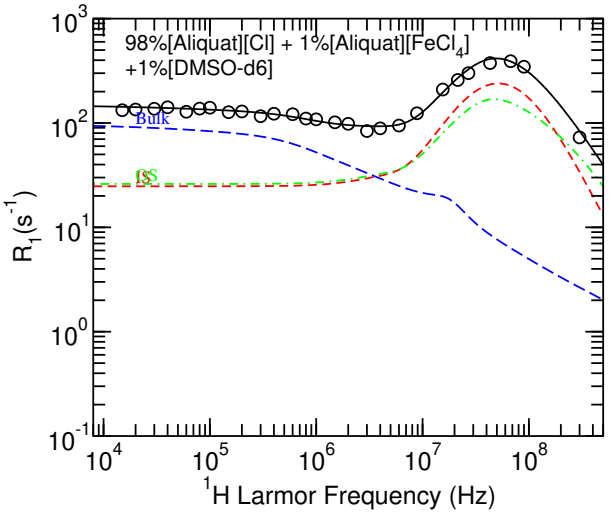

globalmagnetic-2.pdf

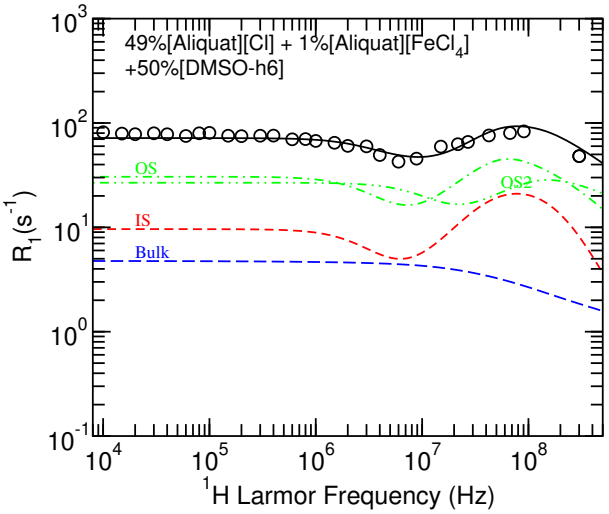

globalmagnetic-5.pdf

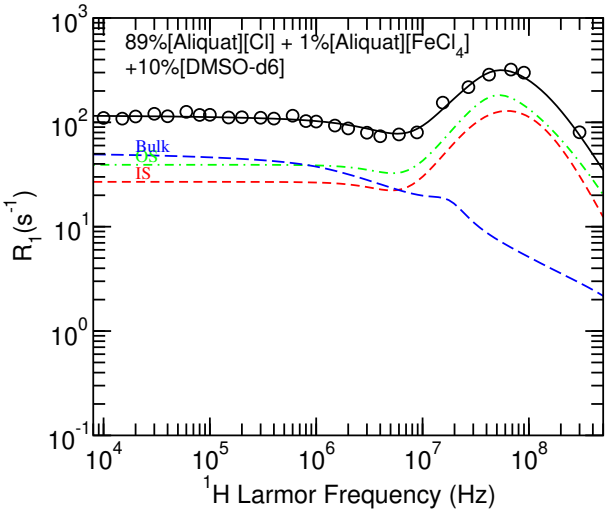

globalmagnetic-3.pdf

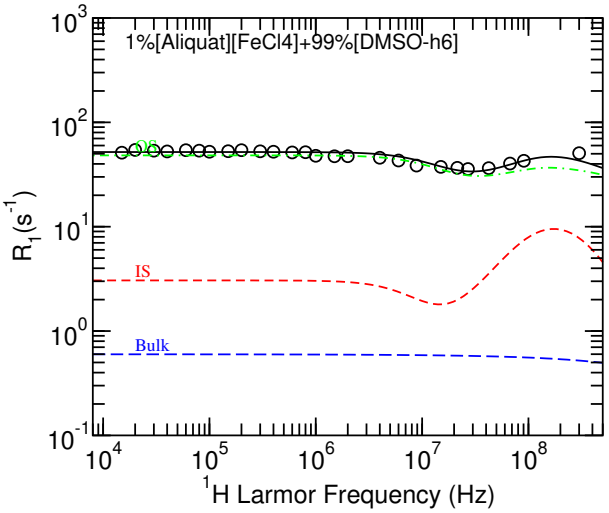

globalmagnetic-6.pdf

Appendix B

Temperature effect on [Aliquat][Cl]

This Appendix shows the pdf report of the global fits for pure [Aliquat][Cl] samples with three different temperatures, 5ºC, 25ºC and 70ºC. This data is part of an unpublished work, but is displayed here with permission of its authors. The terminology used in the pdf report is the same as shown in table A.1. The connection between different temperatures was made by considering an Arrhenius equation for the diffusional and rotational mechanisms, and additional parameters appear, namely the Arrhenius activation energy of the diffusion (ED) and rotation mechanisms (EL) and a reference temperature (Tref), reference rotational correlation time (tauL) and reference diffusion (Dref). The sample at 70ºC was most important, since it demanded a fit where f_{min} is of the order of 7 $\times$ 10$^5 s^{-1}$. Since f_{min} should not decrease with temperature, as it would imply a bigger size for correlated domains with increasing temperature, the other two must be fitted with smaller f_{min}. It was then found that the only way to do so was to increase the value of the OPF curve at the expense of the diffusional curve, which helps to justify the relative relevance given to each mechanism in the [Aliquat]$^+$ samples with varying DMSO concentrations.

fitteia Report

(internet based fitter service)

The Art of Model Fitting to Experimental Results[1]

Subject	Globalfits, AliquatCl_temperature_fits
Date	Thursday 24th September, 2020, 23:37
Affiliation	ruimanuk@hotmail.com 2.80.224.80
Abstract	Fit report produced with the fit results of function: y= (Z_1==1)? BPP(x, Arot, tauL*exp(EL/8.31*(1.0/Z_2-1.0/Tref))):1e-20 + (Z_2==343.15)? Torrey1(x, a70, rtorr70, n, rtorr70*rtorr70*1e-20/(6*Dref*exp(-ED/8.31*(1.0/Z_2-1.0/Tref)))): (Z_2==298.15)? Torrey1(x, a25, rtorr25, n, rtorr25*rtorr25*1e-20/(6*Dref*exp(-ED/8.31*(1.0/Z_2-1.0/Tref)))) : (Z_2==278.15)? Torrey1(x, a5, rtorr5, n, rtorr5*rtorr5*1e-20/(6*Dref*exp(-ED/8.31*(1.0/Z_2-1.0/Tref)))) :1e-20 + (Z_2==343.15)? OPF(x, Aopf70, f070, 0.0, fcM70, 1.00000e + 02) : (Z_2==298.15)? OPF(x, Aopf25, f025, 0.0, fcM25, 1.00000e + 02) : (Z_2==278.15)? OPF(x, Aopf5, f05, 0.0, fcM5, 1.00000e + 02) : 1e-20 + ((Z_1==2)? Dref*exp(-ED/8.31*(1.0/x-1.0/Tref)) : 1e-20) + (Z_2==343.15)? CROSSRELAX(x, ac70, tauc70, f0c):(Z_2==298.15)? CROSSRELAX(x, ac25, tauc25, f0c):(Z_2==278.15)? CROSSRELAX(x, ac5, tauc5, f0c) : 1e-20 to the 82 experimental points, considering 0 free parameters.

$EL = 9776.5$ (fixed)	$ac5 = 8.05 \times 10^{+07}$ (fixed)
$tauL = 9.84 \times 10^{-11}$ (fixed)	$tauc70 = 2.02 \times 10^{-07}$ (fixed)
$Tref = 298.15$ (fixed)	$tauc25 = 1.11 \times 10^{-07}$ (fixed)
$Arot = 5 \times 10^{+09}$ (fixed)	$tauc5 = 1 \times 10^{-07}$ (fixed)
$a70 = 4.3$ (fixed)	$f0c = 1.62 \times 10^{+07}$ (fixed)
$a25 = 19.023$ (fixed)	$Aopf70 = 9929.9$ (fixed)
$a5 = 55.003$ (fixed)	$Aopf25 = 64116$ (fixed)
$rtorr70 = 4.388$ (fixed)	$Aopf5 = 92303$ (fixed)
$rtorr25 = 4.388$ (fixed)	$f05 = 1.4343 \times 10^{+05}$ (fixed)
$rtorr5 = 4.388$ (fixed)	$f025 = 6.871 \times 10^{+05}$ (fixed)
$n = 7.1 \times 10^{+22}$ (fixed)	$f070 = 6.9112 \times 10^{+05}$ (fixed)
$Dref = 1.45 \times 10^{-12}$ (fixed)	$fcM5 = 1.91 \times 10^{+08}$ (fixed)
$ED = 60868$ (fixed)	$fcM25 = 2.63 \times 10^{+08}$ (fixed)
$ac70 = 1.14 \times 10^{+07}$ (fixed)	$fcM70 = 1.56 \times 10^{+08}$ (fixed)
$ac25 = 5.55 \times 10^{+07}$ (fixed)	

$\chi^2[3] = 3.82564$	$\chi^2[1] = 5.51963$
$\chi^2[2] = 7.54346$	$\chi^2_t = 16.8887$

[1] "The Art of Model Fitting to Experimental Results", P.J. Sebastião, *Eur. J. Phys.* **35** (2014) 015017

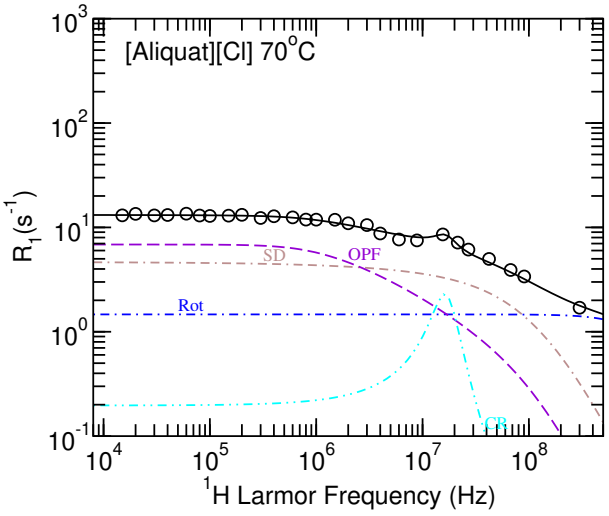

Aliquat_temperature_fit-1.pdf

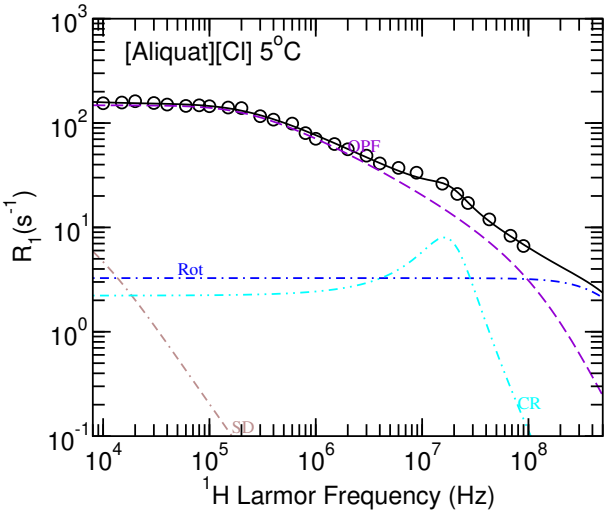

Aliquat_temperature_fit-3.pdf

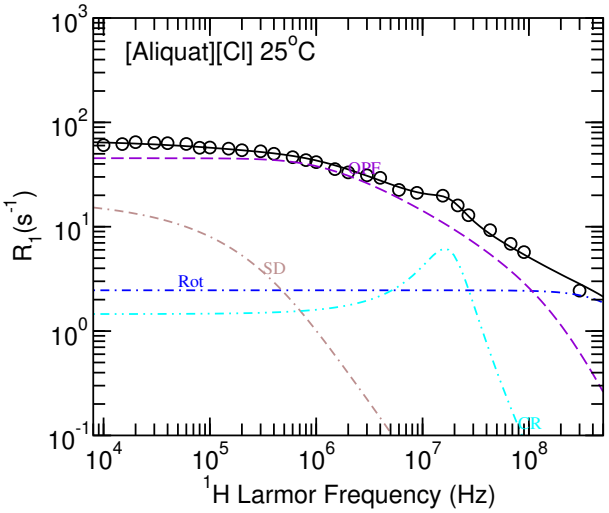

Aliquat_temperature_fit-2.pdf